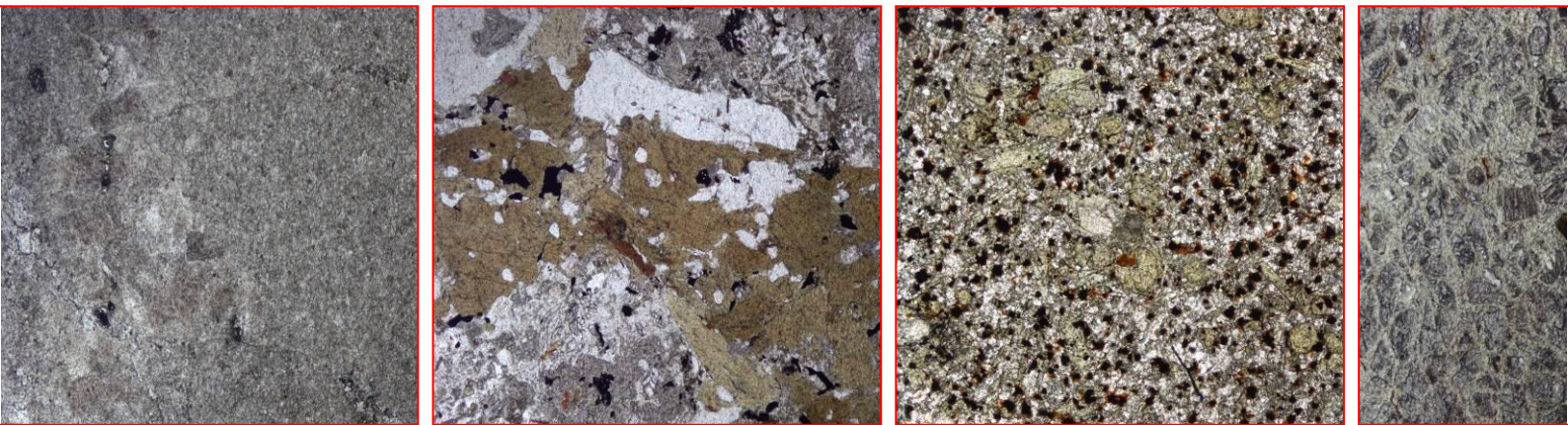


Graz University of Technology
Institute of Applied Geoscience
Institute of Railway Engineering and
Transport Economy

MASTER THESIS



Effect of grain shape and petrographic composition of railway ballast on the Impact Test

March 2014

Elisabeth Uhlig
0710070

Supervisor:
Christine Latal, Mag.rer.nat. Dr.rer.nat.
Holger Bach, Dipl.-Ing. Dr.techn.

STATUTORY DECLARATION

I declare that I have authored this thesis independently, that I have not used other than the declared sources/ resources, and that I have explicitly marked all material which has been quoted either literally or by content from the used sources.

Graz, _____

Acknowledgements

The following master thesis is an interdisciplinary study within the railway ballast test project at the faculty of Civil Engineering and Geosciences at the Technical University of Graz. Laboratory experiments and rock mechanic investigations were carried out at the Institute for Railway Engineering and Transport Economy and the Institute of Applied Geosciences.

First of all I want to show my gratitude to my supervisors. Many thanks to Dr. Holger Bach for giving me the opportunity to be part of this project. I really appreciate the support with various suggestions and constant help to improve this thesis.

Special thanks to Dr. Christine Latal for supporting me throughout my entire academic studies. Thank you for providing quick help and numerous recommendations while working on this master thesis.

At the Institute of Applied Geoscience I want to thank MSc. Markus Kaspar for all the help he provided concerning the analysis of geological and mineralogical aspects of this thesis. Furthermore, my appreciations go to Gerhard Lauk for preparing the thin sections.

At the Institute of Railway Engineering my gratitude goes to Mario Wiesberger who helped me with all problems concerning the impact test device in the laboratory.

Furthermore, I want to thank Sean Cullen for correcting my thesis concerning English misspellings, grammar and expressions.

In the end I want to thank the faculty of NAWI Graz for support.

Abstract

Railway ballast is one of the most important components in the track bed and has to fulfill several quality requirements. Poor quality ballast results in shorter tamping intervals and thus to a shorter lifespan and increased maintenance costs. The quality control of track ballast is executed with the help of various test procedures that verify mechanical properties. Austrian Federal Railways (ÖBB) has used these tests for several years. Resistance to fragmentation, chipping or abrasion of rock material can be verified. Resistance to fragmentation is determined by the Los Angeles-test and impact test, rounding stability is verified with the help of the Deval test. However, the test results are often variable and demonstrate poor repeatability.

The impact test is described in the standards EN13450 and EN1097-2. It is a method, which describes the resistance to fragmentation of rock aggregates. The impact test simulates high peak loads and impact impulses in the track, especially in the sleepers, caused by the traffic load.

In the course of this study, 350 impact tests are carried out, using ballast originating from 15 different quarries. These quarries are found in Austria, Bavaria and Bohemia and are from igneous, metamorphic and sedimentary origin. The geology and mineralogy of all rock types is determined and described by x-ray diffraction and thin sections. Several rock types have been separated into subclasses in order to identify reasons for possible variations in test results within a supplier or one rock type. The particle geometry of all samples is analyzed before and after the test by the device Petroscope 4D[®]. Thus, grain shape and angularity of the ballast can be determined and the effect of these parameters is examined with respect to the variability of the results.

Grain shape, angularity, petrographic composition and the formation of subclasses are analyzed in correlation with the results from the impact test. Petrographic composition and grain shape of the material have a strong influence on the impact test results. The degree of rounding plays a subordinate role. The formation of subclasses shows that railway ballast of one supplier can show different properties in terms of mechanical behavior and petrography.

Zusammenfassung

Bahnschotter ist eine der wichtigsten Komponenten im Gleisbett und muss daher bestimmte Qualitätsmerkmale aufweisen. Geringe Qualität von Gleisschotter führt zu verkürzten Stopfintervallen und somit zu einer kürzeren Lebensdauer und erhöhten Instandhaltungskosten. Die Qualitätskontrolle von Gleisschotter wird mit Hilfe von verschiedenen Testverfahren, die mechanische Eigenschaften überprüfen, durchgeführt. Die Österreichischen Bundesbahnen (ÖBB) lassen diese Tests jährlich seit mehreren Jahrzehnten durchführen. Es werden die Schlagzähigkeit, Kantenstabilität und Abradierbarkeit von Gesteinsmaterial überprüft. Die Schlagzähigkeit wird mittels Los Angeles-Test und Schlagzertrümmerungsversuch bestimmt, die Kantenstabilität kann mit Hilfe des Deval-Tests ermittelt werden. Die Testergebnisse variieren jedoch teilweise erheblich von Jahr zu Jahr.

Der Schlagzertrümmerungsversuch wird in den Normen EN13450 und EN1097-2 beschrieben. Dieser Test stellt ein Verfahren dar, um den Widerstand gegen die Zertrümmerung von Gesteinsaggregaten zu beschreiben. Der Schlagzertrümmerungsversuch soll hohe Lastspitzen und Aufprallimpulse im Gleis und speziell in der Schwelle, durch die Verkehrslast simulieren.

Im Zuge dieser Masterarbeit werden 350 Versuche des Schlagzertrümmerungsversuches an 15 verschiedenen Schottersorten durchgeführt. Die verwendeten Schottersorten stammen aus mehreren Steinbrüchen in Österreich, Bayern und Böhmen und sind sowohl magmatischen, metamorphen als auch sedimentären Ursprungs. Die Geologie und Mineralogie aller Gesteinsarten wird durch Röntgendiffraktometrie und Dünnschliffe ermittelt und beschrieben. Einige Schottersorten werden in Subklassen getrennt, um mögliche Schwankungen in Testergebnissen innerhalb eines Zulieferers oder einer Gesteinsart feststellen zu können. Die Korngeometrie aller Probenchargen wird vor und nach dem Test mit Hilfe des Gerätes Petroscope 4D[®] aufgenommen. Somit kann die Kornform und der Rundungsgrad des Schotters bestimmt und der Einfluss dieser Parameter auf die Variabilität der Ergebnisse untersucht werden.

Kornform, Rundungsgrad, petrographische Zusammensetzung und die Bildung von Subklassen werden im Zusammenhang mit den Ergebnissen aus dem

Schlagzertrümmerungstest analysiert und interpretiert. Petrographische Zusammensetzung des Materials und die Kornform haben einen starken Einfluss auf die Testergebnisse des Schlagzertrümmerungsversuches. Der Rundungsgrad spielt eine untergeordnete Rolle. Die Bildung von Subklassen zeigt, dass Schottermaterial eines Zulieferwerkes unterschiedliche Eigenschaften in Bezug auf mechanische Eigenschaften und Petrographie aufweisen kann.

Table of contents

1. Introduction	9
1.1. Statement of the problem	9
1.2. Purpose of thesis	10
2. Literature review – technical background.....	11
2.1. Functions of railway ballast.....	11
2.2. Requirements for railway ballast.....	12
2.3. Railway ballast in Austria	13
2.4. Loads and stress levels in the track	14
2.5. Ballast fragmentation.....	16
2.6. Ballast geometry	17
3. Methodology.....	20
3.1. Impact test	20
3.2. Petroscope 4D®	25
3.3. Concept of “P2” test series	26
4. Rock type description.....	29
4.1. Criteria for subclasses.....	29
4.2. Thin section and X-ray analysis	30
5. Results	52
5.1. SZ_{TU} -values	53
5.2. Strain.....	63
5.3. Degree of Fragmentation Z.....	72
5.4. Minimum sample size.....	75
5.5. Particle shape.....	77
5.6. Angularity	84
5.7. Comparison between the data Austrian Railways (ÖBB) and TUGraz ..	90
6. Discussion and Conclusion	92
References	97

1. Introduction

1.1. *Statement of the problem*

Rock ballast is one of the main components of railway tracks. In addition to the rock aggregates, the subsoil, drainage and elastic components are also important factors in a railway track. The ballast has to fulfill several requirements to be used as track ballast (Klotzinger, 2008).

Around one million tons of rock ballast per year is used by Austrian Federal Railways (ÖBB). The rock types used are of magmatic, metamorphic or sedimentary origin (Bach, 2013). The quarries that deliver the aggregates can be found all over Austria, as well as in Bavaria and Bohemia. Although the purchase and transport costs are relatively low, the maintenance costs are very cost-intensive. Therefore Railway infrastructure companies are interested in good quality ballast, with which maintenance costs and tamping are reduced. Descriptions of quality standards for the mechanical behavior of ballast exist in several European Standards.

To meet the quality standards, several testing methods have been established. Next to the Los Angeles, and the Deval tests, the impact test is a method to evaluate railway aggregates. Executing the impact test and analyzing the impact test results are the objectives of this thesis.

The testing methods for the mechanical behavior of rock ballast have been carried out by Austrian Railways for several years. The test results vary highly from one test year to another, and the tests do not have a statistical significance as they are repeated only three times as describes in EN 1097-2 (Österreichisches Normungsinstitut, 2006). Austrian Railways test the sieve size of their railway ballast more often than the mechanical behavior (Bach, 2013). Therefore the tests have to be carried out with statistical significance and possible reasons for variations in test results are being considered. The aim of the railway company is to determine the best quality ballast, with long durability, and low maintenance costs.

1.2. Purpose of thesis

This thesis investigates the effects of the grain shape and petrographic composition of railway ballast in connection with the impact test. The aim is to carry out impact tests for the 15 most important suppliers of railway ballast for Austrian Railways. The impact test is a mechanical test that simulates the load regime in the track and the magnitude of loads acting upon the track (Österreichisches Normungsinstitut, 2004a). The outcome of the test is the fragmentation of aggregates. During the project in 2013, the impact test was carried out 350 times. The impact test results are analyzed with statistical and finite element-methods, as well as with the help of literature.

With the help of the device Petroscope 4D[®], various parameters such as particle geometry and petrography, are obtained. An analysis of the influence of petrographic composition and particle geometry of different rock types on the impact test results is made. The results are analyzed in range, with the main goal of finding possible reasons for variations of the test results.

Moreover an important factor of this work is the description of the railway ballast. The variation of petrographic composition will be evaluated by standard mineralogical and geological methods. These methods include the analysis of thin sections, and interpretation of x-ray-diffraction results.

This thesis gives an overview of the technical background from a railway engineering and geological point of view in section 2. Section 3 deals with the methods used in the laboratory. Section 4 describes the used railway ballast in detail. Results that were acquired during the project can be found in section 5. In the end, section 6 discusses the results obtained.

2. Literature review – technical background

Railway ballast is a mass product due to its multiple functions. As a mass product, cost, durability, and maintenance are important factors for production (Bach, 2013). Therefore mechanical tests are carried out to identify the most suitable rock aggregates.

Testing methods for railway ballast are designed to simulate the loads and stress levels on the track and its components (Österreichisches Normungsinstitut, 2004a). The test methods used in the current test project are the Los-Angeles Test, the Deval Test and the Impact Test.

2.1. *Functions of railway ballast*

A homogenous, clean, elastic ballast bed is one condition for a well-functioning train system. Therefore track ballast and the track bed have to fulfil various functions. Uniform load distribution and dynamic load bearing are necessary, as well as resistance to sleeper displacements. In addition, a high resistance against longitudinal and transversal shifts is an important function, requiring an immovable, stable situation of the sleepers. Another function is a simple restoration of the original track geometry. Railway ballast also needs to be permeable to water and air. These functions are met by the right choice of the strength of the bed, its bed profile, the right choice of the ballast, and the quality of compaction of the ballast (Klotzinger, 2008).

However, it is not easy to achieve those functions, especially in the starting states of tracks. The situation in the track changes and requires most efficient rock ballast in terms of geometry and geology (see sections 2.5/2.6 and 4).

Depending on the rock quality, tracks need tamping after several years of use. This leads to new fragmentation and abrasion of particles as the ballast settlement is several mm in the track (Bach, 2013).

2.2. Requirements for railway ballast

As the ballast has a major influence on the durability and quality of the track, several requirements have to be fulfilled for rock aggregates to be used as railway ballast. Track bed strength and drainage are important factors for the quality of the track. As the track is heavily loaded by the high traffic volume and speeds of the trains, it is exposed to dynamic and static stresses. Higher quality of the rock ballast results in longer tamping intervals and lower costs for the railway company (Klotzinger, 2008).

Therefore the track ballast has to fulfill the following requirements:

- Rock ballast must be resistant to weathering and demonstrate low crack formation. Microcracks and crack formation by blasting appear in different forms and sizes. These cracks can reduce the strength of the ballast and lead to shorter life span (Klotzinger, 2008).
- The ballast should show toughness, hardness and low cleavability. Toughness reflects the resistance to loading. Cracks and microcracks play an important role in the breaking behavior, and therefore influence the toughness of the ballast. Hardness of the aggregates refers to the mineral hardness and the hardness of the binding material between the grains. The lower the cleavability is of the rock ballast, the lower the tendency will be of splitting along a natural weakness (Klotzinger, 2008).
- Additions of loam, earth or fine particles are not desirable. Fine particles as loam, earth and clay dry relatively slowly and are not desirable to find in rock ballast, as the track bed should dry out quickly after rainfall.
- Good resistance to fragmentation behavior is required. Good breaking behavior like sharp edges or dicey aggregates is desirable and leads to greater interlocking of the particles to each other and to the sleepers. This leads to better load transfer and higher resistance to displacements in the track (Klotzinger, 2008).

Mechanical properties and thus the requirements for railway ballast are influenced by the particle shape, especially parameters such as shear strength, tensile strength and compressive strength. Thus has an effect on the degree of fragmentation of particles. One would expect that flat particles are more re-

sistant to fragmentation than elongated particles, which tend to interlock with each other easily. Furthermore angular particles also tend to interlock with each other in the track and hence to small displacements. Angularity influences the degree of particle rounding (see section 2.6) (Bach, 2013).

Track ballast originates from the processes of blasting, breaking-down, screening and sieving of solid rock, as well as from washing, as fine particles are not desirable. After European Standard BH 700, the optimal grain size for railway ballast lies between 31.5 and 63mm (Österreichische Bundesbahnen (ÖBB), 2007). However, grain sizes between 22.4 and 31.5 mm are also included in railway ballast.

2.3. *Railway ballast in Austria*

The best suitable rock types for track ballast are hard rocks like granite, diabase and basalt. Those rock types have a high compressive strength and are therefore appropriate aggregates for railway ballast. Weaker materials such as limestone, dolomite and other sediment rocks have a smaller compressive strength and are consequently less suitable aggregates for tracks (Klotzinger, 2008).

Next to physical requirements and geometry the most important criteria for suitable railway ballast are impact strength, resistance to rounding and abrasion resistance (Österreichische Bundesbahnen (ÖBB), 2007). These properties result from mineral hardness, mineral bonding and size of the minerals and the texture of the rock type. One expects that fragmentation behavior is influenced by mineral grain sizes (coarse grained material like granite → higher tendency to break than fine grained material like diabase) (Kuttelwascher, 2011).

The rock types of the most important suppliers of Austrian Federal Railways are listed in Table 1. The table shows that rocks of all classes are used (igneous, metamorphic and sedimentary rocks types). The most widely used ballast in Austria is Granite, as it is found relatively often, especially in the Bohemian Massif. The second most commonly used railway ballast is Diabase. Diabase is also a wide spread rock type in Austria, mostly found in the Grauwackenzone. Basalt is a very suitable rock type, because of its properties. However as it does not occur very often in Austria, it is not used often. Despite its inferior suitability

for railway ballast, dolomite is also used, because it is found relatively often (Kuttelwascher, 2011).

Table 1: rock types used as railway ballast in Austria. Railway ballast is from igneous, metamorphic and sedimentary origin. Most used rock type in Austria is granite, followed by Diabase.

Rock type	Rock class	Number of quarries
Granite	igneous	5
Granite porphyr	igneous	1
Granulite	metamorphic	2
Diabase	metamorphic	3 (4)*
Basalt	igneous	1
Dunite	igneous (metasomatosis)	1
Dolomite	sedimentary	1

*There are four rock types of diabases that have been tested. However, two of these diabases are from the same quarry, but broken down only in different crushers.

2.4. Loads and stress levels in the track

Under the effect of the service of trains, the track is exposed to static and dynamic loads. The rail is positioned in a way that permanent deformations are unlikely. Vertical loads are producing most of the compressions and strains in the track. The stress distribution in the track is not equal at all points. Load chains are built within the tracks that are transformed from one grain to another. Through these loads chains, high load peaks and strong impact impulses are generated (Bach, 2012).

Axle loads transfer stresses from the axle, rail, rail pad, sleeper and ballast layer to the subsoil. In the track, stresses and elastic deformations are generated by static vertical loads and intensified by traffic actions. Just before the axle load hits the rail and consequently the ballast layer, sleepers are lifted up to 0.2mm by the weight of the traffic load and create hollow layers (Figure 1) (Fendrich, 2007). This “uplifting” is a dynamic factor in the track.

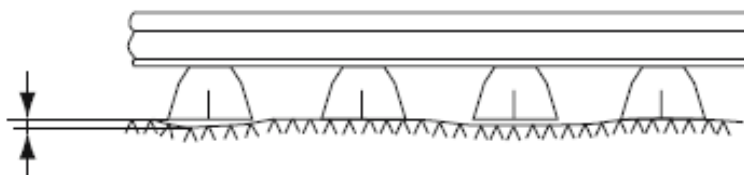


Figure 1: schematic diagram of hollow layer under the sleepers (between the arrows), the hollow layers are created by the dynamic factor in the track, by loads and stresses (Fendrich, 2007). In reality, railway sleepers are filled up to the top with ballast.

When the traffic load hits the hollow layers under the sleepers, the under lying ballast is subjected to a strong impact impulse. The uppermost ballast layer is affected greatest by the impact strength of the traffic load. The impact test (section 3.1) is a testing procedure to simulate the impact impulse of the traffic load that hits the opening and affects the underlying ballast (Bach, 2012). From the sleeper to the lowest layer of ballast the shear stress decreases with depth. Through the impact impulse and high point loads, fragmentation occurs. Next to fragmentation processes, other attrition types that can occur in the track are fragmentation, chipping or abrasion. Figure 2 shows the different attrition phenomena. In the first line, the fragmentation typology is displayed. Fragmentation generates medium sized particles or very fine ones. The angularity does not change significantly during fragmentation. Rounding or chipping and abrasion can also occur. Rounding is caused by high point loads or shear stress. Although the angularity increases, the grain size does not change. During abrasion processes that are caused by shear stress, size and shape remain the same, but many fine particles are produced (Bach, 2013).

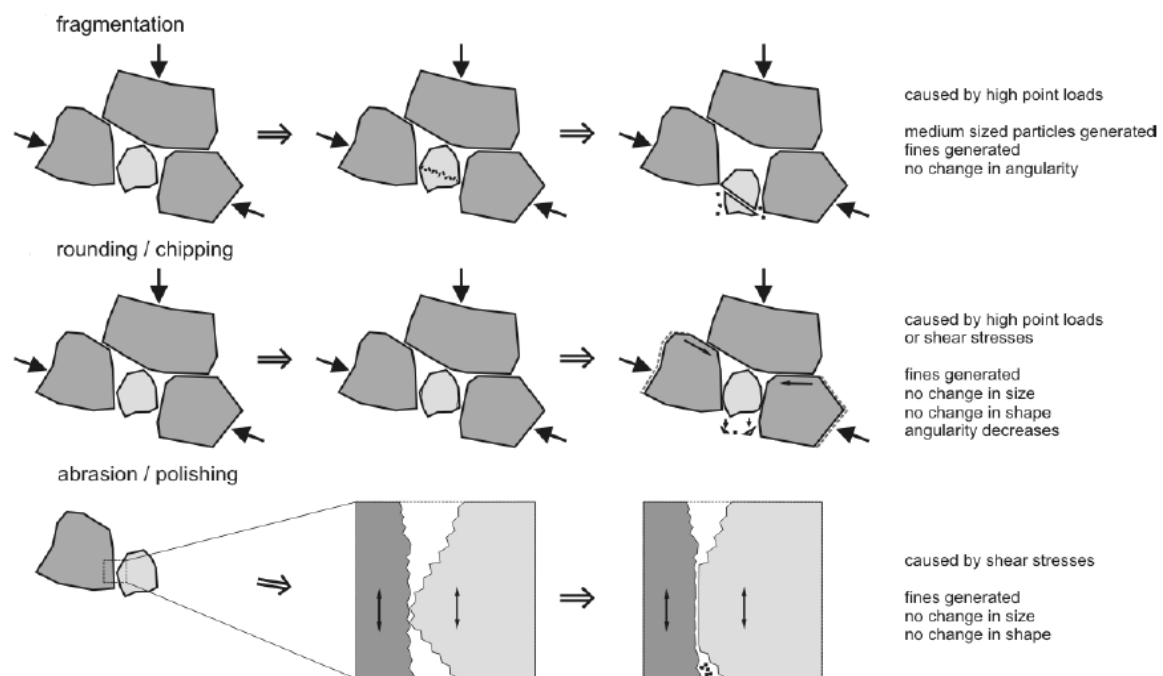


Figure 2: Attrition typology (Bach, 2013), schematic depiction of the process of fragmentation (first line), rounding/chipping (second line) and abrasion (third line).

2.5. Ballast fragmentation

Fragmentation describes the process of particle breakage which changes the grain size distribution of a sample. The original grain size distribution, as described in section 2.6, is changing. One larger particle is destroyed and results in smaller particles (Wieden, 1969).

The change in particle size during fragmentation processes can be seen in Figure 3. The figure displays the grain size distribution before and after the impact test.

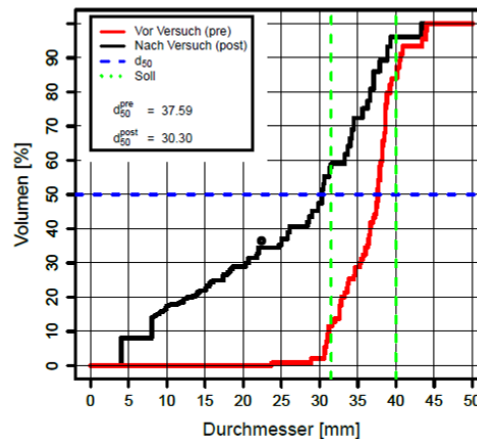


Figure 3: Example of grain size distribution before (red line) (particle size ranges between 31.5/40mm) and after (black line) (particle size ranges between 4/40mm) the impact test. The area between the lines indicates the degree of fragmentation.

The degree of fragmentation can be expressed by the value Z ("Zertrümmerungsgrad"). This value was established by the Swiss Federal Laboratories for Materials Science and Technology, EMPA (Wieden, 1969). It is defined as,

$$Z = 100 * \frac{F_v - F_n}{F_v} [\%]$$

where F_v is the grain fraction area before the test and F_n is the grain fraction area after the test. In Figure 4 the degree of fragmentation is expressed in a diagram.

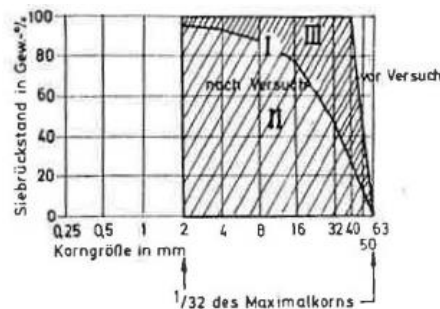


Figure 4: degree of fragmentation, I = F_v , II = F_n , III = I-II, established by EMPA (Wieden, 1969)

The fragmentation value is affected by the fragmentation taking place during the impact test and by abrasion, rounding and chipping between the particles (Wieden, 1969).

2.6. Ballast geometry

The ballast geometry is significant for the track bed properties. Grains must fulfill the functions mentioned in sections 2.1 and 2.2; otherwise, track instability occurs. Unfavorably shaped aggregates can lead to attrition phenomena such as fragmentation, chipping or abrasion (see section 2.4). This leads to shorter tamping intervals and therefore higher maintenance costs (Bach, 2013). Important factors which describe ballast geometry are particle shape, angularity and grain size.

Particle shape

Blott & Pye (2008) describe and summarize different methods of particle shape characterization and classification in their paper.

According to them, the most important properties relating to the form of a particle are the elongation ratio (ER) and the flatness ratio (FR). Therefore it is important to measure the length (L), breadth (I) and thickness (S) of a particle (Blott & Pye, 2008). These parameters can be related to each other in order to describe the elongation ratio and flatness ratio of an aggregate (Zingg, 1935).

$$ER = I/L$$

$$FR = S/I$$

Furthermore Zingg (1935) proposed a classification for shapes and established a terminology which separates the terms with a value of 0.67 to each other (see Figure 5).

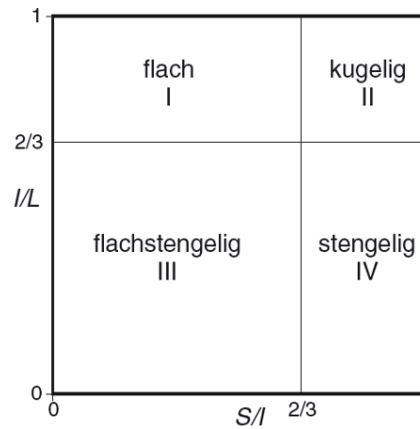


Figure 5: Classification of particle shapes (limiting value: 0.67), proposed by (Zingg, 1935), I = flat; II = cuboidal; III = flat and elongated; IV = elongated.

Angularity

As described above particle angularity is independent of the particle shape. Angularity or roundness of particles is linked to the sharpness of edges and corners on a sphere that can be seen in Figure 6 (Powers, 1953). Powers provides a roundness scale with 6 classes which can be seen in Figure 6 (top).

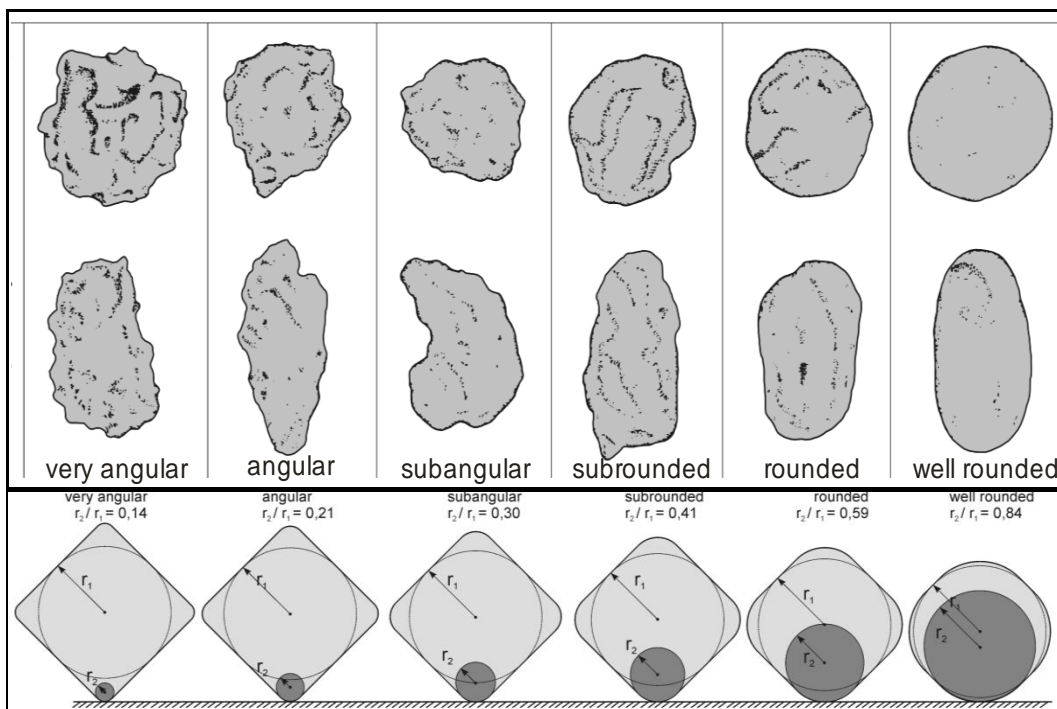


Figure 6: characteristic particles with high sphericity (top) and low sphericity (middle), roundness scale and classes (after Powers, 1953) (bottom).

The roundness scale after Powers (1953) describes the ratio between radii of the corners to the radius of the maximum inscribed circle (see Figure 6 bottom). The angularity can be described by models as seen in Figure 6 or with the help of computational laser techniques. The surface properties are described by laser triangulation. With the help of computer- and laser equipment, detailed 2D and 3D images of the particle can be created. Lee (Lee, Smith, & Smith, 2007) provides a newer model than Powers' scale. In his concept, an ellipsoid is used to determine the elongation and flatness ratio, but scaled down to 1/3 of the size. Edges and corners are that cannot be reached by the ellipsoid, set in relation to the particle volume, are called proportion of angles.

To combine the approach of Lee and Powers (2007) the term "proportion of angles" (PropA) in % is used below. The mean proportion of angles is called "Prop 50%". This term describes the volume loss of particles.

Grain Size distribution

As described in the European Standard EN 13450 the optimal grain size distribution for railway ballast lies in the range between 31.5 and 63mm. The grain size distribution is determined by square perforation sieves (Österreichische Bundesbahnen (ÖBB), 2007). Granulation between 31.5 and 63mm is called K1. K2 describes a granulation between 16 and 31.5mm (Österreichische Bundesbahnen (ÖBB), 2007). The granulation used for the impact test is 31.5/40mm. The selection of the correct granulation influences the results of the impact test. One can expect bigger particles to break into relatively large pieces than smaller particles after the fragmentation process. This is due to the higher compressive strength of large particles. For example, if one would choose a grain size distribution of 40/50mm for the impact test, there would also be a fragmentation of particles. But it could be possible that particles only break into two parts producing bigger particles. The degree of fragmentation would be smaller. Hence fewer particles would pass the 8mm sieve (see section 3).

3. Methodology

Austrian Railways uses various rock ballasts from different quarries in Austria; Bavaria and Bohemia (see section 2.3). The ballast that is tested in the laboratory is from a single-day's production (Bach, 2013). The quarries are delivering between 700kg and 1,000kg for the test series P2 ("Petroscope 2") in 2013. There was a first testing period P1 ("Petroscope 1") in 2012 (Bach & Hofer, 2013). Next to the Impact test, which is the focus of this work, the Los-Angeles and Deval test is carried out.

3.1. *Impact test*

Due to European Standard EN 1097-2 (Österreichisches Normungsinstitut, 2006) the impact test has been developed to quantify the resistance against fragmentation of rock ballast. The standard is used for naturally and artificially produced aggregates that are used in constructions. The impact test is an alternative testing procedure to the Los Angeles test. Aim of the test is to obtain the impact fragmentation coefficient SZ_{RB} . As described in EN 13450 (Österreichisches Normungsinstitut, 2004a) SZ_{RB} is calculated by the equation

$$SZ_{RB} = M/5$$

where M is the sum of screenings in percent and 5 is the number of sieves used. The impact strength value SZ_{RB} is limited to a maximum of 22M-% in Austria (Österreichische Bundesbahnen (ÖBB), 2007).

The impact fragmentation test is carried out as described in the European Standard EN 1097-2 and EN 13450. EN 13450 describes the "Aggregates for railway ballast" (Österreichisches Normungsinstitut, 2004a) and EN 1097-2 contains "Tests for mechanical and physical properties of aggregates – Part 2: methods for the determination of resistance to fragmentation" (Österreichisches Normungsinstitut, 2006).

Testing procedure

For one impact test $5000\text{g} \pm 50\text{g}$ of the aggregates are needed. The sample is placed inside the mortar. After entering the die into the mortar, a blow hammer falls onto the die 20 times. The weight of the fall hammer and die are 75 kg/100kg respectively and the fall height of the hammer is 0.50m. Inside the mortar the sample is crushed (see Figure 8). After the execution of the test, the sample is sieved and weighed with the sieve sizes 22.4/8/4mm. The weight that passes through the 8mm sieve is used to determine the fragmentation value.

The impact fragmentation value SZ_{TU} is calculated according to the equation:

$$SZ_{TU} = M_{<8\text{mm}} / M_{5000\text{g}}$$

$M_{<8\text{mm}}$ is the weight of the sample that passes the 8mm sieve after the impact test and $M_{5000\text{g}}$ is the weight of the whole sample before the test is executed.

The more resistant the rock is to impact stresses, the lower the SZ-value. After the execution of the test the number of particles in the sample has increased. In general, as described in the standard BH 700, rocks with a maximum impact fragmentation value of **22%** are used as track ballast (Österreichische Bundesbahnen (ÖBB), 2007; Österreichisches Normungsinstitut, 2004b).

After the performance of the test a strain analysis is carried out, by measuring the height of the sample in the mortar before and after execution of the drops. The test sample is adjusted arbitrarily in the mortar. Subsequently the height of the sample inside the mortar varies. With the measured height and the following equation the strain in the mortar can be calculated:

$$\varepsilon = \Delta h / h_1$$

ε = strain

Δh = difference in measured height before and after test

h_1 = initial height of sample in mortar

Strain in the mortar can occur through rearrangement of particles and rearrangement in combination with fragmentation. Fragmentation may occur without significant compaction. This is the case, if fragmentation does not lead to particle rearrangement.

Figure 7 shows a schematic picture of the device with which the impact test was carried out by the author (left side). The schematic figure illustrates the dimensions and elements of the machine. On the right side a photo of the device is shown.

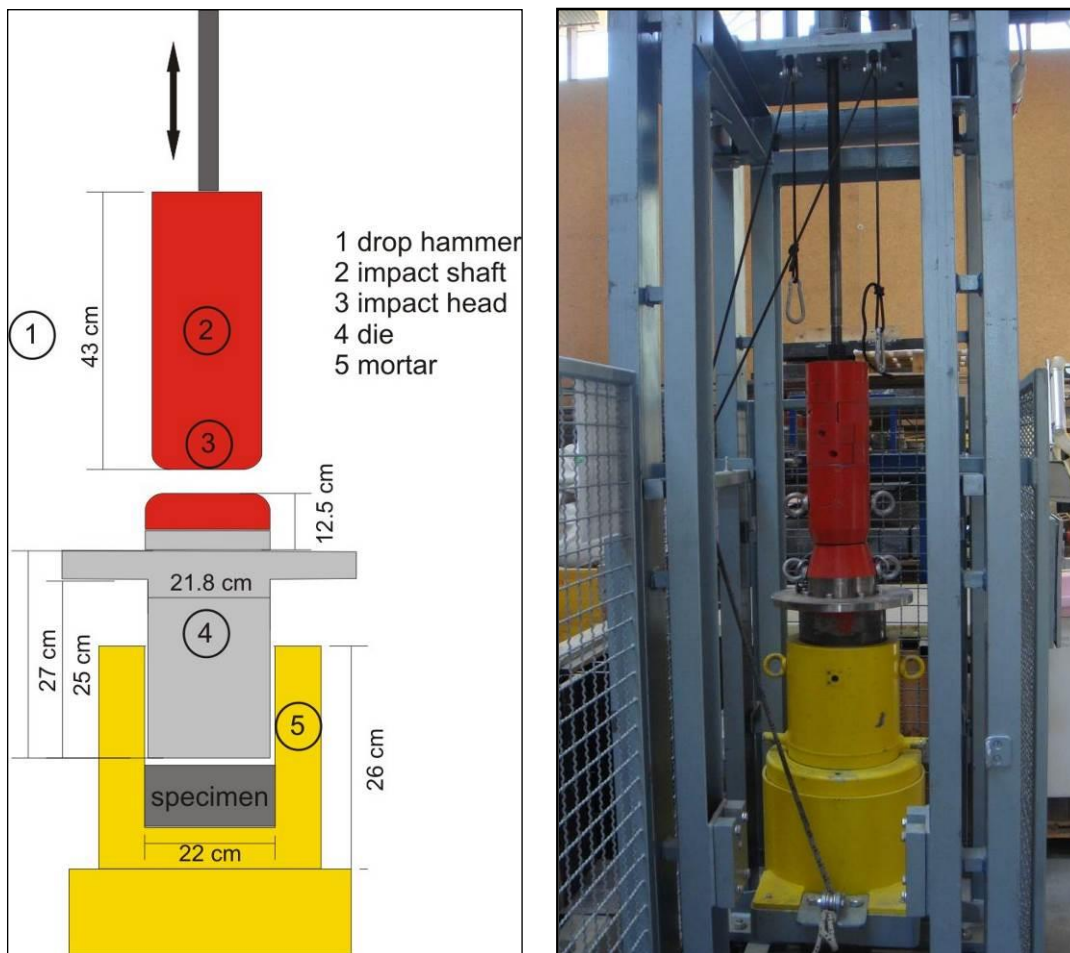


Figure 7: schematic illustration of the impact test device with its dimensions (left) and the device in the laboratory (right).



Figure 8: sample in mortar before (left) and after impact test (right), the sample is adjusted in the mortar by hand, before the test.

In this project, the device used for the test, was adapted. Several changes have been made to the original standard (see Table 2). The impact test device was built by HTL Saalfelden in cooperation with the company Oberhofer-Stahlbau. Some machine parameters do not comply to the standard EN 1097-2. This can be found in their paper “Mechanische Kriterien für Bahnschotter” (Breymann, Nindl, & Scharler, 2012). The same device is now used at the Technical University of Graz and more changes have been made in order to approach the standard EN 1097-2.

Table 2: Parameters of the Impact test, original European Standard values and the changes made to European Standard EN 1097-2, as performed at TUGraz.

		European Standard EN 1097-2 & EN13450	Variation TUGraz
drop hammer	kg	50	75
die	kg	50	100
blows	n	20	20
drop height	m	0.42	0.5
aperture of mortar	mm	170	220
weight of sample	kg	3	5
grain size	mm	31.5/40	31.5/40
<i>momentum</i>			
area	mm ²	22698	38013
velocity	m/s	2.871	3.132
momentum	kg*m/s	143.53	234.91
<i>estimation of filling degree</i>			
volume	m ³	0.00363	0.00608
density of sample	kg/m ³	1500	1500
volume of sample	m ³	0.002	0.00533

As these changes (Table 2) have been made the impact fragmentation value is called SZ_{TU} in this work.

The drop hammer weighs 75kg in this project (compared to 50kg in the European Standard). Weighing 100kg, the die has double the mass than originally described. The number of hammer blows remains the same (20 times), as well as the grain size. As the drop hammer has a higher weight the height has to be adapted too. The aperture of the mortar with a diameter of 220mm is larger than 170mm as described in the standards. To get the similar sample height in the mortar as in the original test, the mass of the sample is raised from 3 to 5kg. Due to the higher weight of die and hammer the velocity and momentum is greater. The changes made to the original standard lead to some problems as discussed in section 6.

As mentioned above, due to the higher weight of the drop hammer the momentum has been changed during testing. This influences the fragmentation and thus the results of the test. Regardless of the weight of the die, the momentum and fall height change throughout the impact test, because of the sample compaction. The alterations to the original standard also change the pressure in the mortar. A heavier die detains the stresses. The pressure that affects the aggregates is therefore lower than in the original test. Figure 9 shows the schematic pressure of the original test (1) and the estimated pressure in this project.

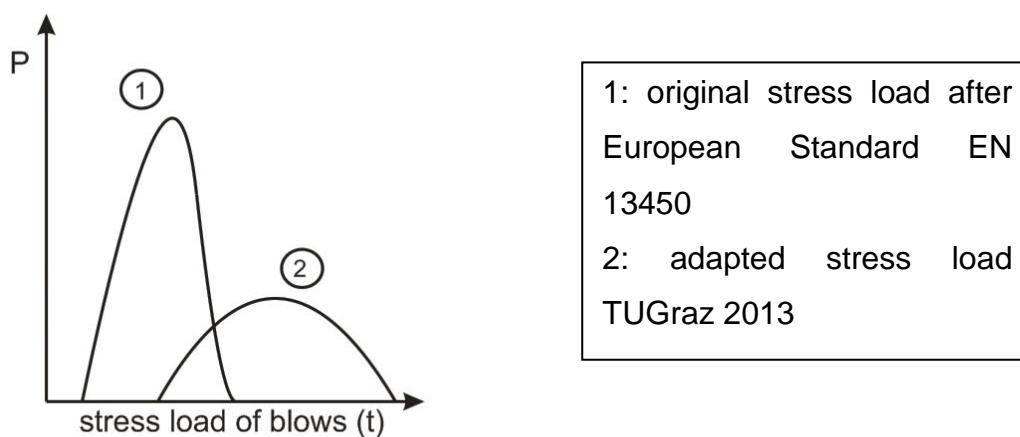


Figure 9: pressure in original test (1) after (Wieden, 1969) and stress load of test at TUGraz (2). The estimated pressure of the stress load in this project is smaller, because the heavier die detains the stresses in the mortar.

3.2. *Petroscope 4D*[®]

To analyze the rock ballast before and after the execution of the Los Angeles-, Deval- and Impact-tests, the device *Petroscope 4D*[®] is used. *Petroscope 4D*[®] was created and developed in the EUREKA projects: 2569 (EUREKA, 2001) and 3665 (EUREKA, 2005).

The device is utilized to analyze rock aggregate properties. *Petroscope 4D*[®] uses a combination of camera and laser equipment to analyze each particle of a rock sample. The parameters that are described with the help of the device are the size of the particle axes, sieve sizes, angularity, elongation ratio, flatness ratio, as well as the volume and sphericity of the particles (Daniel & Lowe, 2011). Next to the geometric properties the device detects spectra of the samples at wavelengths between 400 and 900nm (Hofer, Bach, Latal, & Neubauer, 2013).

As the minimum particle size for the *Petroscope 4D*[®] is 4mm, all particles that were crushed in the test to a smaller size are not included for the last analysis in the device. The device consists of the feeder, the spectrometer, and the scan part (see Figure 10). The feeder provides the spectrometer and the scan-part in moderate time intervals with an aggregate. Various rock types are detected by the spectrometer. In the scan-part, all particles run over a conveyer belt, and two cameras and one laser gather the information about the geometry of each particle.



Figure 10: overview of the device *Petroscope 4D*[®] (left) with the feeder, spectroscope and scan unit; inside the scan unit (right) with the conveyer belt, laser and cameras.

Figure 11 shows the immediate results of the Petroscope 4D[®] that are generated while the test is running. The form class, the angularity class, the grain size distribution, the displayed particle shape, the amount of aggregates, and the aggregate petrology are gathered by the device.

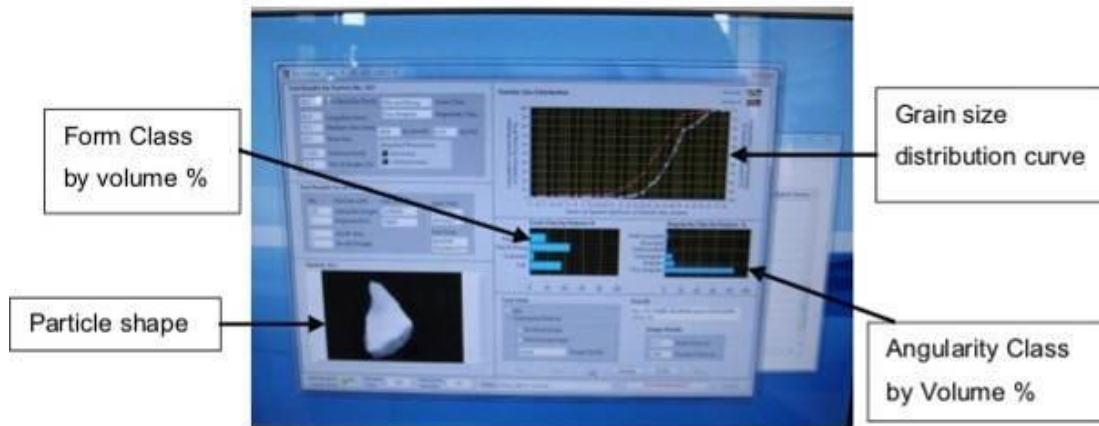


Figure 11: immediate displayed results of the Petroscope 4D[®]. The parameters (grain size distribution curve, form class, particle shape, and angularity class) can be checked during the testing process.

3.3. Concept of "P2" test series

Figure 12 gives an overview of the test series "Petroscope 2" (P2) in the laboratory. This section explains the whole testing procedure step by step.

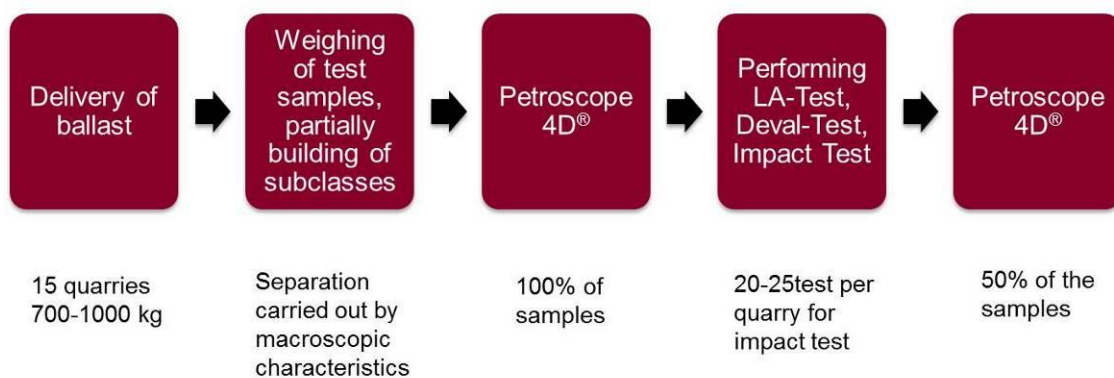


Figure 12: general concept of the test series "Petroscope 2" in 2013. The ballast is delivered from the suppliers, subclasses may be built and the samples are weighed in. Geometry and petrography are analyzed in Petroscope 4D[®], the test is performed and eventually the geometry is measured again in Petroscope 4D[®].

Charges of 700 to 1,000kg of railway ballast are delivered from different suppliers in Austria and Bohemia. The delivered charges contain rock ballast in the gradation according to BH 700 (Österreichische Bundesbahnen (ÖBB), 2007). For the different tests that are executed, different sieve sizes are required. Therefore the ballast has to be first sieved in a sieving machine. The sieves used are 31.5mm, 37.5mm, 40.0mm and 50.0mm. For the impact test the only relevant sieves and grain sizes are in the range between 31.5mm and 40.0mm. The test results given by Austrian Federal Railways are lacking in repeatability and are vary greatly from year to year (Bach, 2013). A possible reason may be the inhomogeneity of the material. Suppliers cannot guarantee ballast material that is completely uniform. In order to quantify the impact of inhomogeneity in terms of petrographic composition on the variation of test results, a separation of the material into subclasses is carried out for these charges in which it has seemed to be useful or successful. After washing the ballast, the aggregates are examined piece by piece for a separation. The subclass which represents the higher amount of particles is titled by the letter “A”. The rock aggregates that have the smaller amount get the letter “B”. “M” is the original – not separated fraction of the track ballast. The test series in 2012 “P1” has already led to several separations into subclasses (Bach, 2013). The test series of 2012 made material distinctions for rock types 03, 04 and 10. In the current test series these ballasts are separated in the same way without considering the amount. For this series 350 impact tests are considered by the author. 20 to 25 samples are tested per quarry. Following the adapted European standards, “Methods for the determination of resistance to fragmentation” EN 1097-2 and “Aggregates for railway ballast” EN 13450, every test sample has a weight of 5,000g ($\pm 50g = 1\%$). If a distinction into subclasses is made, 6 to 10 samples for each class are considered. This depends on the amount of the subclass (see Table 19). After weighing the samples, each one is analyzed in the Petroscope 4D[®] (see section 3.2). The next step is the impact test. The test is executed as described in section 3.1. After the impact test the samples are sieved again with smaller sieve sizes (4, 8 and 22.4mm). The mesh pluses of the sieves $> 4mm$, $>8mm$

and > 22.4mm are weighed. The grain sizes between 8/22.4mm and 22.4/40mm are kept for further analysis. The rest is no longer needed.

The last step after sieving the test samples is another analysis in the Petro-scope 4D[®] (50% of the samples could be analyzed in the device after the test). Most samples are constricted, for the sake of time. The results of the impact test and Petro-scope 4D[®] need to be analyzed. For a better analysis of the petrology, thin-sections and x-ray-analysis are produced for each rock ballast and its subclasses (see section 4).

Figure 13 shows an overview of the testing procedure of the impact test. It illustrates how the test was carried out in the laboratory and shows the most important parameters.

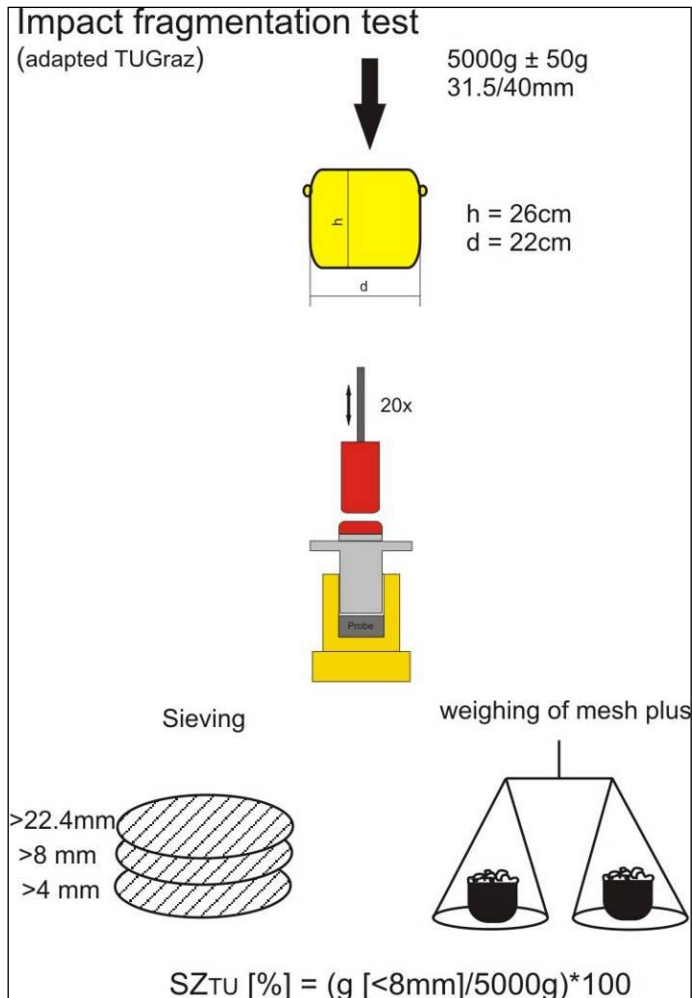


Figure 13: Impact test procedure, as adapted at TUGraz, dimensions of mortar, testing device, mesh sizes, weighing of mesh plus and equation to calculate the SZ_{TU} -value.

4. Rock type description

4.1. Criteria for subclasses

As mentioned in section 3.3, subclasses are built for heterogeneous material. For a distinction to be made, the samples have to differ by the macroscopic point of view. One of the following criteria leads to a separation of a material:

- Foliation: there are particles within one rock type that show a foliation and are separated due to this fact. This can be seen in rock type 03 and 06;
- Grain size: rock type 15 offers different grain sizes visible by macroscopic point of view and has led to a distinction in two subclasses. Subclass “A” has particles with grain size of 1-3mm and subclass “B” holds minerals that have a size of 5 to 15mm;
- Color: This criterion can differ within one shade of color (e.g. light to dark gray) or aggregates can have different colors (e.g. some particle are gray-red, others green-gray). Some particles even show variations of color in the same grain, for example the subclasses of rock type 04 are separated due to its color. Color can differ due to a higher amount of dark minerals;
- Different states of weathering: the material from different suppliers holds various states of weathering. Weathered aggregates can be detected in rock type 09 and 12;
- Absence or existence of quartz, feldspar or carbonate lenses, quartz, carbonates or feldspar veins (see Figure 14). These lenses and veins have a size of at least 3mm up to 5cm. This criterion is found in rock type 07, 08 (and 14).



Figure 14: Example for one of the separation criteria, Diabase “A” and “B” with and without quartz lenses/veins

If a distinction into subclasses takes place for one rock type, there are mainly three classes: Class “A” is the subclass which represents the most amount of the particular samples. Class “B” is the minor representation and class “M” is the original mixture of both “A” and “B”.

Subclasses are built for rock type 03, 04, 06, 07, 08, 09, 12, 14 and 15. An attempt is made to have the same amount of samples for each subclass. That is not always successful (see table 3). For some rock types the number of samples per subclass is very small (for example 08, 09 and 12).

4.2. *Thin section and X-ray analysis*

The first macroscopic rock description has taken place in the laboratory prior to the impact test. For a microscopic description, a thin section is produced out of one representative aggregate per rock type. The thin sections are analyzed with the microscope “Leica DMPLP” (enlargement factor of 5.0). The total mineral content is determined by means of qualitative and semi-quantitative determination. For this purpose a small amount of each sample is ground to x-ray fineness and pressed into a sample carrier. The samples are measured with the x-ray diffractometer Panalytical XPert Pro (Co-tube) in the range of 4° to $85^{\circ} 2\theta$. The phase analysis of the sample is performed with the program High Score Plus (using database PDF2 – ICDD). Afterwards, the semi-quantitative determination of mineral amounts is carried out by comparing characteristic x-ray peak intensities with calibration curves of minerals with an average chemical composition. For minerals that have a great chemically variability, such as garnet, amphibole or feldspar, there can be larger inaccuracies in the calculation of amounts.

Table 3 lists all tested rock types with the most prominent features, their subclasses and the amount of the subclasses. The author has estimated the amount of subclasses during the process of separation and has calculated it based on the number of samples per subclass.

Table 3: provides an overview of the tested rocks that are used as railway ballast in Austria. Subclass, amount of subclass, color and fabric are given for all rock types.

Name	Rock type	Sub-class	Amount [%]	Color	Fabric & texture
01	Granite	-	100	light to dark gray, white	macrocrystalline, non-orientated
02	Basalt	-	100	gray, red, greenish	microcrystalline, non-orientated
03 *	Granite porphyr	(M)	100	gray, red, green	porphyric structure
	Granite porphyr	(A)	50	dark gray, red	foliation, microcrystalline
	Granite porphyr	(B)	50	dark gray, green	non-orientated
04 *	Dunite	(M)	100	gray, green, brown	orientated and non-orientated
	Dunite	(A)	30	greenish-gray	non-orientated, microcrystalline
	Dunite	(B)	70	brown-gray	macrocrystalline, orientated
05	Diabase	-	100	green to gray and red	microcrystalline, brecciated
06 **	Granulite	(M)	100	light to dark gray, yellow	foliation, microcrystalline
	Granulite	(A)	80	light gray to yellow, white	small garnets, biotite veins
	Granulite	(B)	20	gray to dark gray	more dark minerals
07 **	Diabase	(M)	100	gray, blue, greenish	microcrystalline, non-orientated
	Diabase	(A)	75	gray, blue, greenish	microcrystalline, non-orientated
	Diabase	(B)	25	gray, blue, greenish, white	microcrystalline, non-orientated
08 **	Diabase	(M)	100	green, gray, brown	microcrystalline, non-orientated
	Diabase	(A)	80	green, gray, brown	microcrystalline, non-orientated
	Diabase	(B)	20	green, gray, brown, white	microcrystalline, non-orientated



09 **	Granite	(M)	100	gray, pink, brown	macrocrystalline, non-orientated
	Granite	(A) = (M)	97.5	brown	macrocrystalline, highly weathered
	Granite	(B)	2.5	gray, brown	microcrystalline, highly weathered
10	Granulite	-	100	light gray, brown	macrocrystalline, foliation
	Granulite	(A)	-	-	-
	Granulite	(B)	2.5	white	macrocrystalline
11	Dolomite	-	100	gray to rose- gray, ivory	splintering surface, brecciated
12 **	Granite	(M)	100	brown, gray	macrocrystalline, non-orientated
	Granite	(A)	90	=(M)	=(M)
	Granite	(B)	10	brown	highly weathered
13	Granite	-	100	Light gray	homogenous, macrocrystalline, non-orientated
14	Diabase	-	100	= 08	= 08
15 **	Granite	(M)	100	light to dark gray	non-orientated, macrocrystalline
	Granite	(A)	60	gold-brown	fine grained or microcrystalline
	Granite	(B)	40	green-brown	macrocrystalline

* same subclasses as in 2012 (Bach, 2013)

** subclasses generated in this thesis


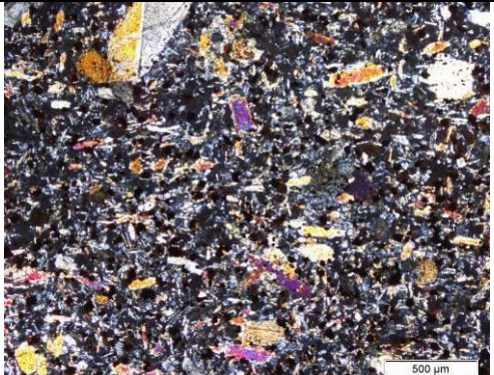
The thin sections are examined with the help of literature by (Nesse, 2012), (Pape, 1972) and (Moorhouse, 1959). In tables 4 to 18, the rock ballast in the test series of 2013 is described. The tables feature the rock type, a macroscopic and microscopic description, photographs of aggregates and thin sections (thin section photographs are taken with crossed polarizer), as well as the minerals (+ amount) that are found within the rock ballast. If a distinction in subclasses was carried out the table also includes these differences. Following these tables, there is a short description of the thin section.

Table 4: shows the macroscopic and microscopic description of 01 Granite. It also lists the mineralogical composition. This igneous rock type is homogenous, as a result no subclasses have been identified.

Sample name	01	
Rock type	Granite	
mineralogical composition	quartz, feldspar, micas	
Macroscopic description		
color	light to dark gray	
fabric/texture	non-orientated, macrocrystalline	
Microscopic description		
grain shape	hypidiomorph, holocrystalline minerals	
grain size	medium grained, 0.5 -3mm	
texture	granular, massive, non-orientated	
special feature	small joints	
additions	intrusive origin	
Mineralogical composition		% (based on x-ray diffractometer)
Plagioclase		18
Alkali feldspar		16
Quartz		40
Muscovite		10
Biotite		16
		

The thin section of 01 granite displays clear grain boundaries between the minerals. The size of the crystals varies; larger feldspars are set amongst smaller quartz crystals. Quartz is typically white-gray and shows undulatory extinction. Plagioclase features the characteristic twins and alkali feldspar holds its specific grid. The muscovite is colorless (uncrossed polarizer) and shows a very good cleavage. Biotite has a high relief and is easily detectable due to its significant brown color.

Table 5: shows the macroscopic and microscopic description of 02 Basalt. It also lists the mineralogical composition. This magmatic rock type is homogenous from the macroscopic view; as a result no subclasses have been identified.

Sample name	02	
Rock type	Basalt	
mineralogical composition	pyroxene, foids, magnetite, amorphous components	
Macroscopic description		
color	gray-greenish, reddish	
fabric/texture	non-orientated, microcrystalline, porous	
Microscopic description		
grain shape	hemocrystalline porphyric	
grain size	very fine groundmass (<0.5mm) that is classy and crystalline with larger phenocrysts (1-2mm)	
texture	porphyric	
special feature	phenocrysts are mainly leucite, nephelin, magnetite	
additions	extrusive origin, amorphous quartz, oxides	
Mineralogical composition		% (based on x-ray diffractometer)
Diopside		detected
Sodalite		detected
Augite		detected
Magnetite		detected
Nephelin		detected
Leucite		detected
Olivine		detected
		

The texture of this thin section is porphyric. Many phenocrysts of different sizes can be found in a very fine groundmass that mainly consists of foids, augite, sodalite and amorphous components. The phenocrysts are mainly leucite, nephelin, augite and olivine. The crystals are idiomorph.

Table 6: shows the macroscopic and microscopic description of 03 Granite porphy. It also lists the mineralogical composition. This magmatic rock type was separated into subclasses due to macroscopic differences.


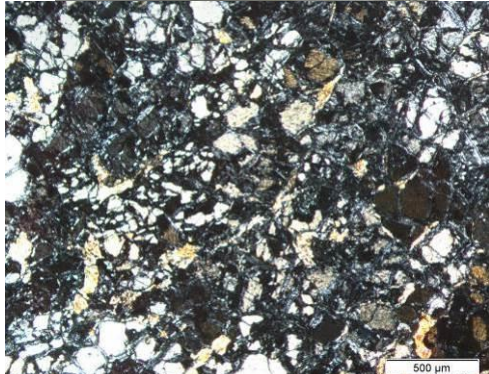
Sample name	03	
Rock type	Granite porphyr	
min. composition	quartz, feldspar, micas (\pm chlorite, garnet, sillimanite)	
Building of subclasses	M, A, B, building due to color and structure \rightarrow in thin sections there is a difference in grain size	
Additions	building of subclasses as in 2012; intrusive origin	
Macroscopic description		
	A	B
color	dark gray, red, white	gray to dark gray, green
fabric/texture	foliation, macrocrystalline, veins	no preferred foliation, microcrystalline
Microscopic description		
grain shape	hypidiomorph	fibrous + idiomorph
grain size	medium grained (0.5-5mm)	very fine grained (<0.5mm)
texture	holocrystalline, porphyric	porphyric
special feature	microcracks, biotite veins	microcracks
Mineralogical composition	% (based on x-ray diffractometer)	% (based on x-ray diffractometer)
Quartz	20	30
Alkali feldspar	10	7
Plagioclase	14	10
Biotite	33	22
Chlorite	10	-
Garnet	-	17
Hornblende	13	14


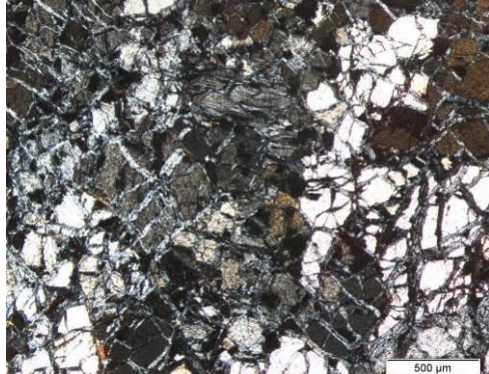
The thin section of 03(A) displays clear grain boundaries between the minerals. The size of the crystals varies. In general, feldspars are larger than quartz crystals. Biotite has a high relief and is easily visible due to its significant brown color. Chlorite is also found in this section with a brown-green color and also shows a high relief. Thin section (B) completely differs from section (A). This section is divided into two parts. On one side, there is typical granulated rock texture as in section (A). This part stands out because it has smaller grain sizes and bears garnets. On the other side of the section, there are no clear boundaries between crystals. These crystals are very small and merge into each other. The structure of this part is porphyric, some larger minerals (phenocrysts) can be found between very small ones (<0.2mm).

Table 7: shows the macroscopic and microscopic description of 04 Dunite. It also lists the mineralogical composition. This magmatic rock type was separated into subclasses due to macroscopic differences.

Sample name	04	
Rock type	Dunite	
mineralogical composition	olivine, amphibole, feldspar, serpentine, (\pm talc)	
Building of subclasses	M, A, B, building due to color and slight foliation in (B) \rightarrow thin sections do not show large differences	
Additions	building of subclasses as in 2012, in 2013 there are less of the (A)-samples (~30%); intrusive origin	
Macroscopic description		
	A	B
color	greenish – gray	brown-gray
fabric/texture	no foliation, microcrystalline	slightly preferred orientation, macrocrystalline
Microscopic description		
grain shape	holocrystalline, granulous	Holocrystalline, granulous
grain size	fine to medium grained (<0.5 – 1mm)	medium grained (0.5 – 2mm)
texture	porphyric, serpentized	Porphyric, strong serpentization
special feature	-	-

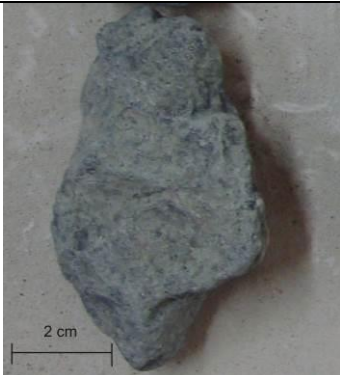
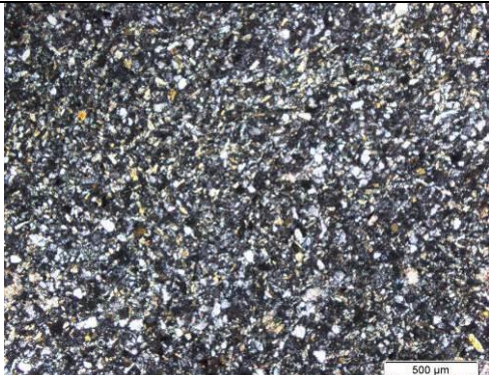
Mineralogical composition	% (based on x-ray diffractometer)	% (based on x-ray diffractometer)
Olivine	detected	detected
Amphibole	detected	detected
Serpentine	detected	detected
Talc	detected	-

The minerals of both thin sections (A) and (B) are clearly traversed by serpentinization. This makes it difficult to distinguish grain shape and size. Thin section (A) shows smaller minerals (<math><0.5 - 1\text{mm}</math>) more clearly than in section (B) (0.5 – 2mm). Olivine, which is the main feature of Dunite, is the colorless mineral in the thin section and appears to be hexagonal or octahedral. Thin section (A) features less brown amphibole than section (B). Except for the slightly different amount of amphibole, the thin sections do not differ in mineralogical composition.

Table 8: shows the macroscopic and microscopic description of 05 Diabase. It also lists the main mineralogical composition. This metamorphic rock type is relatively homogeneous from the macroscopic view; as a result no subclasses were identified.

Sample name	05	
Rock type	Diabase	
mineralogical composition	feldspar, amphiboles, quartz, pyroxene, chlorite	
Macroscopic description		
Color	green - gray, red	
fabric/texture	microcrystalline, brecciated	
Microscopic description		
Grain shape	fine grained, granulous	
Grain size	minerals are very small, very fine grained (<0.2mm)	
texture	isogranular to heterogranular, granoblastic	
Special features	small microcracks	
Additions	-	
Mineralogical composition		% (based on x-ray diffractometer)
Plagioclase		22
Chlorite		17
Quartz		14
Hornblende		46
Clinopyroxene		1
		

A very fine grain matrix can be seen in this thin section (crystals are smaller than <0.2mm). The size of the minerals is uniform. The minerals are so small that it is difficult to distinguish the optical properties of the minerals, which are in this case granoblastic. The most abundant mineral in this diabase is hornblende. This mineral gives the rock its green color. Next to the minerals, some small microcracks are visible.

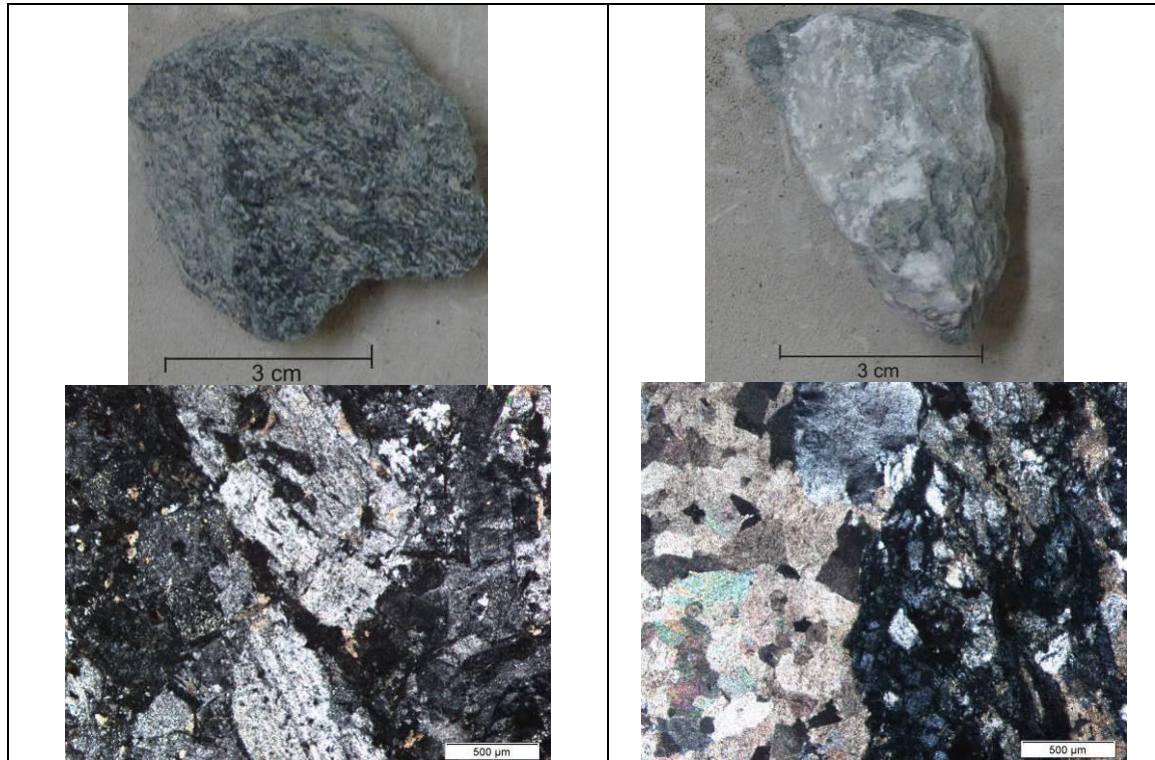
Table 9: shows the macroscopic and microscopic description of 06 Granulite. It also lists the main mineralogical composition. This metamorphic rock type was separated into subclasses due to macroscopic differences.

Sample name	06	
Rock type	Granulite	
min. comp.	quartz, feldspar, biotite, chlorite, garnet	
Building of subclasses	M, A, B, building due to color and amount of dark minerals → both aspects are difficult to prove in thin sections	
Additions	no subclasses in test series 2012	
Macroscopic description		
	A	B
color	light gray to yellow, white	light to dark gray
fabric/texture	foliation, microcrystalline	foliation, microcrystalline
Microscopic description		
grain shape	xenomorph	xenomorph
grain size	fine grained with larger garnets (0.5-3mm)	fine grained with larger garnets (0.5-3mm)
texture	Heterogranular, granoblastic	Heterogranular, granoblastic
special features	some minerals are slightly weathered	some minerals are slightly weathered
Mineralogical composition	% (based on x-ray diffractometer)	% (based on x-ray diffractometer)
Plagioclase	20	15
Alkali feldspar	25	24
Quartz	34	41
Biotite	8	8
Garnet	11	10
Chlorite	2	2

The most abundant minerals in the thin sections of 06(A) and (B) are quartz and feldspars. Both quartz and feldspar have about the same grain size (heterogranular) and one can see clear grain boundaries. Quartz differs from feldspar because it has no twinning and shows no cleavage. Small biotite veins run through thin section (A). (A) shows garnets with a high relief that are larger than quartz or feldspar crystals. Thin section (B) shows smaller garnets and less biotite veins than (A). This is in clear contradiction to the macroscopic description. The macroscopic distinction in subclasses is based on the color and the assumption that there are more dark minerals in subclass (B). Thin section (B) disprove this theory. On the contrary thin section (B) contains more quartz (see XRD results in Table 9), which is a light colored mineral.

Table 10: shows the macroscopic and microscopic description of 07 Diabase. It also lists the main mineralogical composition. This metamorphic rock type was separated into subclasses due to macroscopic differences.

Sample name	07	
Rock type	Diabase	
min. composition	feldspars, chlorite, quartz, carbonates, amphibole, biotite	
Building of subclasses	M, A, B, building due to existence of carbonate veins and lenses → this can be proved in the thin sections, dolomite/calcite veins are found in section (B)	
Additions	no subclasses in test series 2012	
Macroscopic description		
	A	B
color	gray-blue, greenish	gray-blue, greenish, white
fabric/texture	microcrystalline, non-orientated	microcrystalline, non-orientated
Microscopic description		
grain shape	skeletal	skeletal and xenomorph
grain size	medium grained (0.5-3mm)	medium grained (0.5-2mm)
texture	heterogranular, intersection structure, granoblastic	heterogranular, granoblastic with overlapping dolomite
special features	voids (porosity), microcracks filled with calcite, partly weathered	+ carbonate veins (3mm to 5cm)
Mineralogical composition	% (based on x-ray diffractometer)	% (based on x-ray diffractometer)
Plagioclase	21	18
Alkali feldspar	21	21
Quartz	14	10
Chlorite	18	19
Calcite	12	4
Muscovite	4	5
Dolomite	10	23




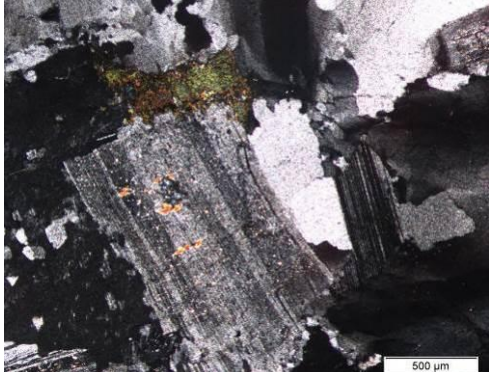
Thin section 07(A) shows granoblastic minerals that intersect with each other and build a skeletal texture. Quartz, feldspar and carbonates are the most prominent crystals in the section. Chlorite is difficult to detect here, as its color is gray to blue. Carbonates shine through feldspar and quartz crystals. Thin section (B) shows, next to quartz and feldspar minerals, clearly visible dolomite and calcite veins running through the section. The veins are easily visible (macroscopic and under the microscope) and are the main characteristic feature for a distinction into subclasses. Chlorite is easier to recognize in this section due to its green to blue color. Muscovite is detectable in the x-ray results. However, it is difficult to find it in both thin sections.

Table 11: shows the macroscopic and microscopic description of 08 Diabase. It also lists the main mineralogical composition. This metamorphic rock type was separated into subclasses due to macroscopic differences.

Sample name	08	
Rock type	Diabase	
min. composition	quartz, feldspar, micas, carbonate, chlorite, amphibole	
Building of subclasses	M, A, B, building due to existence of quartz veins and lenses → this can be proved in the thin sections, quartz veins and lenses are found in thin section (B)	
Additions	08 = 14	
Macroscopic description		
	A	B
color	green-gray, brown	green-gray, brown
fabric/texture	microcrystalline, laminated	microcrystalline, laminated
Microscopic description		
grain shape	xenomorph	planar, xenomorph
grain size	fine grained (~0.5mm)	fine grained (~0.5mm)
texture	heterogranular, lepidoblastic	heterogranular, lepidoblastic
special features	ores	ores; quartz veins
Mineralogical composition	% (based on x-ray diffractometer)	% (based on x-ray diffractometer)
Plagioclase	30	24
Quartz	21	32
Chlorite	15	10
Biotite	10	8
Micas	8 (Muscovite, Margarite)	8
Calcite	3	2
Hornblende	13	16
Ores, pyroxene	detected (magnetite, rutile)	detected


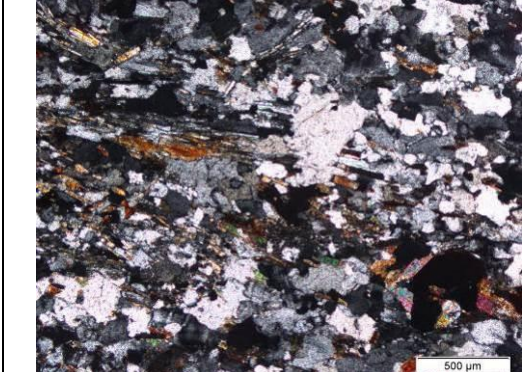
Feldspar and quartz are the most abundant minerals in this rock type. Grains in both sections feature heteroblastic minerals. Both thin sections show plagioclase with typical twins and some quartz crystals with the characteristic undulatory extinction. Micas are also found in both sections. Biotite, muscovite and margarite can be found in both thin sections. Brown hornblende is also existent in both thin sections. It is smaller than the other minerals and seems to intersect with the other minerals. In thin section (B) quartz veins can be found that run through the thin section. The veins are clearly visible and are the main characteristic feature for a differentiation into subclasses. In both sections, black dots are detectable that are ores (rutile and magnetite), however it is more apparent in section (A). A very small amount of pyroxene was also found in the x-ray analysis.

Table 12: shows the macroscopic and microscopic description of 09 Granite. It also lists the main mineralogical composition. For this magmatic rock type one sample per subclass was built. The differences from the main properties are described in Table 3.

Sample name	09	
Rock type	Granite	
mineralogical composition	quartz, feldspar, biotite, garnet , chlorite	
Macroscopic description		
color	gray, pink, brown	
fabric/texture	macrocrystalline, mineral sizes of several mm	
Microscopic description		
grain shape	holocrystalline, hypidiomorph	
grain size	medium grained (0.5-3mm)	
texture	granular, volume ratio is massive and non-orientated	
special features	microcracks	
additions	1 sample per subclass: A=M; B is a highly weathered sample of this granite, no thin section or x-ray analysis, because of the very small amount; intrusive origin	
Mineralogical composition		% (based on x-ray diffractometer)
Plagioclase		23
Alkali feldspar		20
Quartz		39
Biotite		9
Chlorite		2
Garnets (Pyrope)		7
		


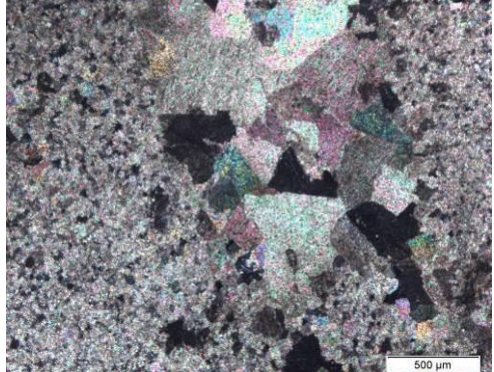
The thin section of 09 granite shows clear grain boundaries between the minerals. The size of the feldspar and quartz crystals does not vary. Quartz shows typical undulatory extinction. Plagioclase features the characteristic twins and alkali feldspar holds its specific grid. Biotite shows a high relief and is easily detectable due to its significant brown color. The color of biotite also appears in green color. Garnets are small. Small microcracks run through the thin section.

Table 13: shows the macroscopic and microscopic description of 10 Granulite. It also lists the main mineralogical composition. For this metamorphic rock type one sample per subclass B was built. The difference from the main properties is described in Table 3.

Sample name	10
Rock type	Granulite
mineralogical composition	feldspar, quartz, micas, garnets, sillimanite
Macroscopic description	
color	light to dark gray, brown
fabric/texture	slight foliation, macroscopic
Microscopic description	
grain shape	xenomorph, fibrous
grain size	fine grained (<0.5mm) with larger minerals (0.5-2mm)
texture	porphyroblastic
special features	sillimanite fibers
additions	1 sample for subclass B, it is a very light, white material, that has stood out between the brown one, no thin section or x-ray analysis, because of the very small amount
Mineralogical composition	
	% (based on x-ray diffractometer)
Plagioclase	15
Alkali feldspar	14
Quartz	54
Biotite	10
Garnet	9
Sillimanite	detected
	

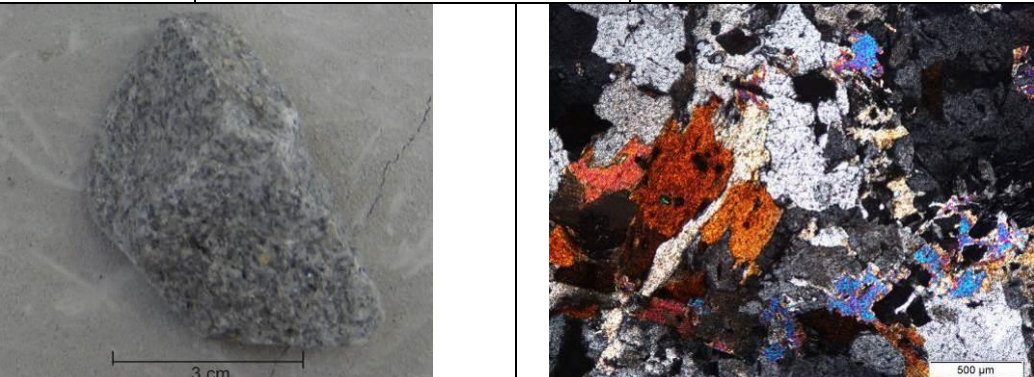
This granulite thin section mainly consists of quartz, feldspar and biotite. Garnet can be found which is mostly surrounded by biotite. The grains are heteroblastic minerals and the most prominent feature are the sillimanite fibers that draw through the thin section. Sillimanite is a fibrous, colorless mineral with perfect cleavage.

Table 14: shows the macroscopic and microscopic description of 11 Dolomite. It also lists the main mineralogical composition. This sediment is homogenous; as a result no subclasses were identified.

Sample name	11	
Rock type	Dolomite	
mineralogical composition	dolomite, calcites	
Macroscopic description		
color	gray to rose-gray, ivory	
fabric/texture	brecciated structure, splintering surface	
Microscopic description		
frame	crystalline	
grain size	very fine grained (<0.2mm)	
fabric	compact, no grains	
special features	calcite veins cross matrix	
additions	-	
Mineralogical composition		% (based on x-ray diffractometer)
Dolomite		85
Calcite		15
		

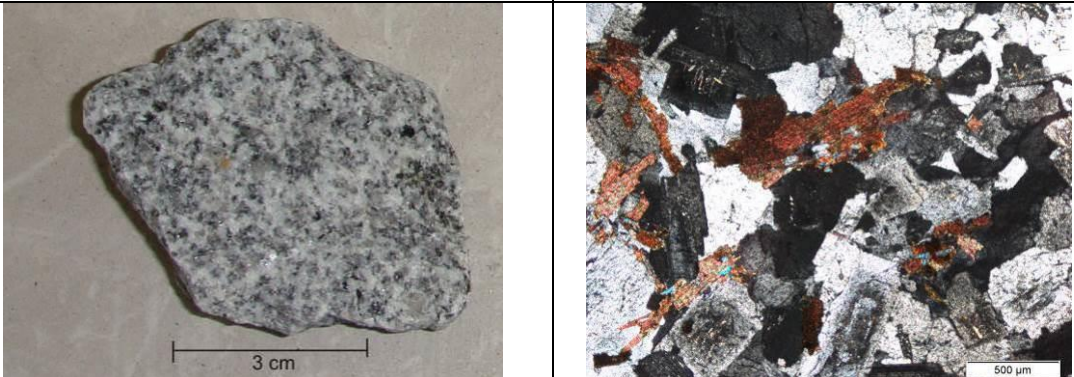
The dolomite in this thin section shows a very fine grained matrix consisting of only dolomite and calcite. Its fabric is compact and the frame is crystalline. Calcite veins with larger minerals (0.2-0.5mm) run through the thin section. The color of dolomite crystals varies between gray and pink. The mineral dolomite is a rhombohedral crystal with high birefringence. Calcite minerals are not easily distinguishable from dolomite minerals in thin sections. Dolomite does not contain organisms.

Table 15: shows the macroscopic and microscopic description of 12 Granite. It also lists the main mineralogical composition. For this magmatic rock type two subclasses were built. The differences from the main properties are described in table 3.

Sample name	12	
Rock type	Granite	
min. composition	feldspar, quartz, micas, clay	
Building of subclasses	M, A (=M), B → highly weathered M, building due to highly weathered material	
Additions	no thin section and x-ray of B; intrusive origin	
Macroscopic description		
	A	B
color	gray	brown
fabric/texture	macrocrystalline, non-orientated	macrocrystalline, non-orientated
Microscopic description		
grain shape	hypidiomorph, holocrystalline	-
grain size	medium grained (0.5-2mm)	-
texture	massif, granular	-
Mineralogical composition	% (based on x-ray diffractometer)	% (based on x-ray diffractometer)
Quartz	46	-
Plagioclase	20	-
Alkali feldspar	15	-
Muscovite	6	-
Biotite	10	-
Chlorite	3	-
		


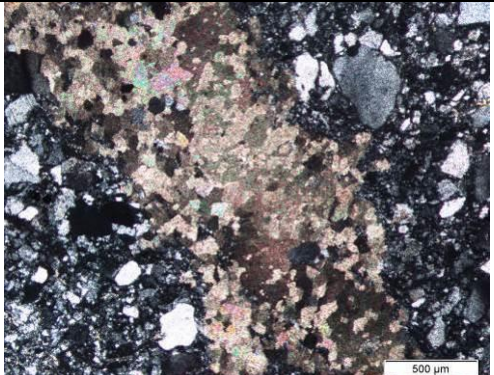
This granite displays clear grain boundaries and the size of the crystals varies as larger feldspars are set amongst smaller quartz crystals. Biotite, muscovite and chlorite show a high relief and protrude out of quartz and feldspar minerals. Plagioclase features the characteristic twins and alkali feldspar holds its specific grid. Quartz is recognizable due to its white-gray color and absence of cleavage. Mica minerals have their typically good cleavage. Chlorite and biotite cannot be differentiated easily in this section as the thin section is a little bit too thick (blue minerals).

Table 16: shows the macroscopic and microscopic description of 13 Granite. It also lists the main mineralogical composition. This magmatic rock type is relatively homogenous; as a result no subclasses were identified.

Sample name	13	
Rock type	Granite	
mineralogical composition	feldspar, quartz, micas	
Macroscopic description		
color	light gray	
fabric/texture	macroscopic, homogenous, non-orientated	
Microscopic description		
grain shape	hypidiomorph	
grain size	medium grained (0.5-3mm)	
texture	granular, holocrystalline, massif	
special features	-	
additions	intrusive origin	
Mineralogical composition	% (based on x-ray diffractometer)	
Quartz	37	
Plagioclase	22	
Alkali feldspar	22	
Biotite	8	
Muscovite	10	
Chlorite	1	
		

The thin section of 13 granite displays clear grain boundaries between the minerals. Quartz and feldspar crystals have almost the same sizes. Biotite is easily detectable under the microscope as it has a high relief and features the typical brown color. Muscovite and chlorite are found in the x-ray-analysis but cannot be seen in the thin section.

Table 17: shows the macroscopic and microscopic description of 14 Diabase. It also lists the main mineralogical composition. This metamorphic rock type is relatively homogeneous, as a result no subclasses were identified.

Sample name	14	
Rock type	Diabase	
Macroscopic description		
color	= 08, broken down in different crushers	
fabric/texture		
Microscopic description		
grain shape	xenomorph	
grain size	fine grained (~0.3mm)	
texture	heterogranular	
special features	microcracks filled with calcite	
additions	same subclasses as in 08 (=14)	
Mineralogical composition		% (based on x-ray diffractometer)
Quartz		35
Plagioclase		23
Calcite		23
Hornblende		10
Chlorite		8
Pyroxene		1
Ores (hematite, rutile)		detected
		

The thin section and XRD-analysis for rock type 14 has been performed to compare the results with rock type 08. This thin section can be especially compared to rock type 08(B), but instead of quartz veins, as seen in 08(B), carbonate veins run through this section. Feldspar and quartz are the most abundant minerals in this rock type. Grains in both sections feature heteroblastic minerals. Instead of biotite as in thin sections 08(A) + (B), chlorite is found here. Hornblende, ores, and a very small amount of pyroxene can also be detected (as seen in 08).

Table 18: shows the macroscopic and microscopic description of 15 Granite. It also lists the main mineralogical composition. This magmatic rock type was separated into subclasses due to macroscopic differences.

Sample name	15	
Rock type	Granite	
min. composition	feldspar, quartz, mica, amphibole (\pm chlorite)	
Building of subclasses	M, A, B, building due to different grain size \rightarrow clearly visible in thin sections	
Additions	intrusive origin	
Macroscopic description		
	A	B
color	brown, green	dark gray
fabric/texture	very fine grained , microcrystalline	macrocrystalline
Microscopic description		
grain shape	hypidiomorph, holocrystalline	hypidiomorph, holocrystalline
grain size	fine grained (<0.5mm)	medium grained (0.5-5mm)
texture	granular	granular
special features	microcracks	microcracks
Mineralogical composition	% (based on x-ray diffractometer)	% (based on x-ray diffractometer)
Quartz	42	25
Plagioclase	15	24
Alkali feldspar	13	14
Biotite	20	20
Chlorite	1	-
Amphibole	9	17

Both thin sections show granite with its typical minerals: feldspar, quartz and micas. The main difference between subclass (A) and (B) is the grain size. Although thin section (A) has the same mineralogical composition as in section (B) it has different grain sizes. (A) features very small crystals with a size <0.5mm. In section (B), the minerals have a size between 0.5-5mm. Biotite is particularly striking in these sections (amount: 20% and typical brown color dominate the thin section). A small amount of chlorite can be detected in (A) and amphibole is found in subclasses (A) and (B).

Difference between granites 01, 09, 12, 13 and 15

The various granites are quite uniform. They differ mostly in color and grain size. Their main mineral components are quartz, feldspars, micas (\pm chlorite, and \pm garnet). Rock types 01, 12, 13, and 15 show the same color of gray. 09 granite appears pinker due to a higher amount of orthoclase (alkali feldspar). The grain sizes of the individual granites differ between several μm (100-900 μm) and several mm (up to 5mm in 09 granite).

Difference between diabases 05, 07, 08 and 14

All diabase rocks in this project are very fine grained (except 07 = medium grained), dense material that has a green to blue color. Most abundant minerals are plagioclase, quartz, chlorite and hornblende. In rock type 05, a very small amount of sillimanite is detected. Rock type 07 also holds micas and dolomite. In 08 and 14 a certain amount of carbonate, calcite, and ores are detectable. 07 and 08 (=14) are separated into subclasses due to the same macroscopic feature (quartz, calcite, dolomite veins and lenses).

Difference between granulites 06 and 10

Granulites 06 and 10 consist of feldspars, quartz and garnet. In 06 granulite, biotite and chlorite are found. These two minerals cannot be detected in 10 granulite, in which a relatively high amount of sillimanite exists. A foliation is more prominent in 06. Two subclasses were built here due to its color. Rock type 10 is relatively uniform and there are only small color variations.

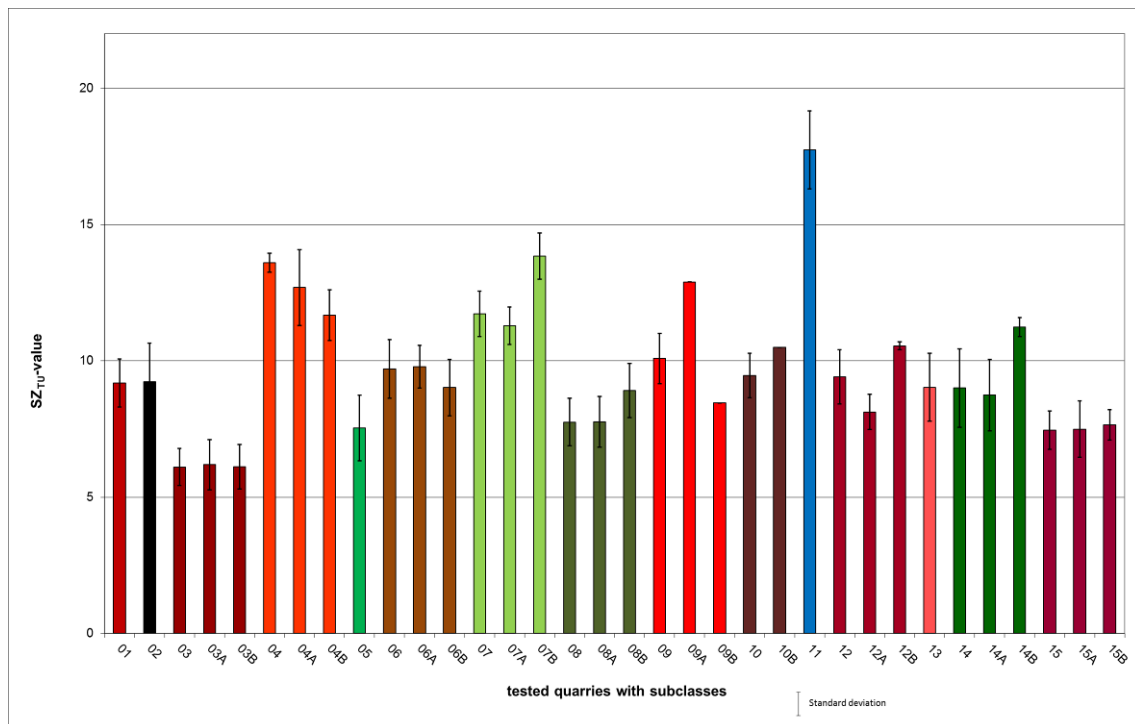
5. Results

Table 19: compilation of all impact tests carried out in the test series of 2013 and the number of samples tested in the device Petroscope 4D®.

Rock type	Petroscope 4D® prior to test	Impact test	Petroscope 4D® after test
01	25	25	0
02	24	24	4
03	8	8	8
03A	8	8	8
03B	8	8	8
04	5	5	5
04A	6	6	6
04B	6	6	6
05	25	25	25
06	15	15	15
06A	6	6	6
06B	4	4	4
07	8	8	8
07A	6	6	6
07B	6	6	6
08	12	12	12
08A	8	8	8
08B	4	4	4
09	22	22	22
09A	1	1	1
09B	1	1	1
10	24	24	0
11	24	24	24
12	18	18	0
12A	4	4	0
12B	2	2	0
13	22	22	0
14	17	17	0
14A	4	4	0
14B	2	2	0
15	8	8	8
15A	9	9	9
15B	6	6	6
SUM	350	350	188

5.1. SZ_{TU} -values

Figure 15 shows the mean test results of the impact test SZ_{TU} for all rock types and their subclasses. Moreover the standard deviation is displayed here as well. Most impact fragmentation values vary between 5 and 15 %. Only dolomite (rock type 11) shows a higher result with a medium SZ_{TU} value of 17.74%. High SZ_{TU} -values indicate high fragmentation and small impact strengths of rocks. The chart in Figure 15 also illustrates that there are differences in the results for the subclasses for some of the rock types (see also Table 20).



01 Granite	02 Basalt	03 Granitporphyr	04 Dunite	05 Diabase	06 Granulite	07 Diabase	08 Diabase
09 Granite	10 Granulite	11 Dolomite	12 Granite	13 Granite	14 Diabase	15 Granite	

Figure 15: mean impact test results of all rock types (with subclasses) and the standard deviation of the results. The diagram illustrates that there are rock types with and without subclasses and that the results differ between these subclasses or may not.

For the analysis of the results, the following considerations must be taken into account: There are rock types with and without subclasses; the author was able to identify the subclasses and to separate them, and the results of the subclasses offer different impact test results. Rock types 04, 07, 09, 12, and 14 show different results for their subclasses. There is almost no difference in the

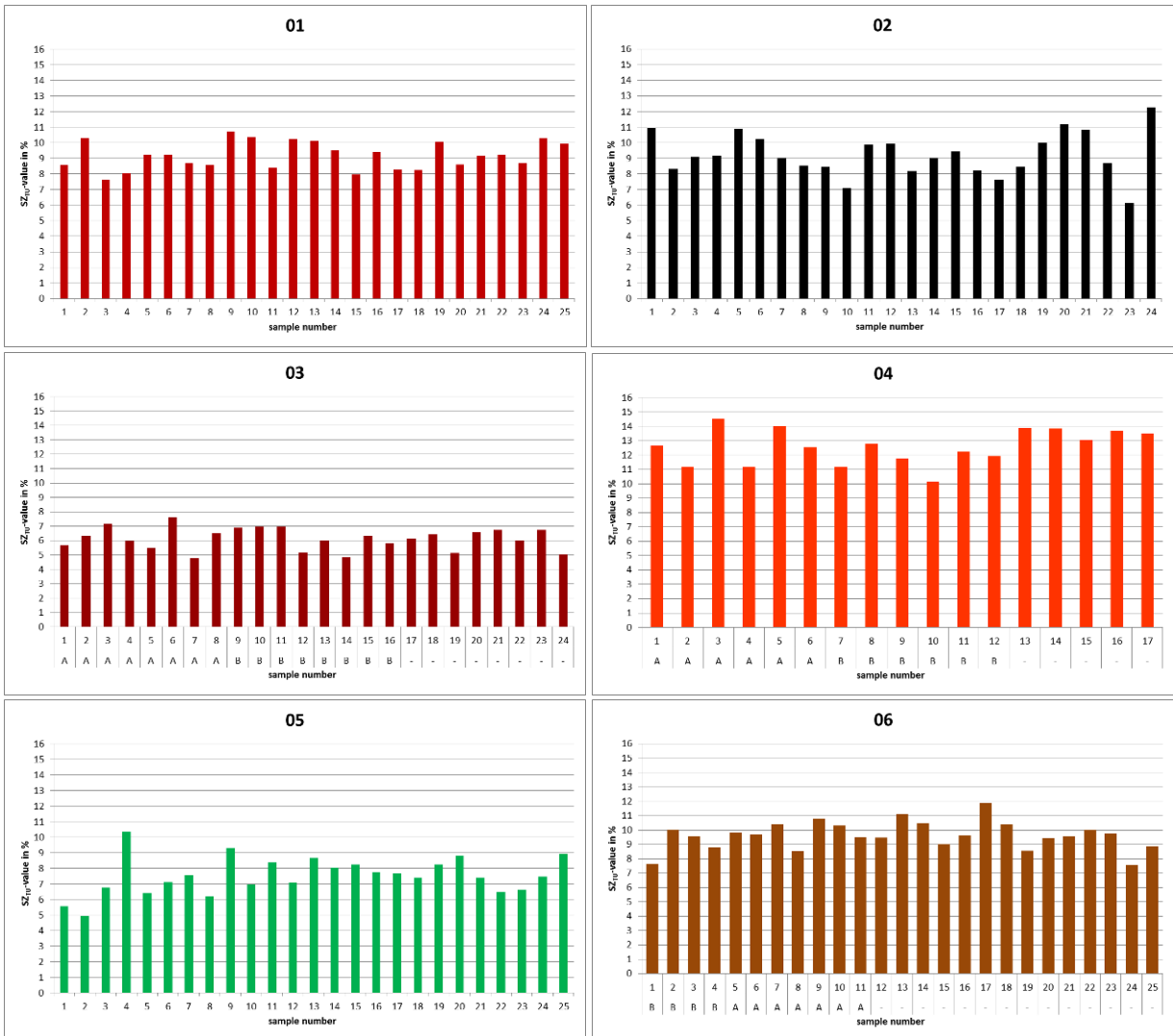
mean values of the subclasses for rock types 03, 06, and 15. If one assumes that the separation was successful but the results do not show differences, then one can conclude that the mechanical properties concerning fragmentation are the same for the subclasses. There is no overall trend that one rock type shows a better fragmentation performance than others.

Table 20: shows the mean SZ_{TU} -value, the minimum and maximum values and the median values in [%], as well as the standard deviation (σ) based on the SZ_{TU} -value and the number of tests executed per rock type and its subclasses.

	mean [%] SZ_{TU} -value	min [%]	max [%]	σ [-]	median [%]	number of tests n
01	9.19	7.63	10.72	0.88	9.22	25
02	9.24	6.14	12.28	1.41	9.05	24
03	6.10	5.04	6.76	0.68	6.28	8
03A	6.19	4.80	7.63	0.92	6.14	8
03B	6.12	4.86	6.95	0.81	6.16	8
04	13.60	13.05	13.90	0.35	13.68	5
04A	12.69	11.20	14.53	1.39	12.60	6
04B	11.67	10.13	12.80	0.93	11.83	6
05	7.53	4.94	10.34	1.20	7.47	25
06	9.70	7.59	11.89	1.08	9.61	15
06A	9.79	8.52	10.79	0.79	9.76	6
06B	9.02	7.66	10.04	1.04	9.19	4
07	11.73	10.62	13.14	0.83	11.71	8
07A	11.29	9.99	11.86	0.69	11.54	6
07B	13.84	12.74	14.80	0.85	13.79	6
08	7.75	6.54	8.99	0.87	7.70	12
08A	7.76	6.05	8.97	0.93	7.95	8
08B	8.91	7.80	10.21	0.99	8.81	4
09	10.09	8.24	11.38	0.93	10.26	22
09A	12.90	-	-	-	-	1
09B	8.46	-	-	-	-	1
10	9.46	7.74	10.69	0.82	9.36	23
10B	10.49	-	-	-	-	1
11	17.74	15.38	21.36	1.43	17.36	24
12	9.41	7.86	11.82	0.99	9.48	18
12A	8.12	7.18	8.66	0.65	8.32	4
12B	10.55	10.45	10.65	0.15	10.55	2
13	9.03	6.44	11.06	1.25	9.03	22
14	9.01	6.65	12.26	1.44	8.68	17
14A	8.74	6.97	9.90	1.31	9.05	4
14B	11.24	10.99	11.49	0.35	11.24	2
15	7.46	6.37	9.04	0.70	7.40	8
15A	7.50	5.65	8.81	1.04	7.38	9
15B	7.66	7.03	8.41	0.56	7.67	6

Table 20 shows all calculated results related to the SZ_{TU} -value. Next to the mean value of all rock types and their subclasses, the minima and maxima values, the standard deviation, and the median value are given in this table. For subclasses 09A, 09B, and 10B only the SZ_{TU} -value is given, as there was only one sample in these subclasses. Diagrams in Figure 17, Figure 18, Figure 19, Figure 20 and Figure 21 display the range of results of all rock types.

The following diagrams in Figure 16 show all single results for every rock type from the impact test. Each SZ_{TU} -value for all 350 samples is represented in %. It becomes more clearly from the charts that the results differ within one rock type both in rock types with subclasses and without. The results sometimes differ by several percents from each other.



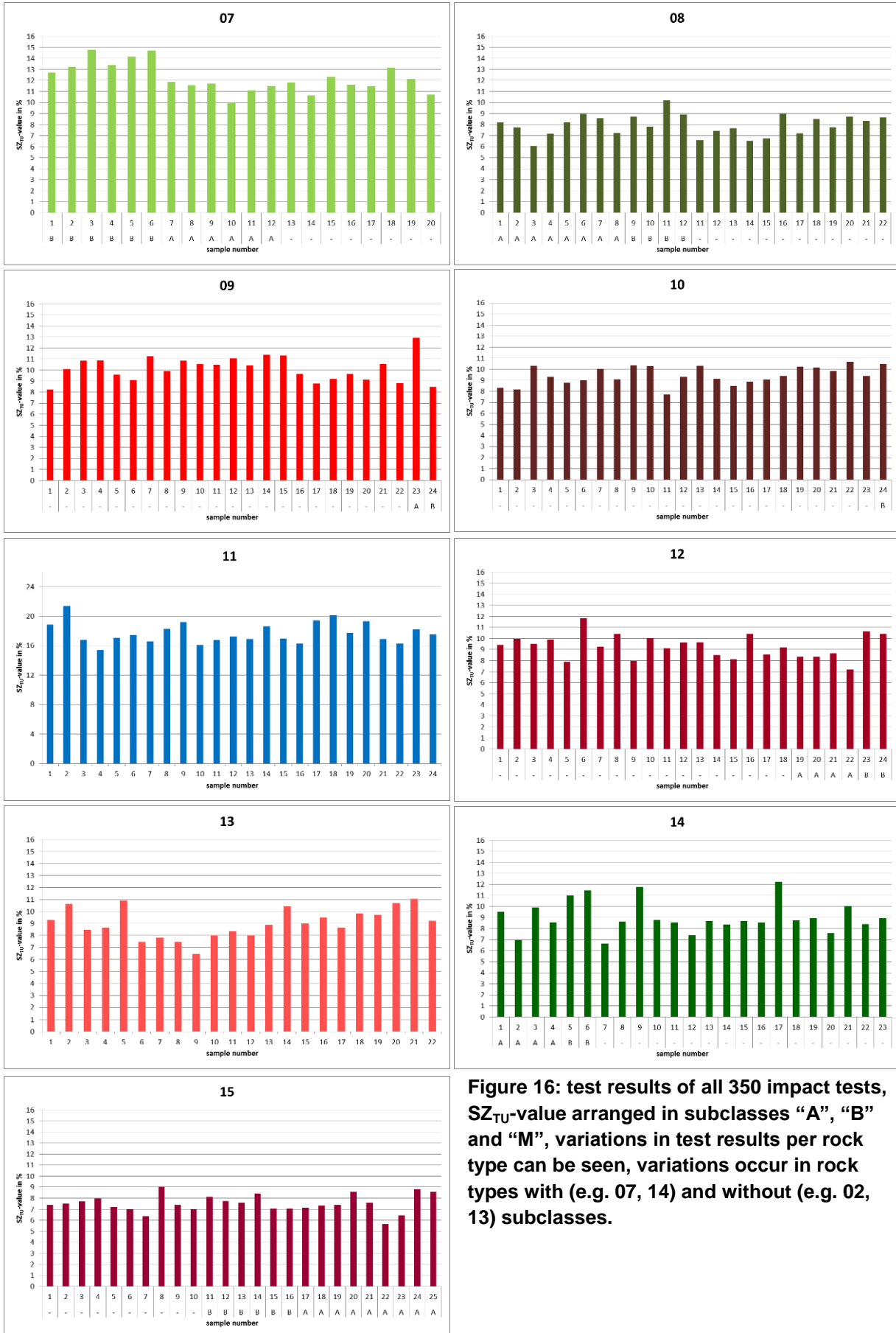


Figure 16: test results of all 350 impact tests, SZ_{TU}-value arranged in subclasses “A”, “B” and “M”, variations in test results per rock type can be seen, variations occur in rock types with (e.g. 07, 14) and without (e.g. 02, 13) subclasses.

The following Figure 17 displays the variations of rock types with respect to the SZ_{TU} -value. One representative of every rock type is offered. Comparing these with each other shows the range of results from the test. Dolomite has the highest values between 15 and 22% (see also Table 20). This means, dolomite shows the highest degree of fragmentation. The results for basalt, granite and granulite range around the same values, near 10%. Whereas the values of the basalt ballast display a high variability, the range of values for granite and granulite is slightly less. The smallest values and therefore the least fragmentation occurs in the samples of granite porphyr. Dunite and diabase show values between 12 and 14%.

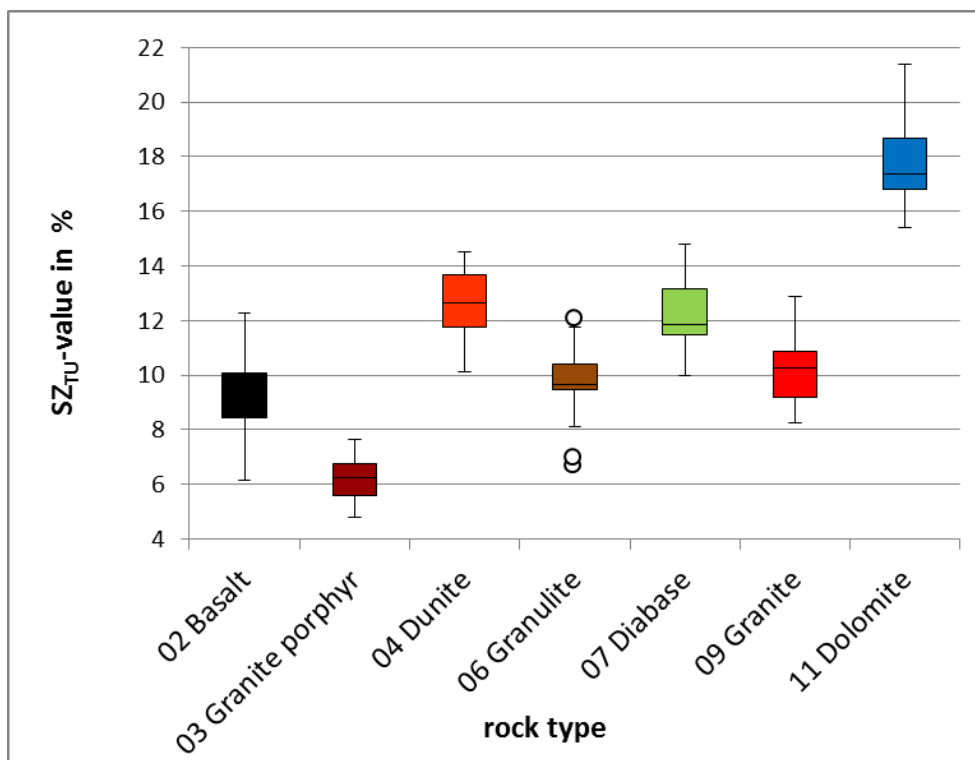


Figure 17: Box plot diagram of one representative of each rock type, all tested rock types show variations within their results and to each other.

Figure 18 to Figure 21 compare the same rock types, but of different quarries. The data is given in the same chart type as in Figure 17.

Granites show quite uniform results, except for rock aggregates from quarry 15. The latter SZ_{TU} -values lie in a range from 7 to 8%. Granites from quarries 01, 09, 12, and 13 have approximate fragmentation values between 8 and 11 %.

The comparison of the different diabase rocks in Figure 19 shows a wider range of results. The fragmentation values for this rock type are not uniform. Diabase rocks from 05 and 08 show almost the same results. Railway ballast from 07 has higher values than the other diabases (at ~12% around 4% higher) (Figure 19). Interesting to notice is that SZ_{TU}-values of 08 and 14 differ in their results. These are diabases from the same supplier, however a different crusher was used (see Table 20 and Figure 19).

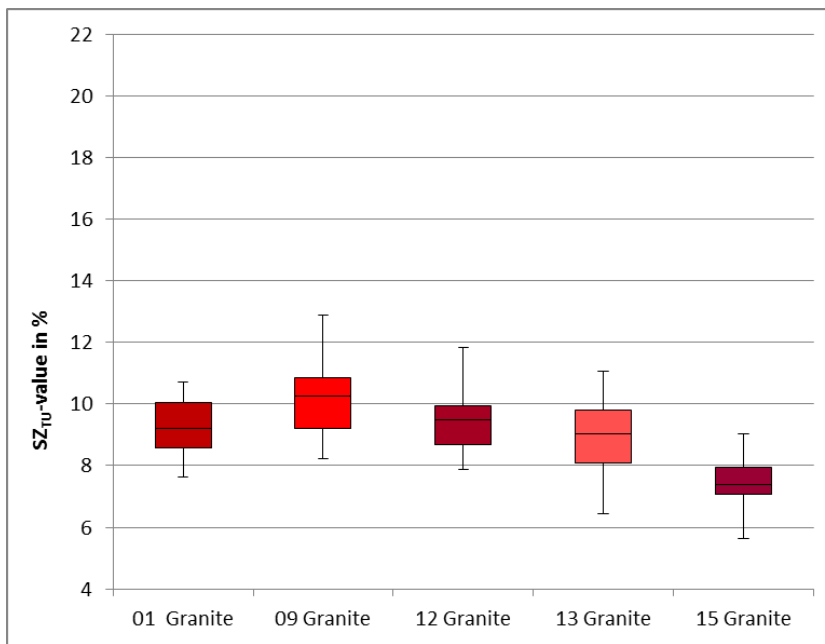


Figure 18: Box plot diagram, comparing SZ_{TU}-values of all granites, the mean results for rock types 01, 09, 12 and 13 are quite uniform with mean SZ_{TU}-values of about 9%, mean values of 15 granite are smaller (~7%).

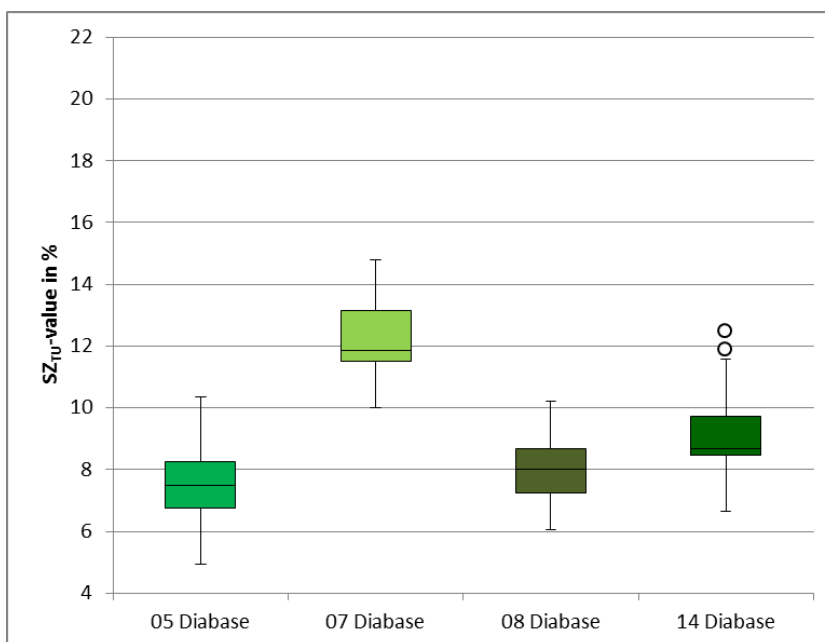


Figure 19: Box plot diagram, comparing SZ_{TU}-values of all diabase rocks, the mean results differ from each other. The fragmentation is only small for 05 diabase (with values around 7%) and relatively high for 07 Diabase (with values around 12%).

Figure 20 compares the granulites from suppliers 06 and 10. Both show results for the impact test between 9 and 10%. Only the range of values differ slightly. 06 granulite shows a higher range of data.

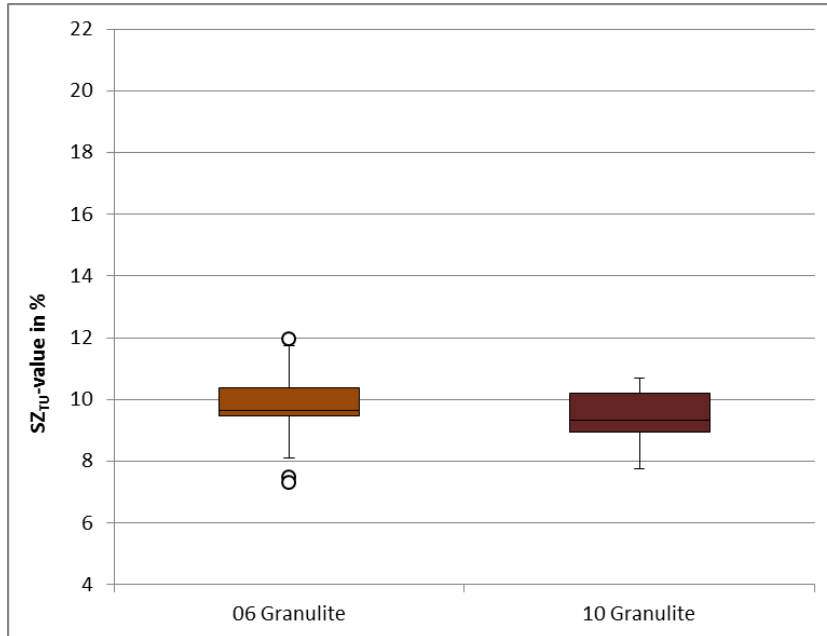


Figure 20: Box plot diagram, comparing SZ_{TU}-values of all granulite rocks, the mean results lie in a range between 9 and 10% SZ_{TU}-value.

The rock types that occur only once in this project are compared again in Figure 21 (see also Figure 17).

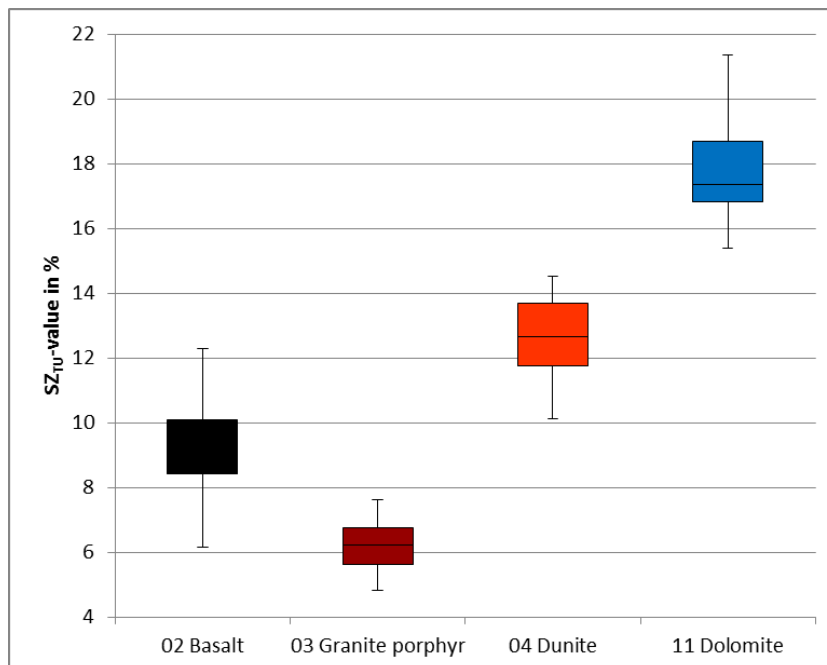


Figure 21: Box plot diagram, comparing SZ_{TU}-values of all other rock types. The least fragmentation has occurred for 03 granite porphyry. The most fragmentation has occurred for 11 Dolomite.

Results SZ_{TU} -value: Diabase

As mentioned above, the rock aggregates from suppliers 08 and 14 are actually the same rock type from the same quarry, but broken up in different crushers. As a result, grain shape and angularity can differ (see Figure 34 and Figure 42). Another possible reason for differences may be microcracks that can result in different crushers. As one can see in Figure 22 the results for the SZ_{TU} -value differ as well. Diabase 14 has slightly higher SZ_{TU} -values, but the mean values do not differ much from each other.

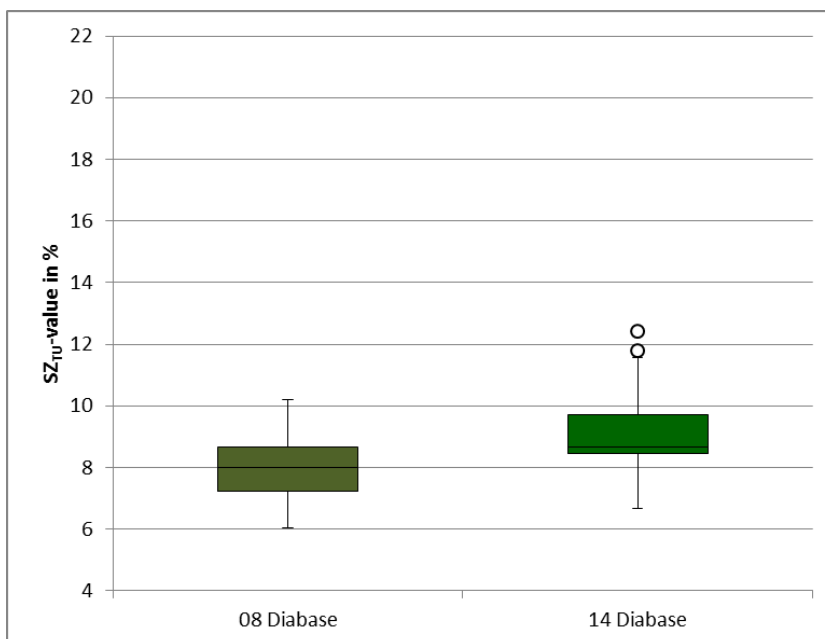
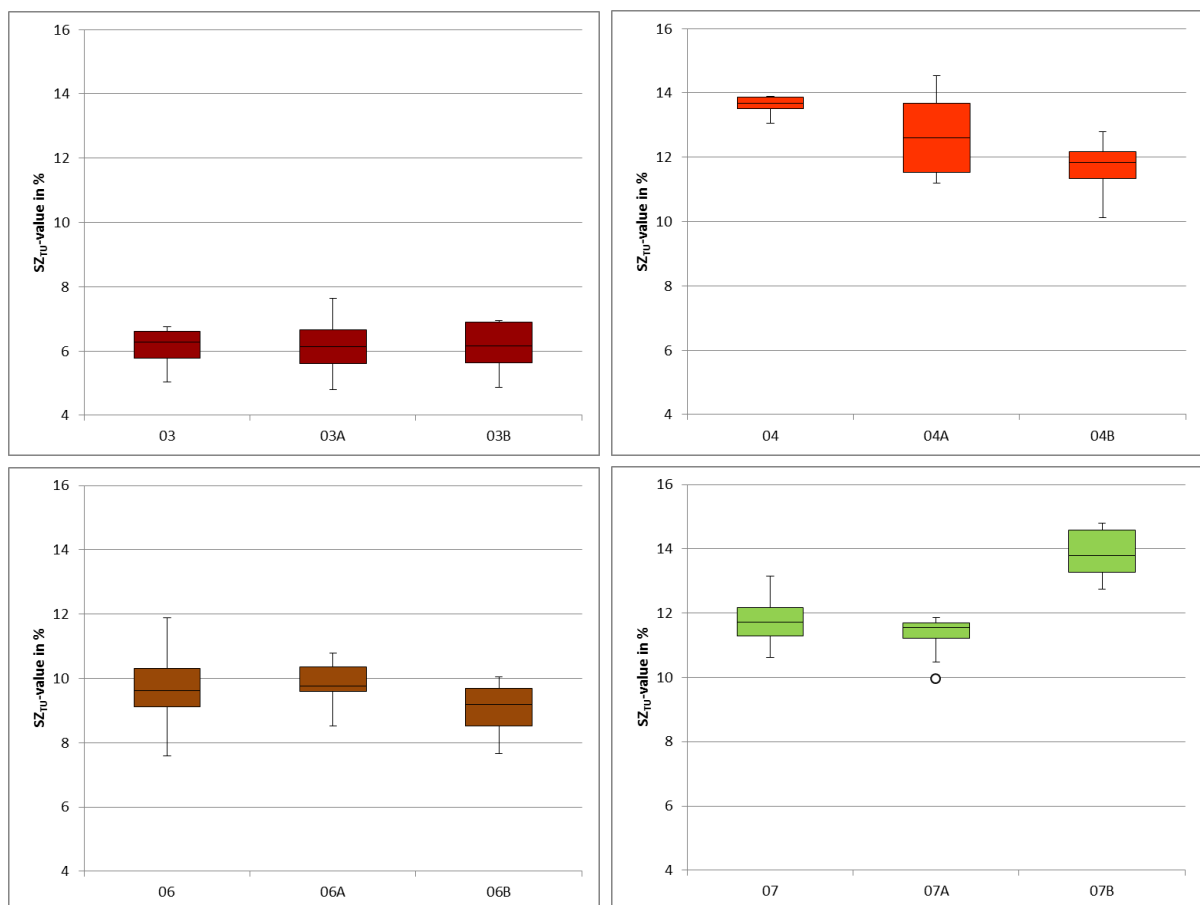


Figure 22: Box plot diagram, comparing SZ_{TU} -value of the same rock type (diabase) 08 and 14. The mean SZ_{TU} -value for 08 Diabase is 8.00 and for 14 Diabase it is 8.68. In general the aggregates of 14 have been fragmented more than those of 08.

Subclasses

Subclasses are built for several rock types in this test series. The diagrams in Figure 23 show the SZ_{TU} -value variations for these rock types. Minimum, maximum, and mean value are displayed for class “M”, “A” and “B”. Differences between the subclasses can be seen for rock types 04, 07, 12, and 14. The differences mostly exist between the subclass “M” and “B”. Subclass “A” is more similar to the non-separated group “M” (e.g. 06, 07, 08). Alterations between the subclass show different mechanical properties for these subclasses (impact strength).

If the difference in the subclass is only small or non-existent, the classes have either the same impact strength (e.g. 03) or the test has not delivered different results. The high variations between the subclasses for rock type 12 and 14 can be the result of small number of samples in the subclasses (see Table 19).



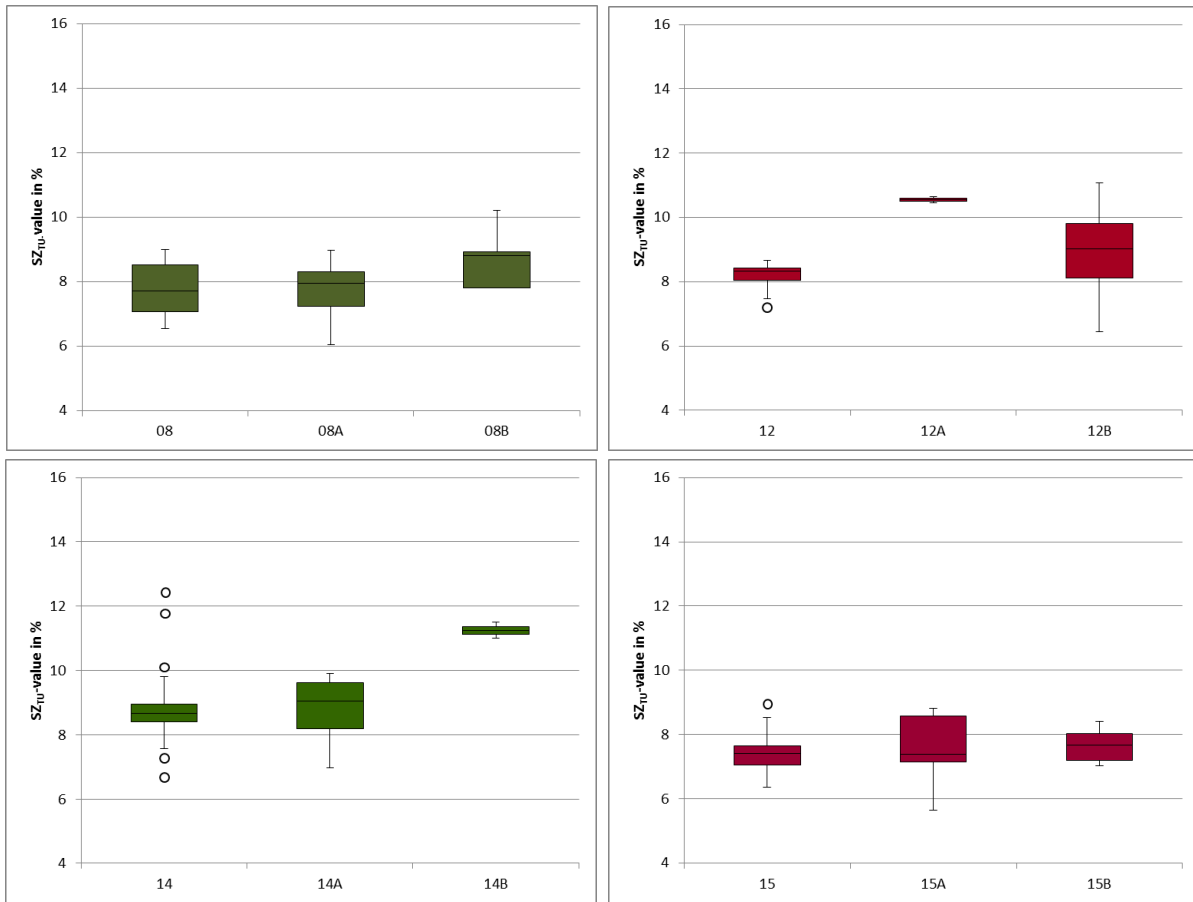


Figure 23: Box plot diagram, comparing SZ_{TU}-value of the subclasses within one rock type; strong differences between the subclasses can be seen for rock type 04, 07, 12 and 14, small differences can be seen for rock type 06 and 08, no differences can be seen for rock type 03.

Diagrams for rock types 09 and 10 do not exist as there is only one sample for each subclass. Rock type 03, 06, 08 and 15 show almost no or only small explicit result differences and also (exception 08) no distinct mineralogical changes. Rock types 04, 07, 12 and 14 show distinct different results in the subclasses, but only rock types 07 and 14 have clearly different mineralogy.

Impact strength values differ between the tested rock aggregates. The various rock types have different mechanical behavior and show a range of results within one rock type. Building of subclasses also shows variances in mechanical behavior within one rock type.

5.2. Strain

The initial height of the sample in the mortar changes during the test, because the aggregates are compacted by the weight of the impact. Using the initial height and the height of the sample after the test, the strain ϵ can be calculated (see section 3.1). The medium strain for every rock type in this project can be seen in Figure 24.

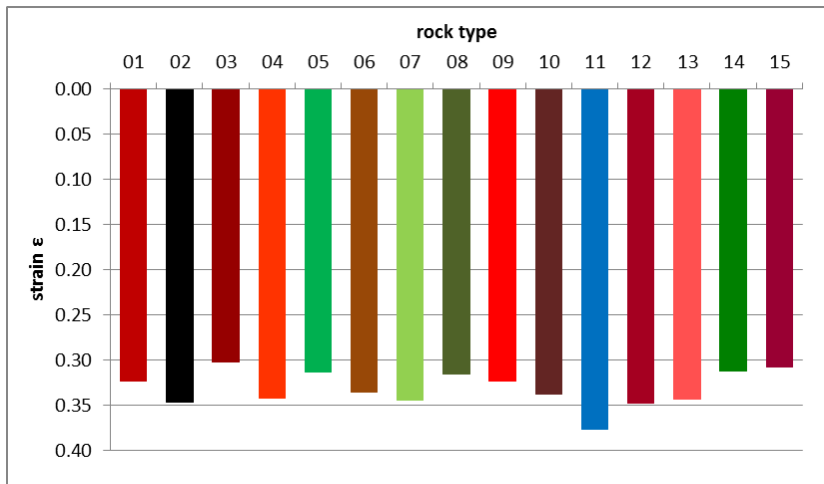


Figure 24: strain values ϵ [-] for the different rock types, calculated by the equation $\epsilon = \Delta h/h_1$. The strain value is given in reversed order, to display the compression in the mortar (0.00 is the height before the test in the mortar).

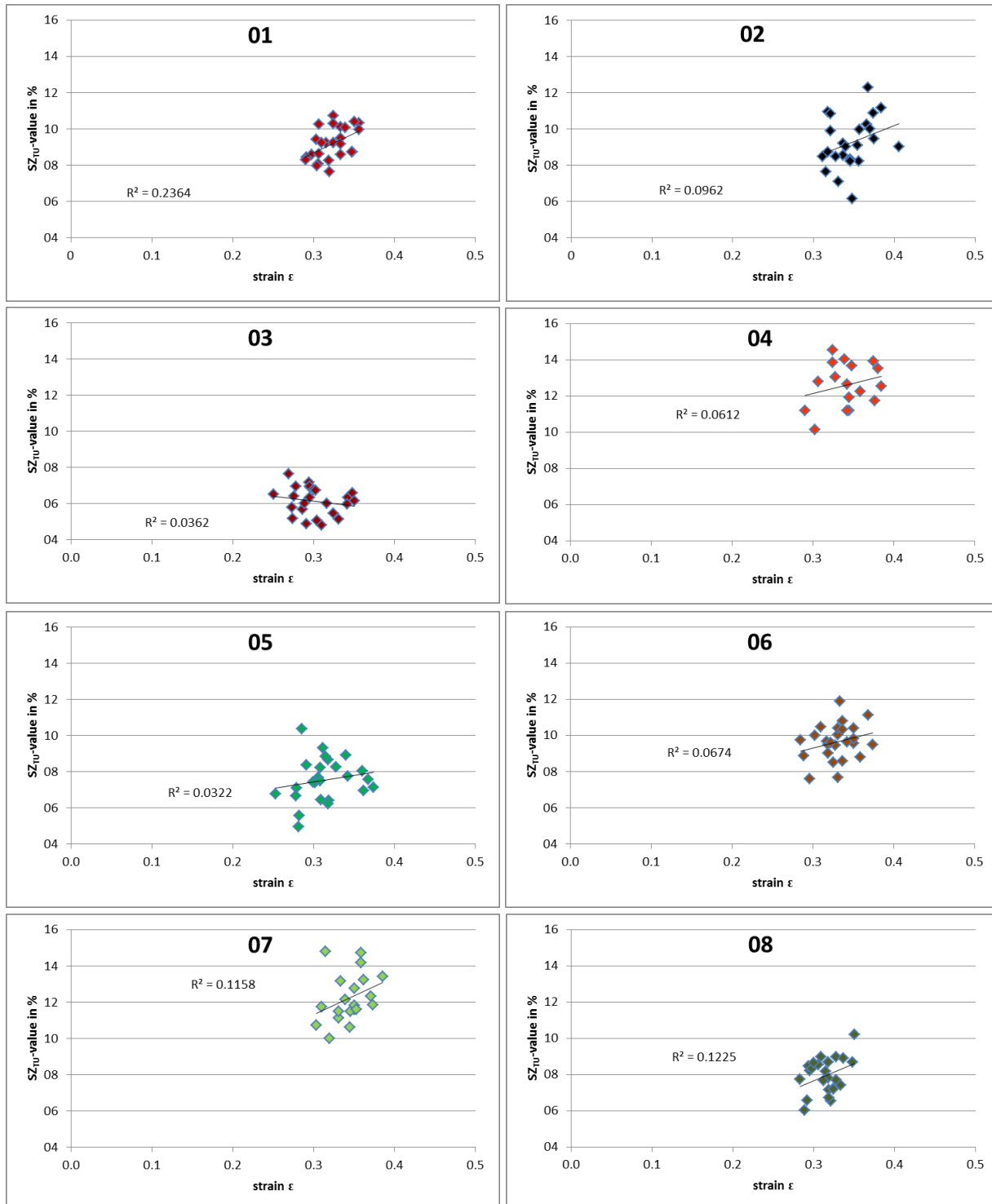
The strain values for the different rock types do not vary much among each other. Strain values fluctuate between 0.3 and 0.35. Only rock type 11 dolomite has a slightly greater strain value with 0.38.

The strain is mainly dependent on the height of the sample in the mortar before the execution of the impact test. If the sample is better compacted prior to the test, the strain may also be smaller. Rearrangement and rearrangement linked with fragmentation processes of the sample particles are responsible for the strain during the test. The strain is not necessarily dependent on whether rocks have high or low compressive strength. However, one must not ignore the impact strength.

In Figure 26, Figure 27, and Figure 28 the previous discussed parameters, such as SZ_{TU} -value, strain, and height before and after the test (consequential density), are plotted against each other and their dependency on each other is discussed.

Plots strain ϵ versus SZ_{TU} -values

When plotting the SZ_{TU} -values against strain results, there is no clear correlation recognizable. The coefficient of determination (R^2) in all digramms is smaller than 0.3. Figure 25 displays these plots.



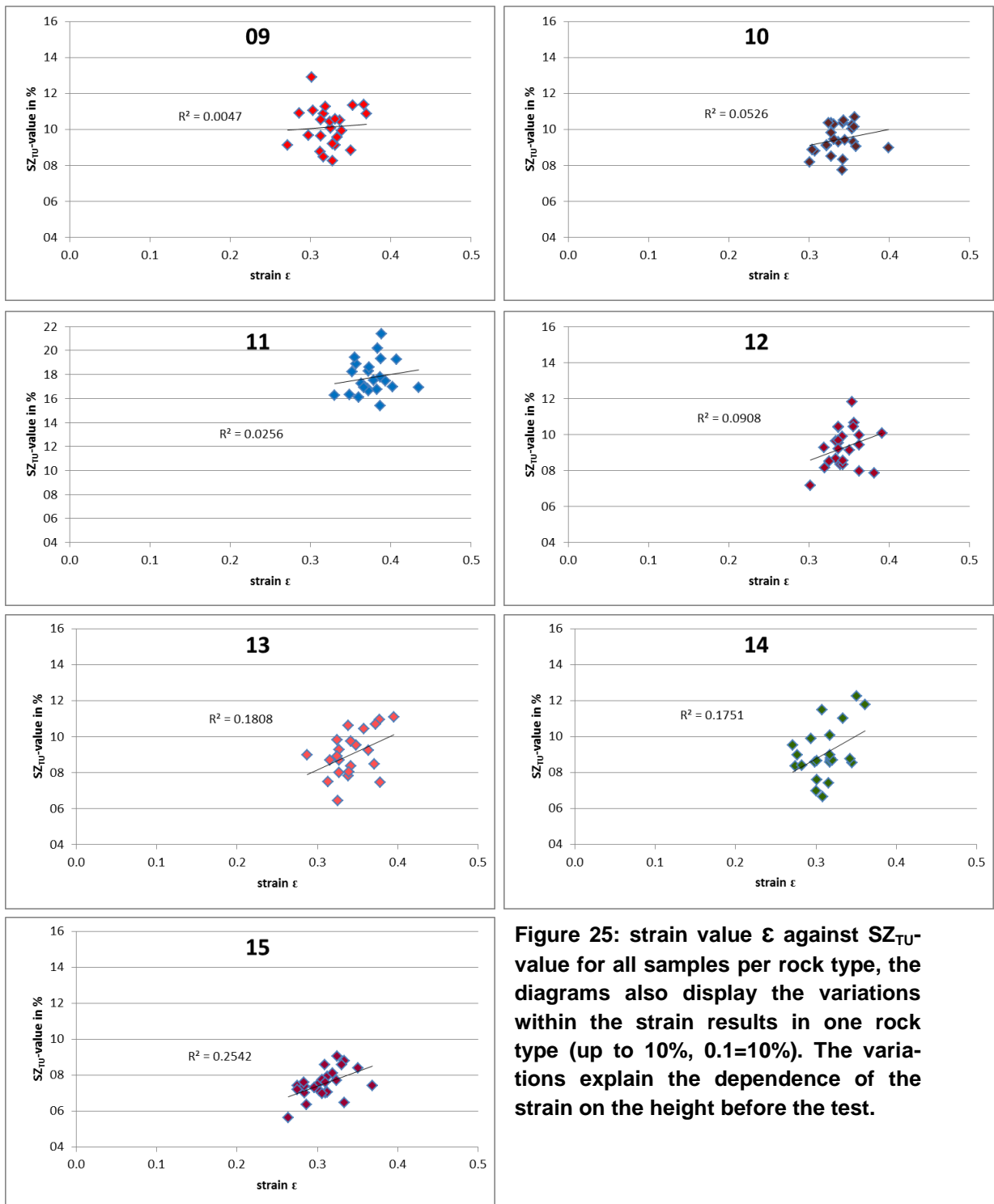
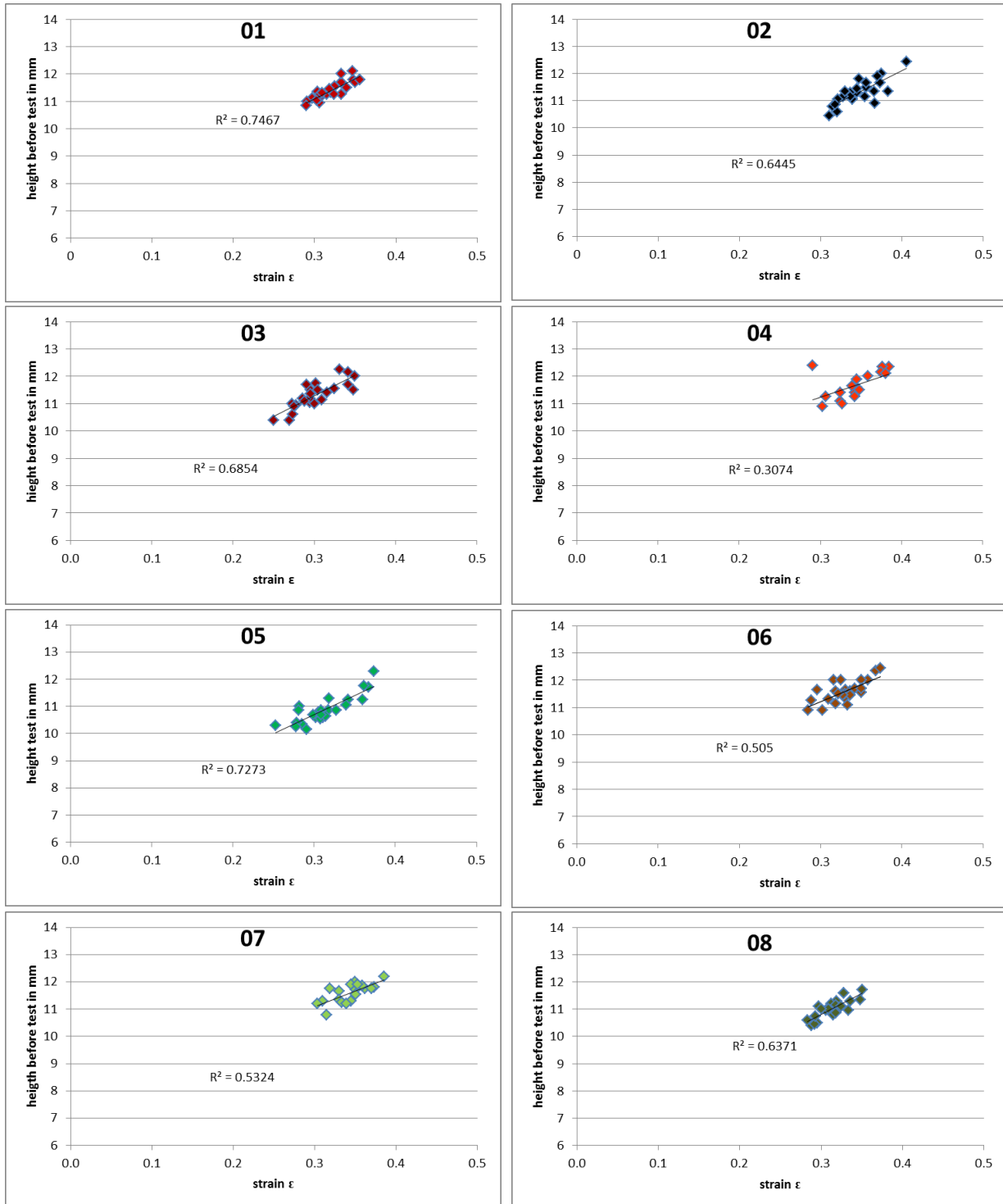


Figure 25: strain value ϵ against SZ_{TU} -value for all samples per rock type, the diagrams also display the variations within the strain results in one rock type (up to 10%, 0.1=10%). The variations explain the dependence of the strain on the height before the test.

The weak correlation between the strain ϵ and the SZ_{TU} -value indicates that the SZ_{TU} -value has little dependency on the strain and moreover not the height of the sample in the mortar (see Figure 26). Furthermore one can assume that as the SZ_{TU} -value is dependent on the impact strength of rock particles, the strain is mostly independent of the impact strength.

When plotting the height of the sample in the mortar before the test against the strain, a strong correlation can be seen (Figure 26). The coefficient of determination (R^2) is higher than 0.4.



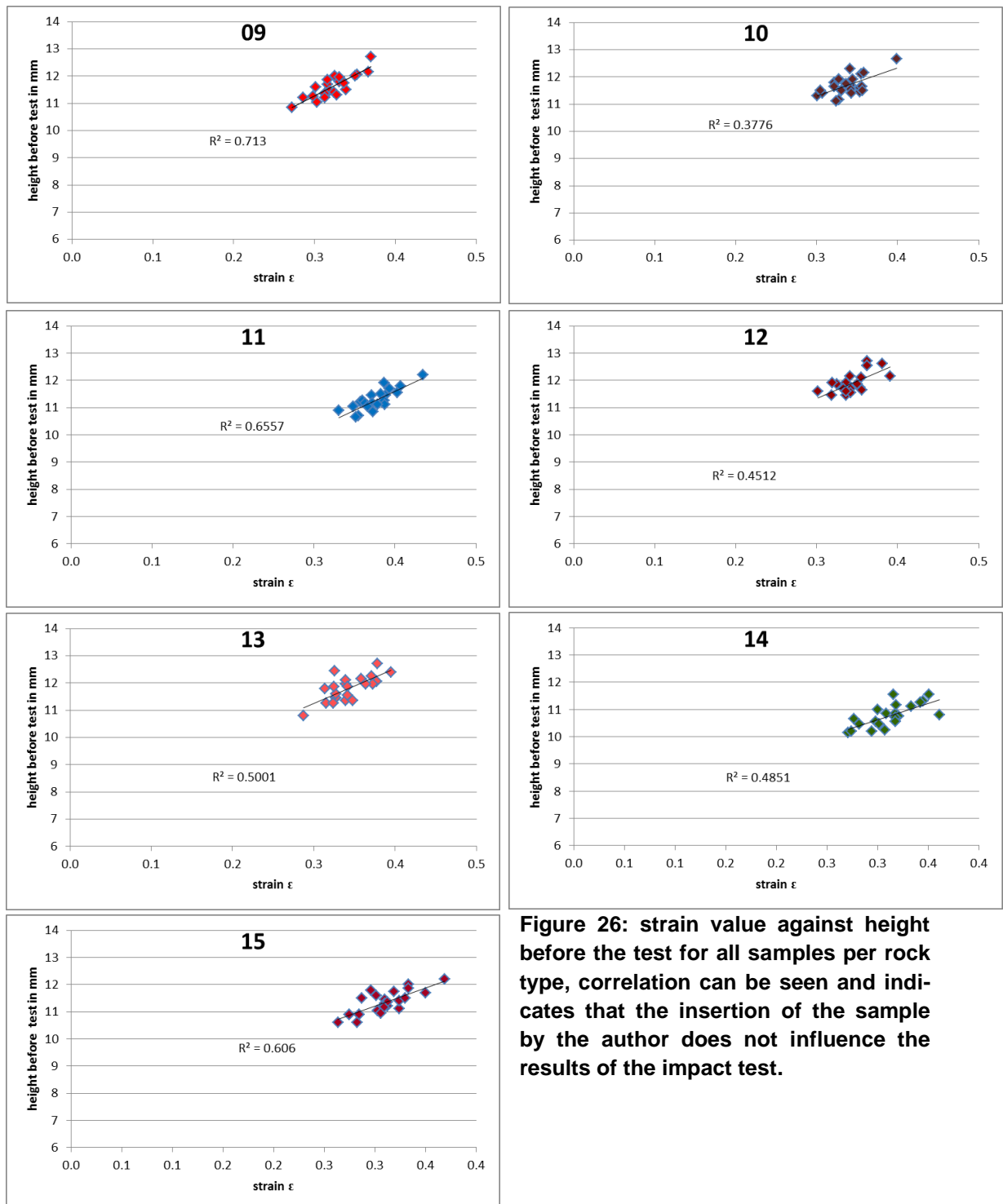
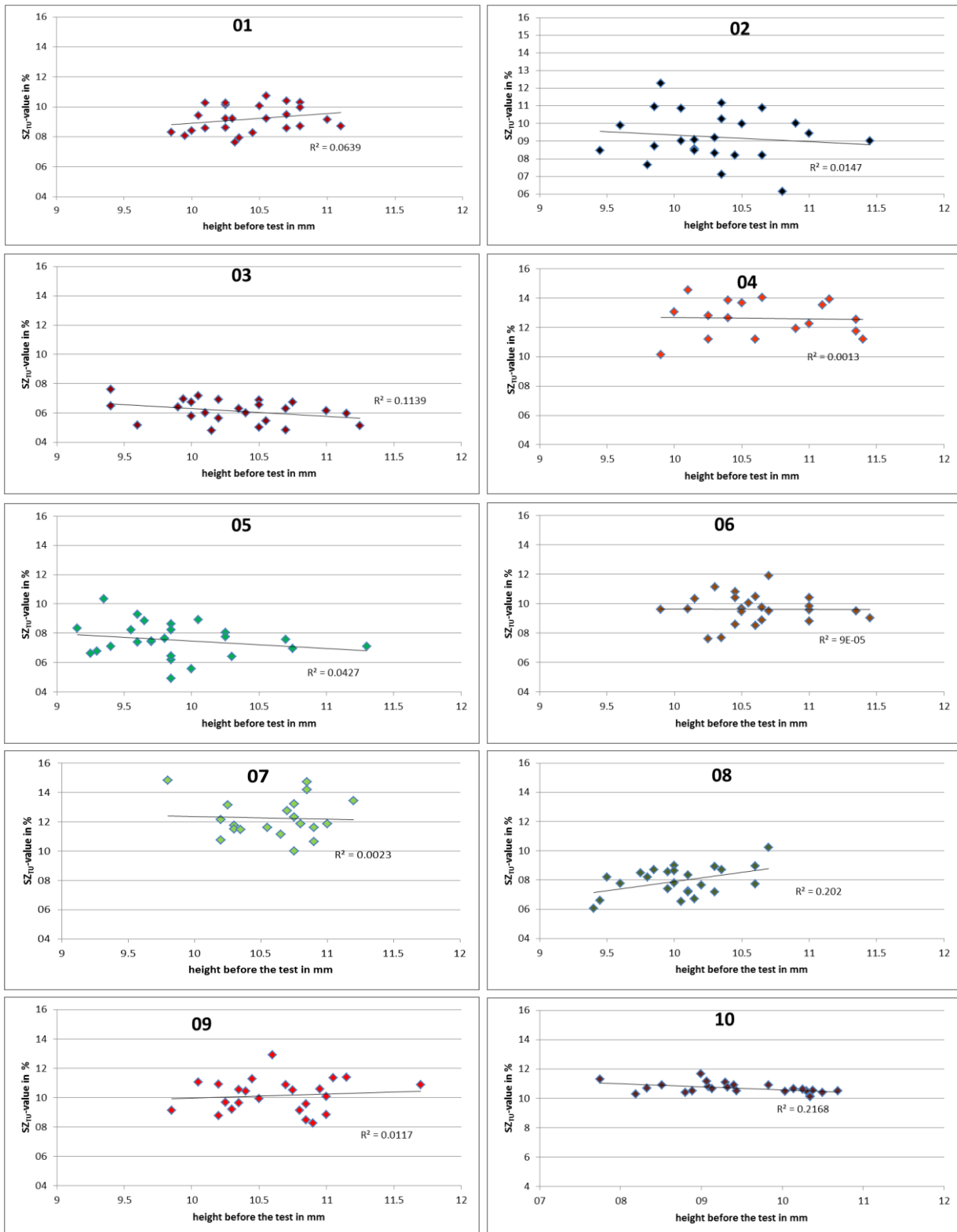


Figure 26: strain value against height before the test for all samples per rock type, correlation can be seen and indicates that the insertion of the sample by the author does not influence the results of the impact test.

This correlation indicates that strain depends on the height of the sample in the mortar before the test. Furthermore, one can assume that the human influence of sample insertion does not play a role on the impact test. When the initial height is low, the strain is smaller and vice versa.

A comparison of the SZ_{TU} -value and the height before the test in the mortar can be seen in Figure 27.



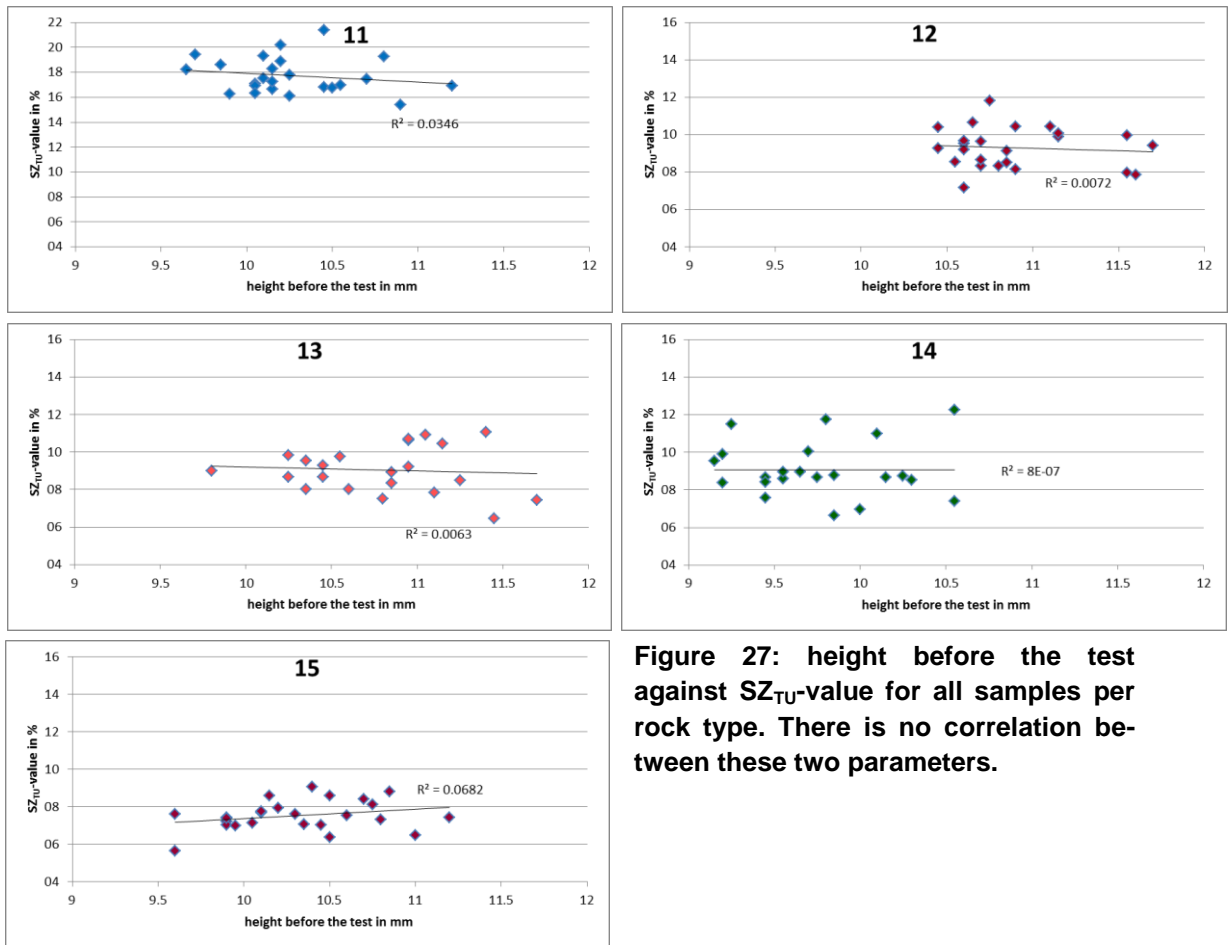
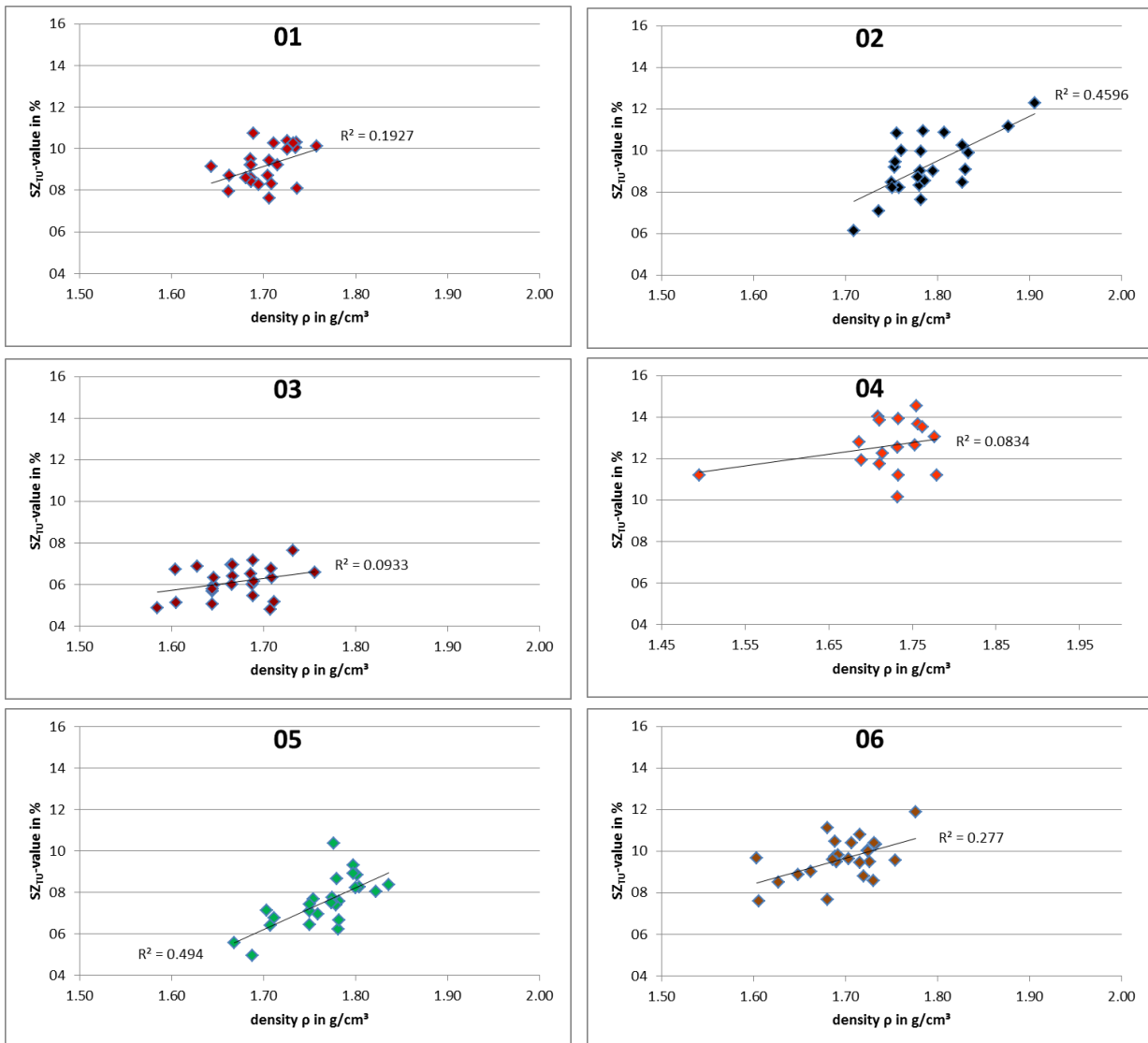


Figure 27: height before the test against SZ_{TU}-value for all samples per rock type. There is no correlation between these two parameters.

There is no link between these two parameters. This lack of correlation also supports the statement in Figure 25. In Figure 25, the SZ_{TU}-value is plotted against the strain ϵ and there is only a weak correlation. It also emphasizes the statement in Figure 26, that the human influence of insertion of particles does not have an effect on the impact test result.

To complete these plots, the SZ_{TU} -value is plotted against the density of the sample after the test. As there is a weak to moderate correlation between these two parameters, the SZ_{TU} -value is only slightly dependent on the height of the sample in the mortar after the experiment. Moreover, the same height of all samples after the testing procedure would indicate that the petrology and grain shape does not play a role. However, the height of the sample in the mortar after the test can be dependent on petrology and grain shape of the aggregates.



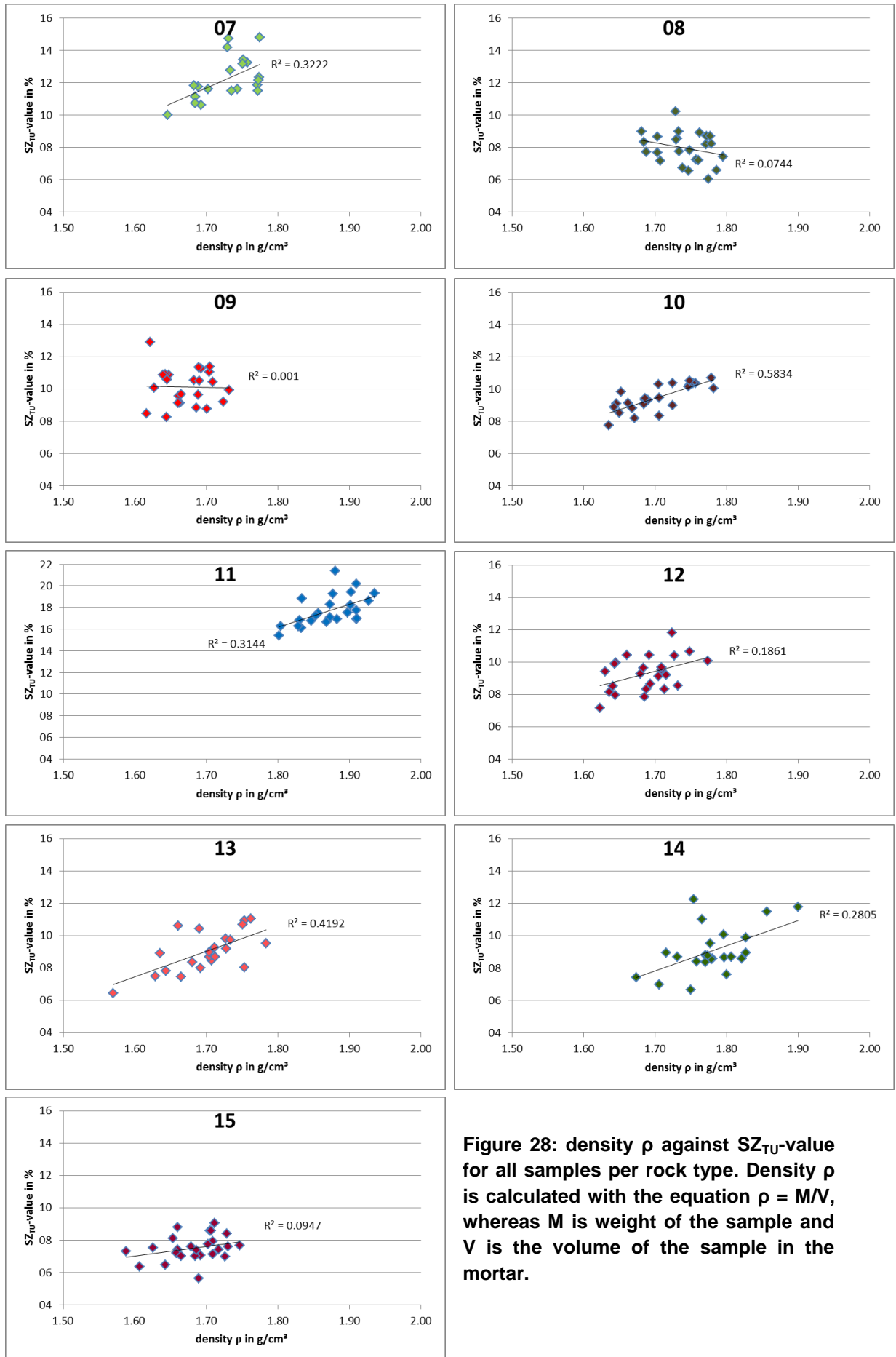


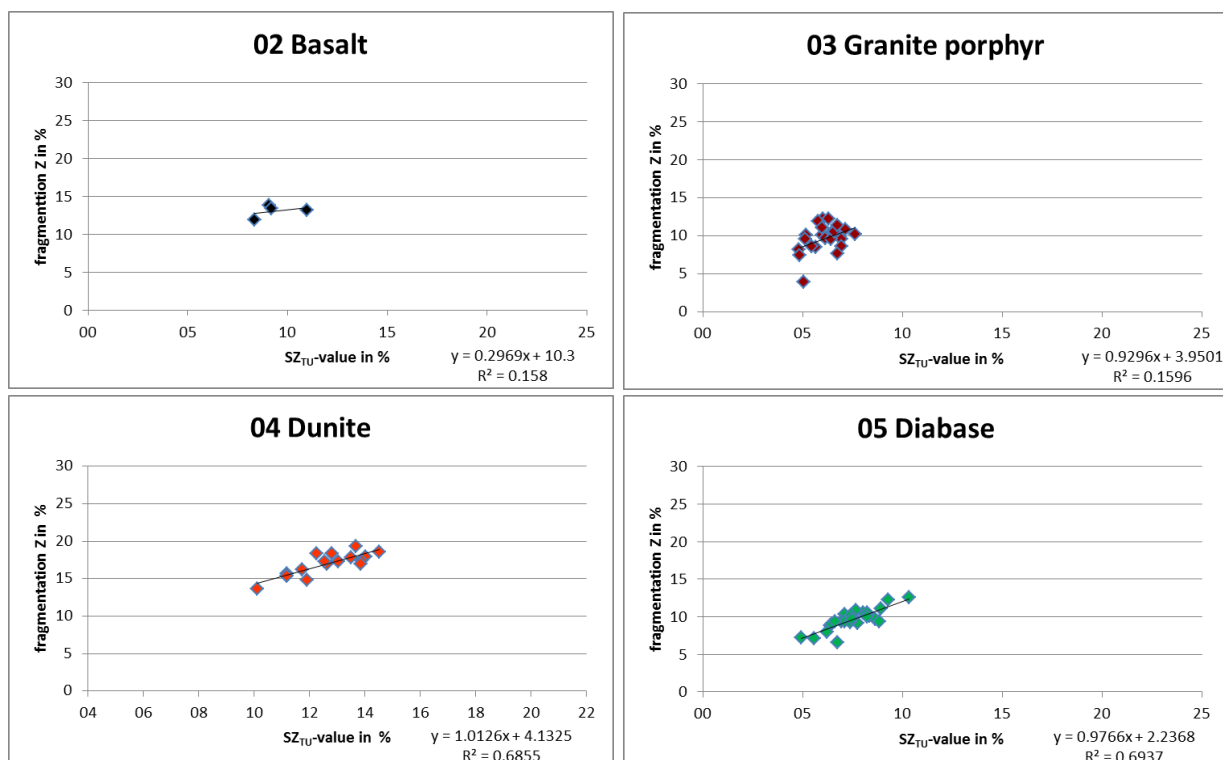
Figure 28: density ρ against SZ_{TU} -value for all samples per rock type. Density ρ is calculated with the equation $\rho = M/V$, whereas M is weight of the sample and V is the volume of the sample in the mortar.

5.3. Degree of Fragmentation Z

From the second analysis of samples in the Petroscope 4D[®] and by comparing these results with the analysis of the first run, the degree of fragmentation Z can be determined. Z is the integrated area between the grain size distribution curves before and after the impact test (see section 2.6). The degree of fragmentation Z and the SZ_{TU}-value are compared with each other in Figure 29. The values show a good correlation for all rock types. Furthermore the mean degree of fragmentation Z is shown in Table 21. As it can be seen in Table 19, only 180 samples could be analyzed in Petroscope 4D[®] after the impact test. Therefore the plots SZ_{TU}-value/fragmentation Z are only displayed for selected rock types (Table 21). There is not a good correlation for 02 Basalt because of a lack of data. The data of 03 granite porphyry also show larger variations.

Table 21: mean degree of fragmentation Z in % for selected rock types

Rock type	Degree of fragmentation Z in %
02 Basalt	13.09
03 Granite porphyry	9.65
04 Dunite	16.89
05 Diabase	9.59
06 Granulite	13.56
07 Diabase	16.03
09 Granite	13.17
11 Dolomite	20.15



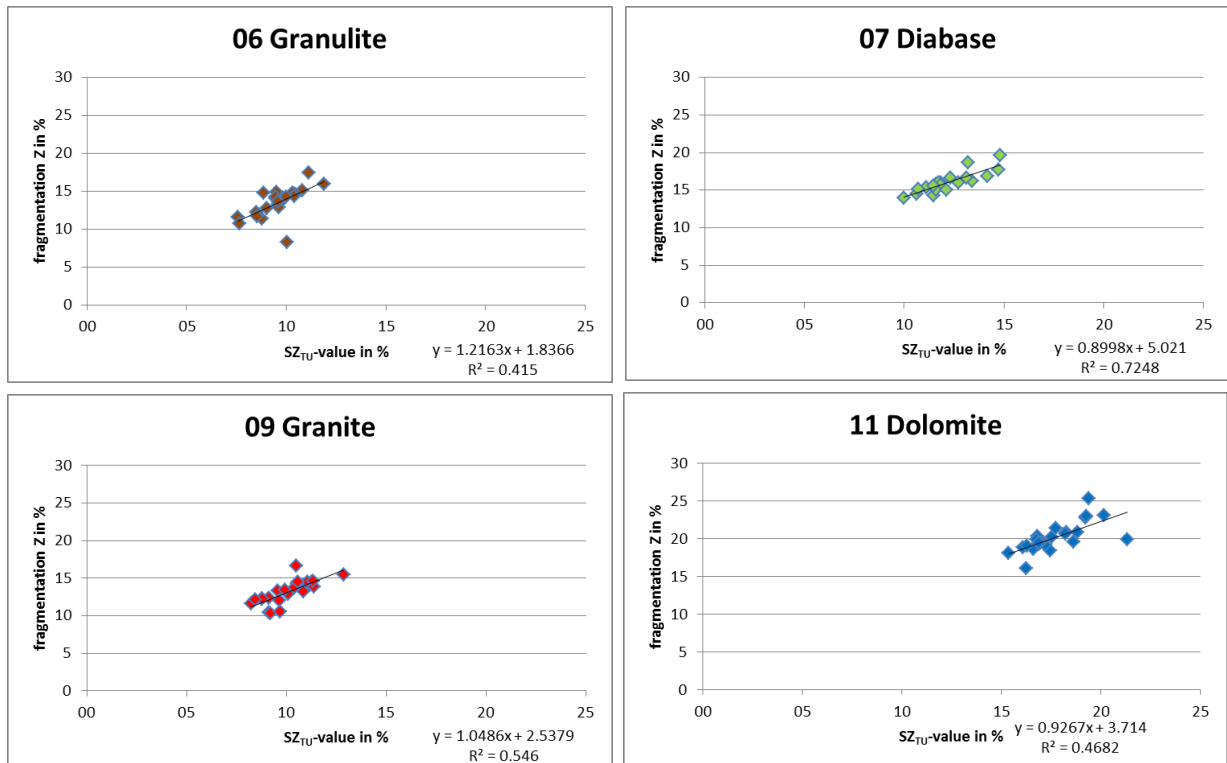


Figure 29: selected rock types with correlation between SZ_{TU}-value (%) and fragmentation Z (%), good correlation between both values, as both describe a sort of fragmentation.

Figure 30 combines all the trendlines and coefficients of determination (R^2) between the fragmentation Z and the SZ_{TU}-impact value. SZ_{TU}-value and fragmentation correlate very well because both demonstrate the degree of fragmentation. Almost all the trendlines run parallel (exception: basalt due to a lack of results). All trendlines have a similar gradient, but the point where the line hits the y-axis is different for all rock types. This indicates that fragmentation took place, but to a different degree. Moreover the point where the trendline meets the y-axis is $\neq 0$. This means that fragmentation took place, but that the fragmentation process does not only create particles that are <8mm (condition of SZ_{TU}-value).

Due to the correlation of the individual curves, a general empirical equation for the relationship between the degree of fragmentation and the SZ_{TU}-value can be derived:

$$Z = 0.98SZ_{TU} + 3.40$$

0.98 is the gradient of the general equation and 3.40 the point where the line hits the y-axis. This means that when $x=0$ there would not be any particles $<8\text{mm}$, but fragmentation had taken place nonetheless and had created particles with a size $>8\text{mm}$ only.

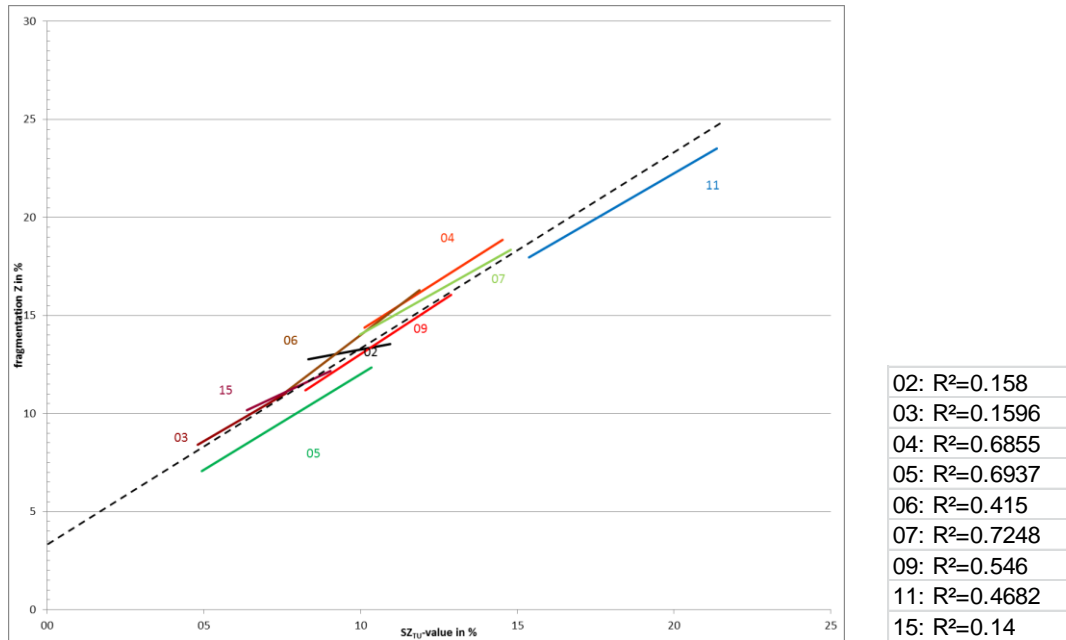


Figure 30: correlation between SZ_{TU} -value and fragmentation Z , the dotted line expresses the general correlation between both values, $Z=0.98SZ_{TU}+3.40$.

5.4. Minimum sample size

For a deviation of the test results, it is important to know how many tests must be completed to achieve a 95% confidence interval. The standard deviation σ must be known to ensure a confidence interval smaller than 5% of SZ_{TU} -value. The minimum number of necessary sample size can be calculated by the equation

$$n \geq \frac{z^2 \sigma^2}{d^2} \quad (\text{after (Liu, 2010)})$$

n represents the minimum number, z is the confidence interval value (1.96) for a 95% confidence interval, σ the standard deviation and d a limiting boundary. The calculation uses the limiting boundaries $d = 0.5\%$ and $d = 1\%$ (absolute) and the limiting boundary $d = 10\%$ of the resulting value (relative). This means that the calculated number n lies in the CI of 95% and the SZ_{TU} -value does not differ more than 0.5%, 1% absolute, and 10% relative from the mean value. For the standard deviation σ , a correction factor c is also introduced due to the small number of tests. Therefore $\sigma^2 = s^2 \cdot c$.

Table 22: number of tests that were executed n , approximated correction factor c (after (Liu, 2010)).

n	3	6	8	10	12	14	15	20	24	25
c	1,443	1,33	1,225	1,071	1,064	1,055	1,049	1,036	1,031	1,030

Table 23 lists the calculated results. If the results of the impact test should differ $\pm 0.5\%$ from the mean absolute value in a 95% confidence interval, the number of tests must increase in most cases, especially for rock types with subclasses. For a limiting factor of $\pm 1\%$ based on the SZ_{TU} -value, more than enough tests have been executed in the test series 2013. If one raises the limiting factor to $\pm 2\%$ from the SZ_{TU} -value, the necessary sample size n would drop under 3, the proposed number of tests in the European Standard 1097-2 (Österreichisches Normungsinstitut, 2006).

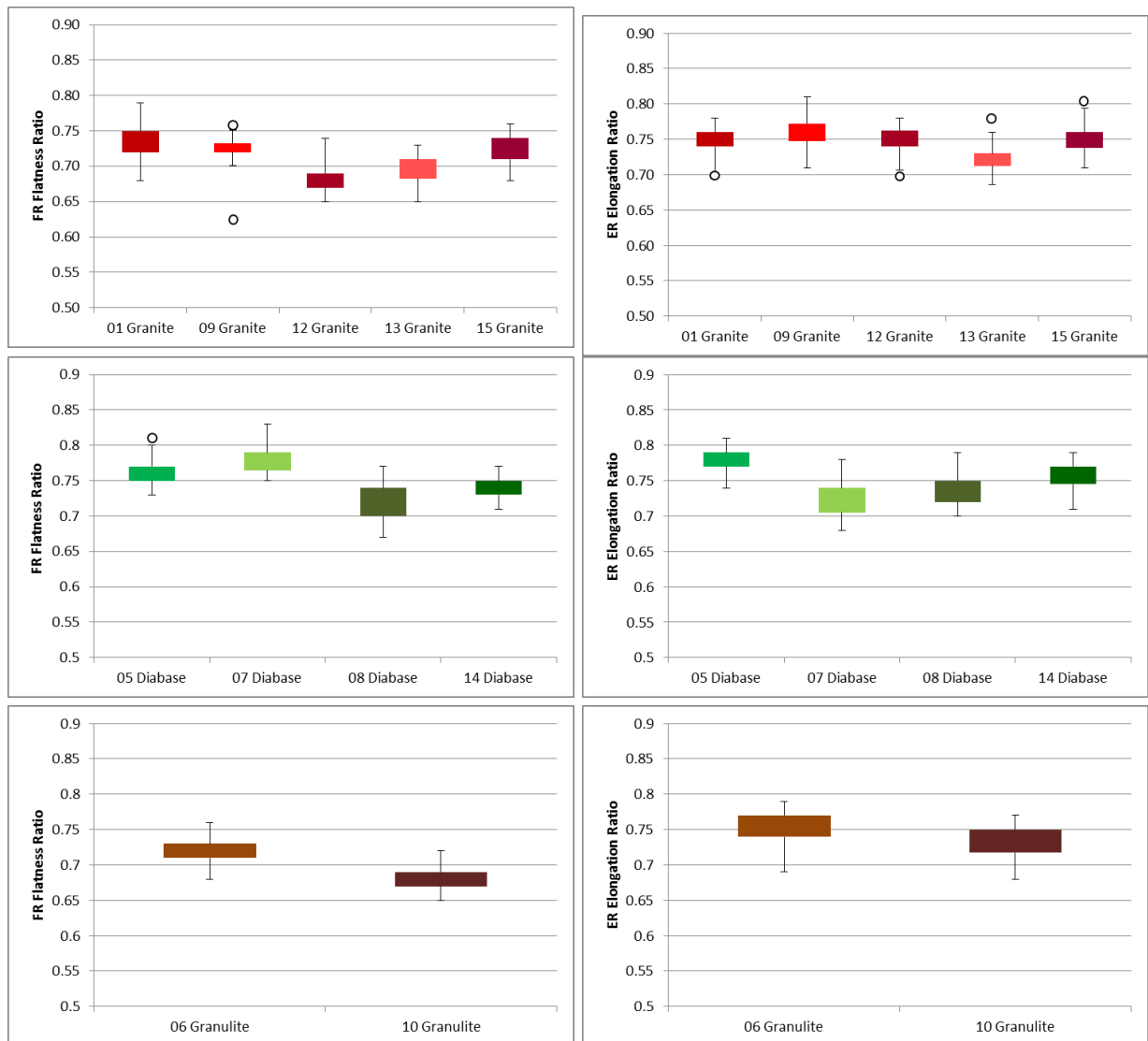
Table 23: deviation of results with respect to the SZ_{TU} -values, mean SZ_{TU} -values, standard deviation based on the test number, number of tests that were executed in the test series of 2013, calculated number of tests needed for a confidence level of 95% and an absolute value that may not exceed 0.5 or 1% of the mean SZ_{TU} -value (d_a) and a relative value that may not exceed 10% of the mean SZ_{TU} -value (d_r).

Rock type	Mean [%] SZ_{TU} -value	σ [-]	n of tests	Min. n of tests for $CI_{0.95}$ and $d_a \leq 0.5\%$	Min. n of tests for $CI_{0.95}$ and $d_a \leq 1\%$	Min. n of tests for $CI_{0.95}$ and $d_r \leq 10\%$
01	9.19	0.88	25	13	4	4
02	9.24	1.41	24	31	8	10
03	6.10	0.68	8	9	2	6
03A	6.19	0.92	8	16	4	11
03B	6.12	0.81	8	13	4	9
04	13.60	0.35	5	3	1	1
04A	12.69	1.39	6	40	10	7
04B	11.67	0.93	6	18	5	4
05	7.53	1.20	25	23	6	11
06	9.70	1.08	14	19	5	5
06A	9.79	0.79	6	13	4	4
06B	9.02	1.04	4	24	6	8
07	11.73	0.83	8	14	4	3
07A	11.29	0.69	6	10	3	2
07B	13.84	0.85	6	15	4	2
08	7.75	0.87	12	13	4	6
08A	7.76	0.93	8	17	5	7
08B	8.91	0.99	4	22	6	7
09	10.09	0.93	22	14	4	4
09A	12.90	-	1	-	-	-
09B	8.46	-	1	-	-	-
10	9.46	0.82	23	11	3	3
10B	10.49	-	-	-	-	-
11	17.74	1.43	24	33	9	3
12	9.41	0.99	18	16	4	5
12A	8.12	0.65	4	10	3	4
12B	10.55	0.15	2	1	1	1
13	9.03	1.25	22	25	7	8
14	9.01	1.44	17	34	9	11
14A	8.74	1.31	4	38	10	13
14B	11.24	0.35	2	3	1	1
15	7.46	0.70	10	9	3	4
15A	7.50	1.04	9	20	5	9
15B	7.66	0.56	6	7	2	3

5.5. Particle shape

Flatness and elongation ratio are determined by the Petroscope 4D[®]. It is expected that grains which are flat before the impact test, will tend to display fragmentation to a larger degree than grains which are spherical before the test. As mentioned above, mechanical properties vary from one rock type to another and even show variations within one rock type. This leads to the question of whether particle shape properties vary in the same way.

The diagrams in Figure 31 compare the flatness and elongation ratio before the test from the same rock types but from different suppliers.



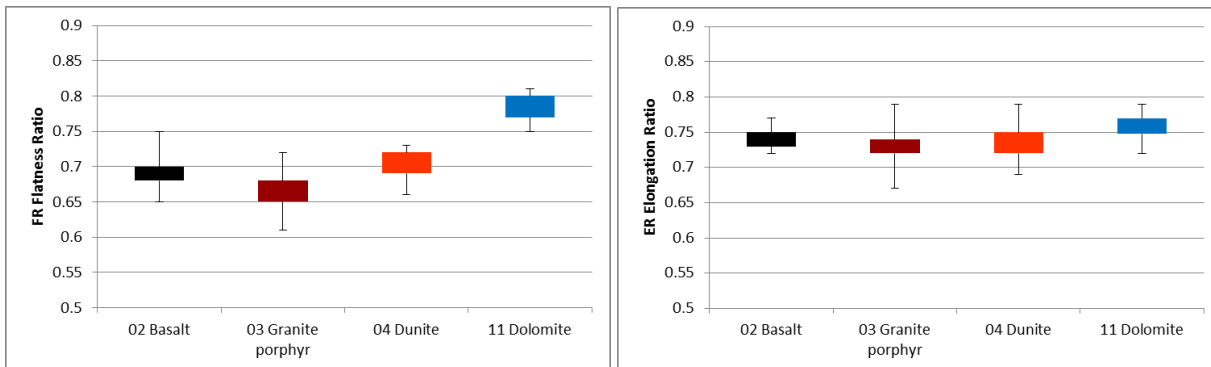


Figure 31: FR (left) and ER (right), comparison of rock types before the impact test. Diagrams show the range of ER/FR values within one rock type and different rock types.

Same rock types do not indicate the same particle shapes. Figure 31 illustrates simply the differences in elongation and flatness ratio between the individual rock types. Rock types can have similar mechanical properties, but particle shape can differ significantly. Diagrams in Figure 31 also show the range of results within one rock type. Flatness ratio varies between 0.6 and 0.85 and elongation ratio varies between 0.65 and 0.8 for all rock types.

Even in rock types that have been considered to be homogenous (e.g. 02 basalt), the distribution of geometric properties differs. This leads to the assumption that subclasses should not only be built by geological/mineralogical aspects, but also due to grain shape.

The following diagrams in Figure 32 show the flatness and elongation ratio for all rock types that were analyzed before and after the test (divided in subclasses). The mean flatness and elongation ratios for rock types without consideration of the subclasses can be seen in Table 24.

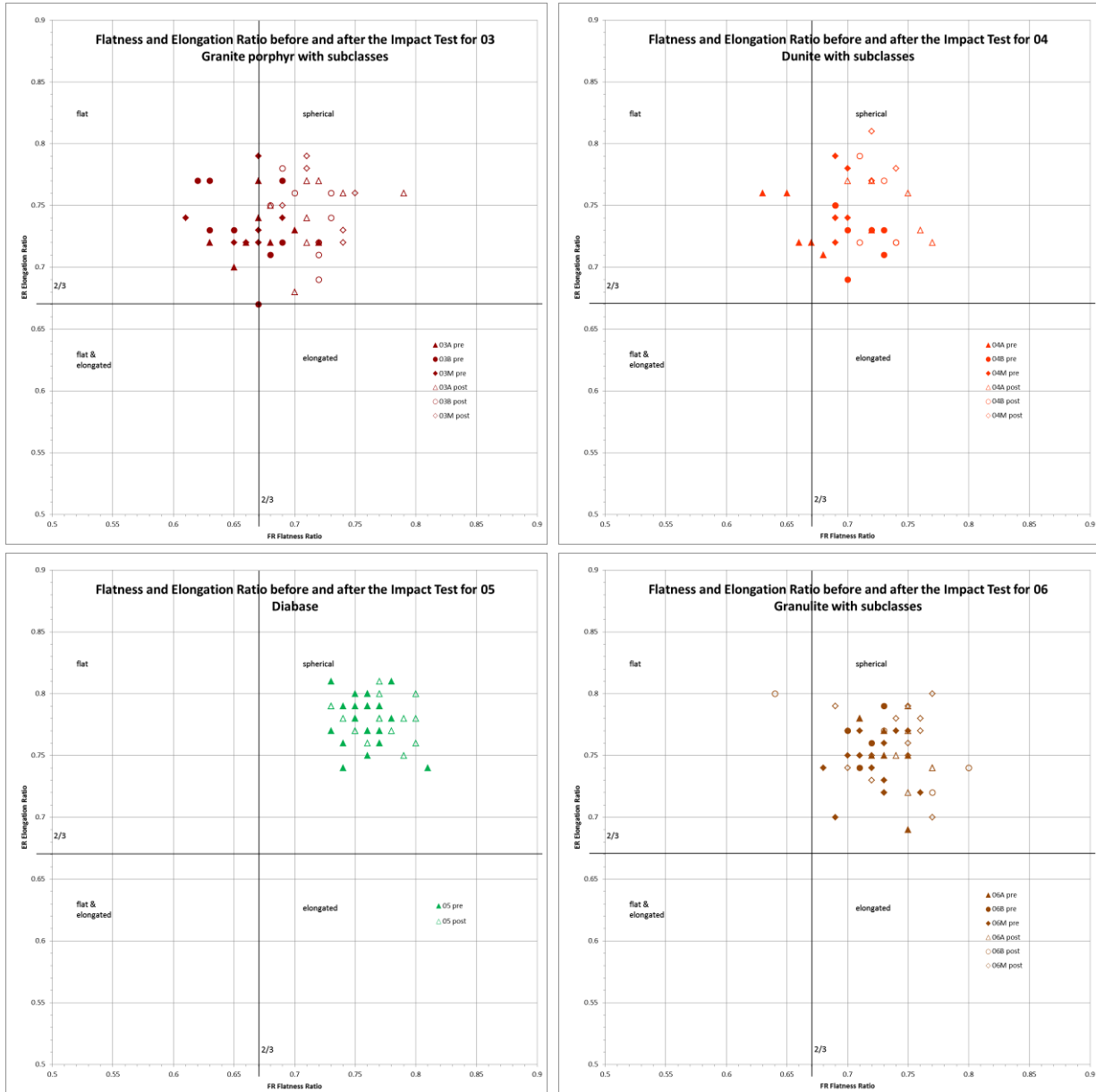




Figure 32: Particle shape geometry (flatness and elongation ratio) of all rock types (with subclasses) that have been tested in the Petroscope 4D[®] before and after the impact test (after Zingg, 1935).

The diagrams in Figure 32 indicate that the particle shape (ER and FR) changes during the impact test (for a better confirmation see Figure 33). One can assume that the impact strength during the test affects the particle shape. It also shows that the particle shape varies samplewise within one rock type.

As mentioned in section 4.1, the author did not build the subclasses according to particle geometry, but mineralogy/geology. Particle shape can influence the process of fragmentation. Unfavourable shaped particles can lead to more fragmentation. But as mentioned above, fragmentation also depends on the

impact strength of the material. However, as the subclasses have been built due to geological/mineralogical aspects, there are no clearly recognizable trends of different ER and FR visible between them in the results for rock type 03, 06, 07, 09, and 15. A trend for different particle shape properties can only be seen within the subclasses of rock type 04. Subclass “A” offers more flat particles before the test than subclasses “B” and “M” offer before the impact test. However, mineralogical composition between these subclasses does not differ. The strong variations in the results for both particle shape as well as SZ_{TU} -value could be a coincidence, as there are also not distinct variations in angularity (see section 5.6).

Table 24: values for elongation and flatness ratio before and after the impact test and the calculated differences. The difference was calculated by $FR/ER_{post} - FR/ER_{pre}$.

	mean					
	pre		post		difference	difference
rock type	FR	ER	FR	ER	FR	ER
01	0.74	0.75	-	-	-	-
02	0.68	0.75	0.76	0.77	+0.08	+0.02
03	0.66	0.73	0.72	0.74	+0.06	+0.02
04	0.71	0.74	0.73	0.76	+0.02	+0.02
05	0.76	0.78	0.77	0.78	+0.01	0
06	0.72	0.75	0.74	0.76	+0.02	+0.01
07	0.78	0.72	0.77	0.74	-0.01	+0.02
08	0.72	0.74	-	-	-	-
09	0.73	0.76	0.75	0.77	+0.02	+0.01
10	0.68	0.73	-	-	-	-
11	0.78	0.76	0.77	0.78	-0.01	+0.02
12	0.69	0.75	-	-	-	-
13	0.70	0.73	-	-	-	-
14	0.74	0.76	-	-	-	-
15	0.72	0.75	0.76	0.76	+0.04	+0.01

Figure 33 summarizes the mean flatness and elongation ratio per rock type. The arrows indicate the mean values of each rock type before (beginning of arrow) and after the impact test (top of the arrow). Rock types 02, 03, 04, 06, 09, and 15 show explicit changes in the flatness ratio, but smaller changes in elongation ratio. Rock type 05 does not change its particle shape at all (see Table 24). Rock types 07 and 11 demonstrate the opposite behavior. There is a negative change in the flatness ratio of the particles and a larger change in the elongation ratio.

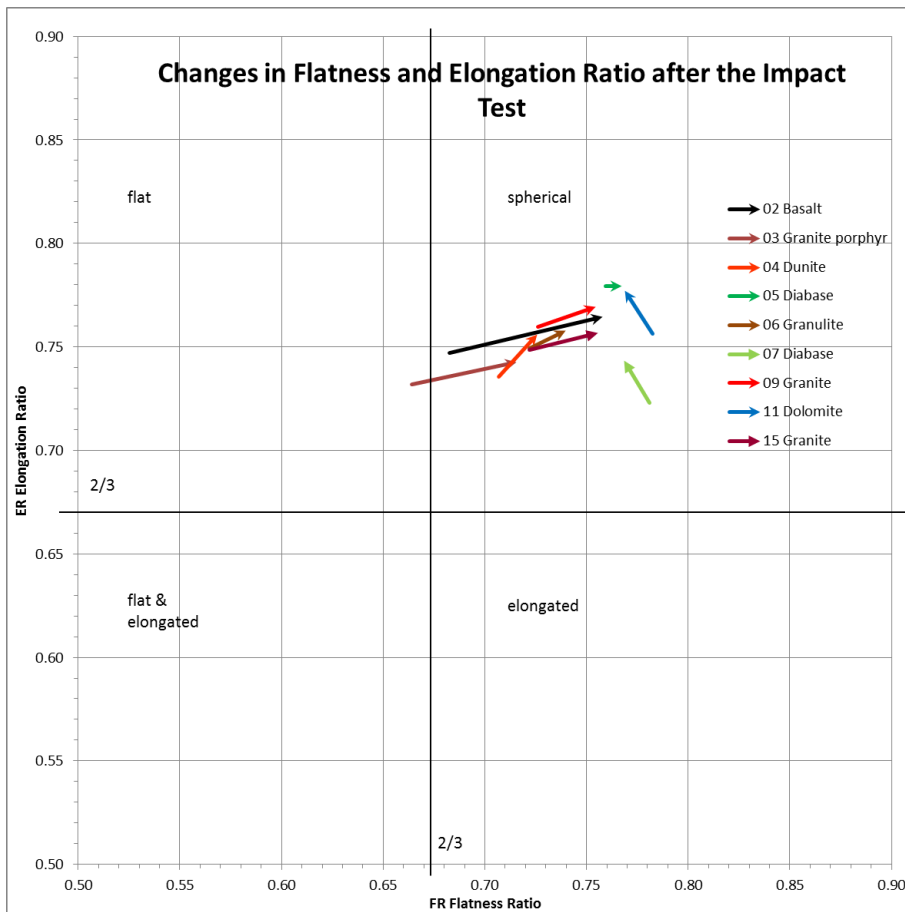


Figure 33: changes in flatness and elongation ratio (after Zingg, 1935) after the execution of the impact test. Beginning of arrow indicates the mean FR/ER before the test, top of the arrow indicates the mean FR/ER after the impact test.

Figure 33 displays that there are changes in both flatness and elongation ratio. The mean flatness ratio for most of the rock types increases more than the mean elongation ratio. The higher increase in mean FR means an increase of flat particles during the impact (e.g. by chipping) test compared to the increase of elongated particles.

As mentioned before, the diabase rocks from supplier 08 and 14 are the same aggregates, but broken down in different crushers. Figure 34 displays the differences in their particle shape.

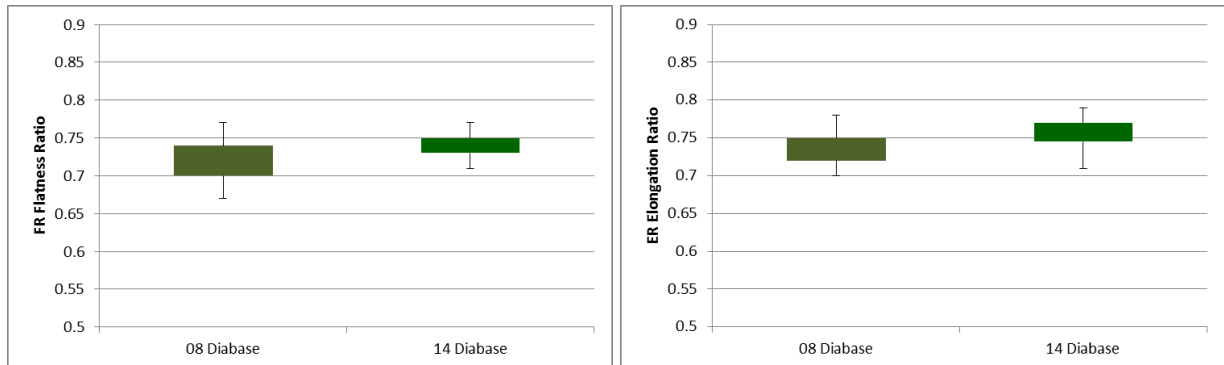


Figure 34: comparison of flatness (left) and elongation (right) ratio for diabase rock 08 and 14, before the impact test.

As they were broken down differently, the particle shapes differ. The diabase that came from the crusher 14 has both a higher flatness and elongation ratio. Therefore we can assume that breaking of particles in different crushers leads to different particle shape properties. As mentioned before, particle shape influences the impact test results, thus the mechanical properties. One can assume that the right choice of the crushing machine influences the quality of railway ballast.

5.6. Angularity

The angularity was also measured in device Petroscope 4D. The diagrams in Figure 35 and Figure 36 display cumulative frequency curves (expressed as proportion of angles, PropA, see section 2.5). The angularity classes after Powers (1953) are supplemented for a better allocation. Those two diagrams show these rock types that were measured in the device Petroscope 4D[®] before and after the test.

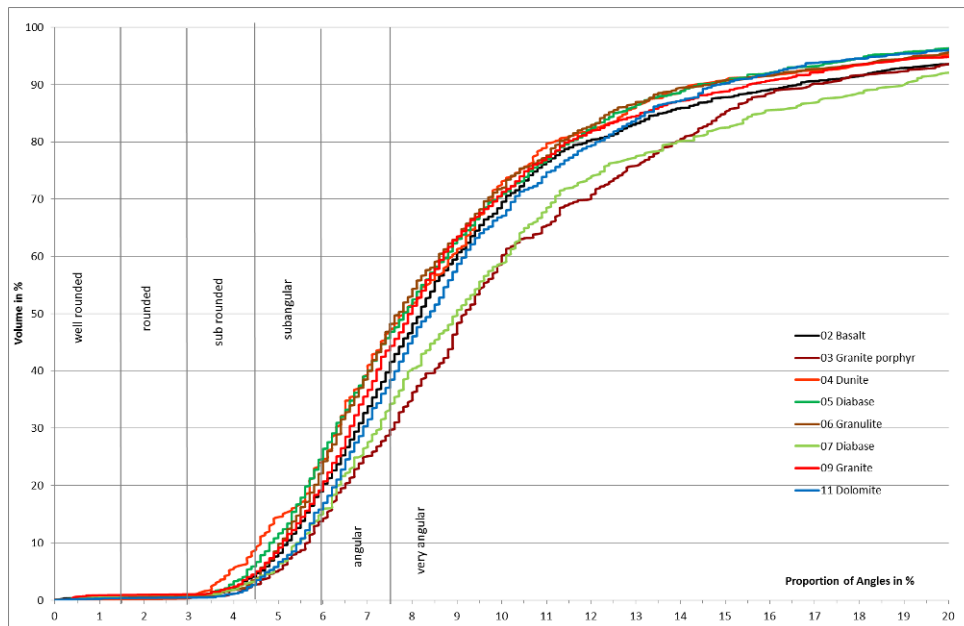


Figure 35: Angularity expressed as proportion of angles (PropA) in % before the impact test of selected rock types.

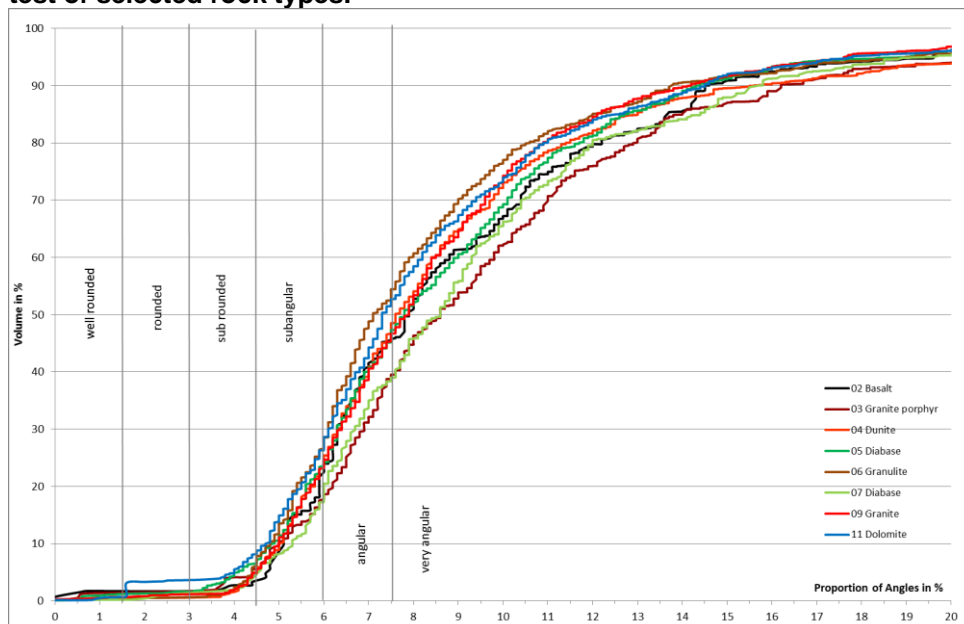


Figure 36: Angularity expressed as proportion of angles (PropA) in % after impact test on selected rock types.

The cumulative frequency curves before the impact test (Figure 35) show that all rock types are “angular” and “very angular” particles (around 80 Volume-%). Less than 5 Volume-% are “well-rounded”, “rounded” or “subrounded” particles. The mean angularity ranges between 6 and 11% PropA (see Figure 35) and the cumulative frequency curves show a similar gradient for all rock types.

After the test, the angularity has only changed slightly. 75 Volume-% are still lying in the range of “angular” and “very angular” particles. The number of “subangular” aggregates has increased by around 5 Volume-%. The gradient of the cumulation curves has not changed.

The following Figure 37, Figure 38 and Figure 39 display the cumulative frequency curves of angularity for three selected rock types divided into subclasses, before and after the test. Black cumulative frequency curves indicate the angularity after the test and the coloured curves, before the test. The selected rock types are 03 granite porphyr, 04 dunite, and 07 diabase.

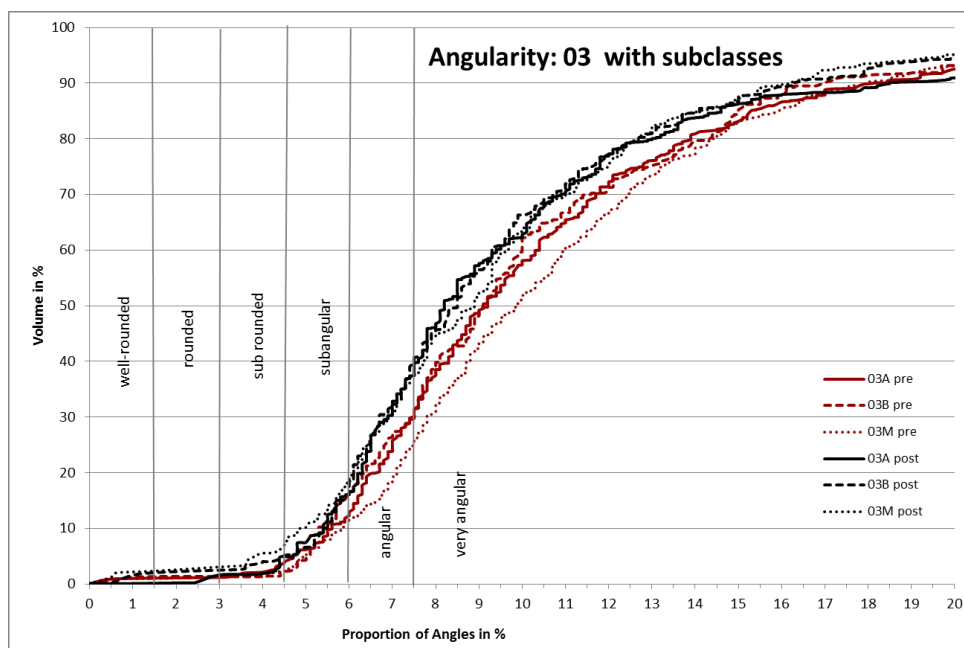


Figure 37: Angularity expressed as proportion of angles (PropA) in % for 03 granite porphyr with subclasses, before (red curves) and after (black) impact test.

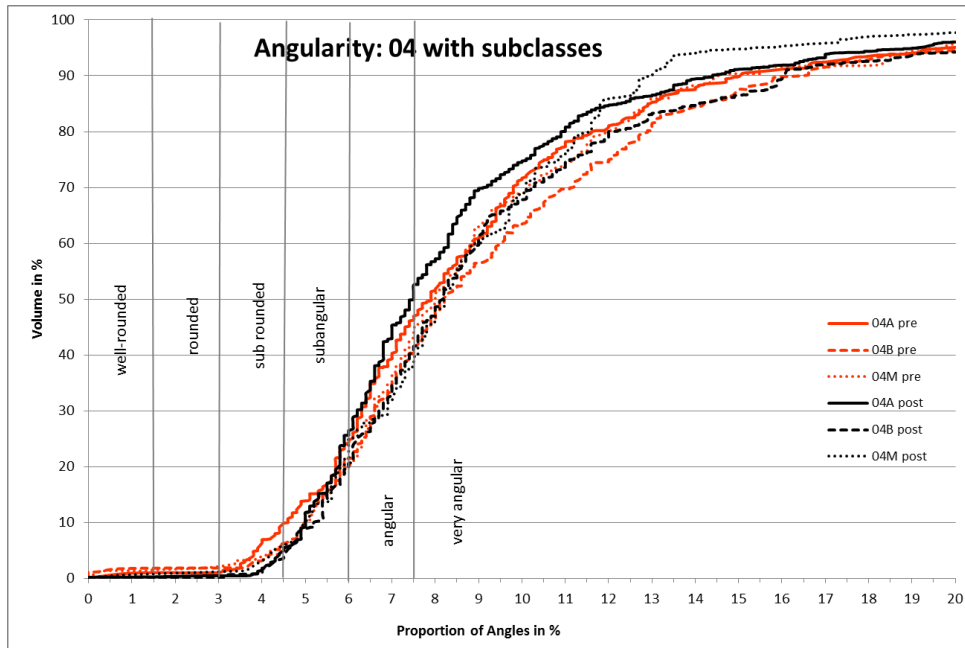


Figure 38: Angularity expressed as proportion of angles (PropA) in % for 03 dunite with subclasses, before (orange curves) and after (black) impact test.

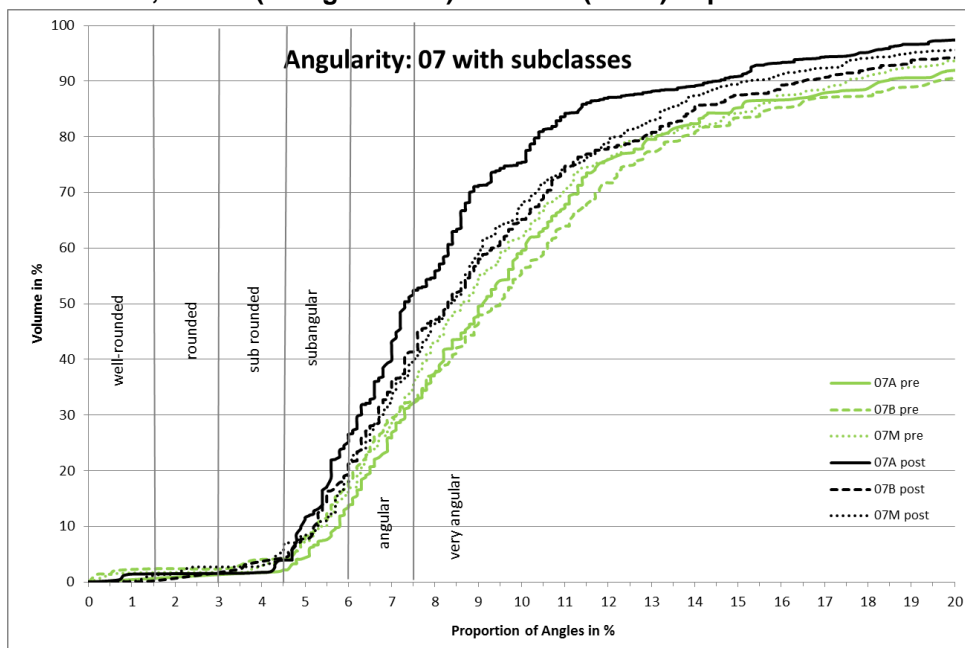


Figure 39: Angularity expressed as proportion of angles (PropA) in % for 07 Diabase with subclasses, before (green curves) and after (black curves) impact test.

When dividing the cumulative frequency curves of the rock types into their subclasses, there are small result differences from those displayed in Figure 35 and Figure 36. For rock type 03 and 07, the amount of “angular” particles increases to the disadvantage of “very angular” particles. Rock type 03 offers different cumulative curves for the mixture group of aggregates and both subclasses

(prior to test). (M) consists of more “very angular” particles than the subclasses (A) and (B). After the test, differences between the subclasses of 03 are only very small. Changes for rock type 04 between the subclasses are only minimal (prior and after the test). The amount of “subrounded” particles is slightly higher in 07(M) than in the subclasses (A) and (B) of 07 (prior to the impact test). The Volume-% fraction of “angular” particles increases in rock type 07(A) compared to classes (M) and (B) (after the test).

In Figure 40 the mean angularity of different rock types is plotted against the SZ_{TU} -value before the impact test. Table 25 lists the values of the mean angularity (Prop 50%) of all rock types before the test and after the impact test (50% of all samples).

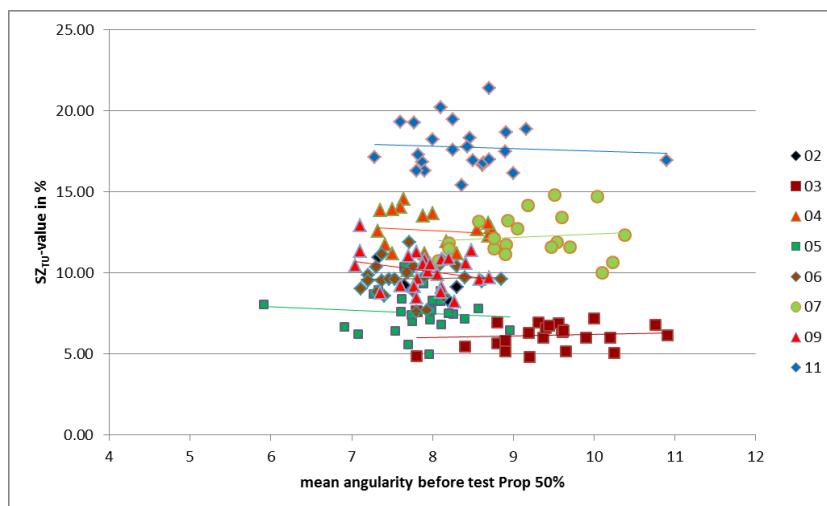


Figure 40: correlation of mean angularity (prop50%) before the impact test with the SZ_{TU} -value of selected rock types.

There is no correlation between the mean angularity and the fragmentation value. If there would be a correlation, then the SZ_{TU} -value would depend on the degree of rounding of the particles. Since this is not the case, the impact strength does not depend on the angularity, at least not for the obtained results.

Table 25: lists the values for mean angularity Prop 50% before and after impact test and the difference of mean angularity before test - difference of mean angularity after test ΔpropA

rock type	Mean angularity before test Prop 50%	Mean angularity after test Prop 50%	ΔpropA in %
01	7.57	-	-
02	7.87	7.94	0.07
03	9.39	8.52	-0.87
04	7.94	8.12	0.18
05	7.79	8.01	0.22
06	7.76	7.57	-0.19
07	9.21	8.44	-0.77
08	8.30	-	-
09	7.91	7.87	-0.04
10	7.97	-	-
11	8.41	7.65	0.24
12	8.24	-	-
13	8.53	-	-
14	6.69	-	-
15	8.52	8.02	-0.5

Figure 41 shows the difference between the mean angularity after the test minus the mean angularity before the test. This value is called ΔpropA in %.

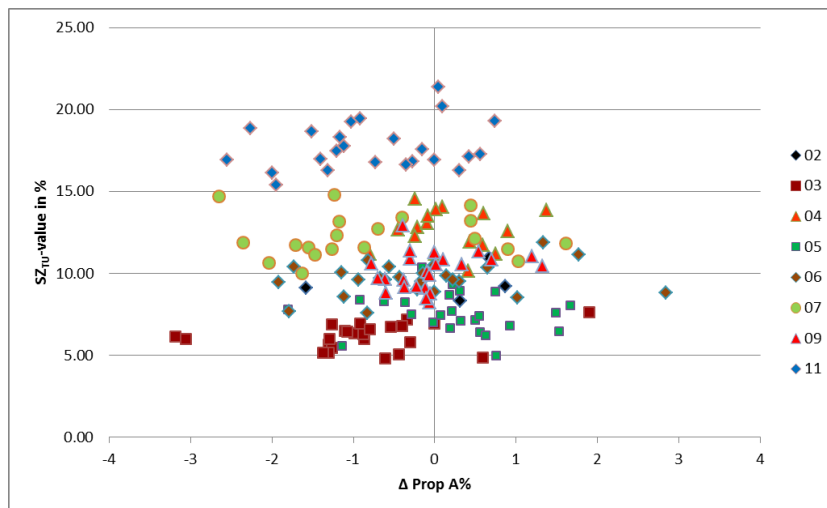


Figure 41: difference of mean angularity before test (Prop50% pre) and mean angularity after test (Prop 50 post), ΔpropA in % = Prop 50 post - Prop50% pre, positive ΔpropA – value indicate an increase in angularity, negative ΔpropA – value indicate a decrease in angularity.

A positive ΔpropA – value indicates an increase in angularity (more “angular” and “very angular” particles) and a negative ΔpropA – value directs to a decrease in angularity (more “subangular” and “subrounded” particles).

There are different angularities for different rock types and the variations within one rock type also differ (mostly in the range of “angular” and “very angular” particles).

However, all provided angularity results do not show significant changes with regard to the impact test. The impact test does not affect the rounding of particles. Fragmentation processes do not lead to rounding of particles.

Figure 42 compares the mean angularity before the test for 08 Diabase and 14 Diabase.

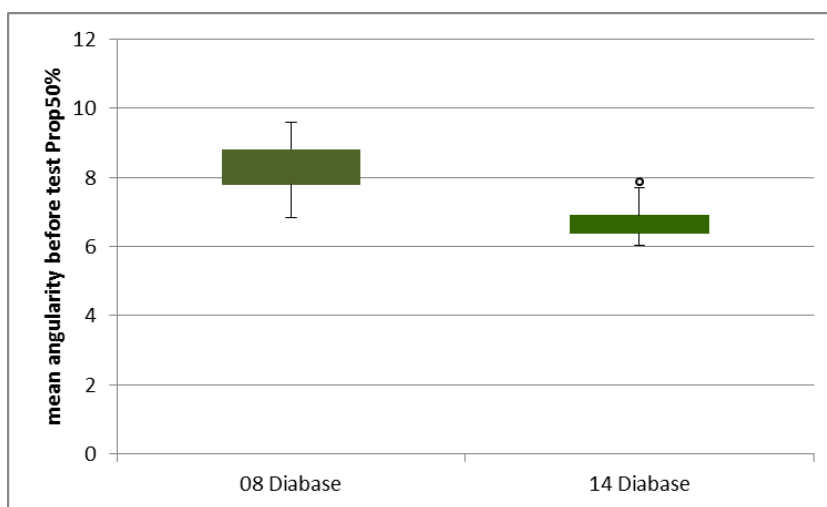


Figure 42: comparison of mean angularity Prop50% before the test of 08, 14 Diabase. Prop50% of 08 Diabase is 8.30% and of 14 Diabase is 6.69%.

Diabase 08 and 14 are the same rock aggregates, as mentioned before. The mean angularity of 08 is much higher than the one of 14. The mean angularity of 08 (Prop50% = 8.30%) indicates mainly “very angular” particles, whereas 14 (Prop50% = 6.69%) leads to the assumption of mostly “angular” particles. Therefore we can conclude that breaking of particles in different crushers leads not only to different particle shape, but also to different rounding of particles.

5.7. Comparison between the data Austrian Railways (ÖBB) and TUGraz

Austrian Railways (ÖBB) has provided their test results. The following diagram in Figure 43 compares the results of ÖBB with the ones obtained by the author at TUGraz. Table 26 provides the data given by the railway company ÖBB as well as the mean values by the author. All test results from TUGraz are smaller than those provided by ÖBB. As these results are all lower, a weak correlation can be seen (Figure 44).

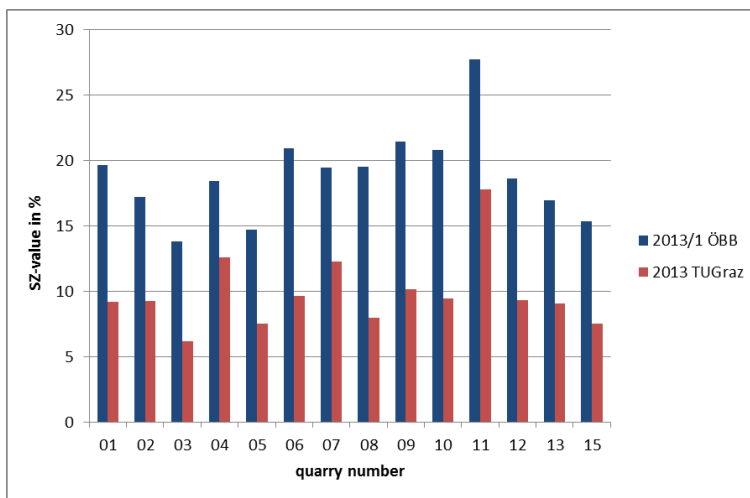


Figure 43: comparison of ÖBB SZ_{RB} and SZ_{TU} -values in % from 2013. Quarry 14 is not included in this diagram, because 08 and 14 Diabase have not been the same rock type at the ÖBB project.

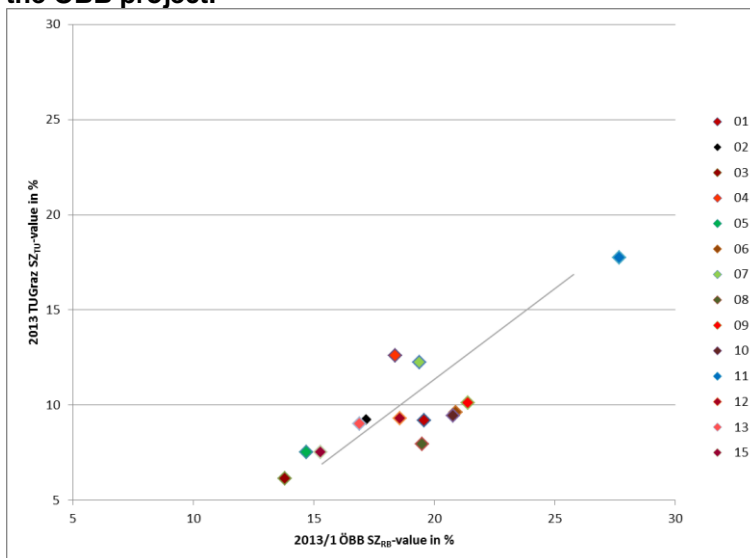


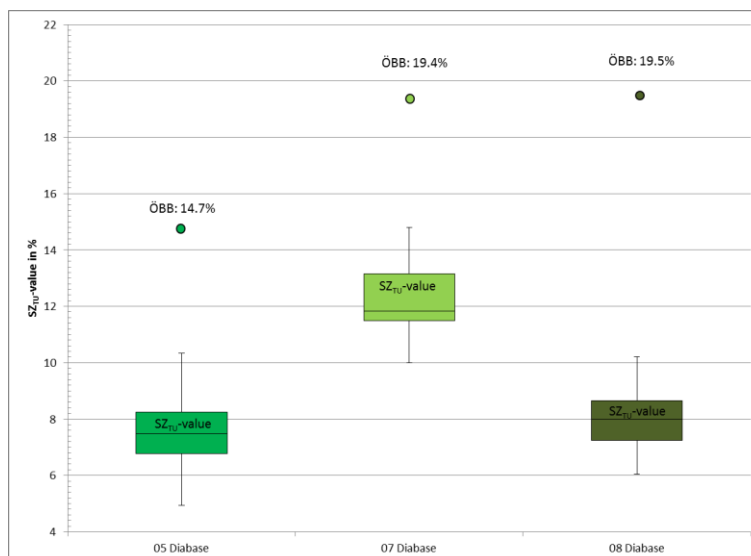
Figure 44: weak correlation between SZ_{RB} values provided by ÖBB and SZ_{TU} -values in %, a weak correlation can be seen, as all test results from TUGraz are smaller than those from ÖBB, quarry 14 is again not included (see description in Figure 43).

Table 26: Compilation of SZ_{RB} -values provided by ÖBB and SZ_{TU} -value from 2013.

	2013/1 ÖBB [%]	2013 TUGraz [%]
01	19.6	9.19
02	17.2	9.24
03	13.8	6.14
04	18.4	12.60
05	14.7	7.53
06	20.9	9.64
07	19.4	12.23
08	19.5	7.95
09	21.4	10.13
10	20.8	9.46
11	27.70	17.74
12	18.6	9.29
13	16.9	9.03
14	12.7	-
15	15.3	7.52

All values from the project at the Technical University are much smaller than the ones provided by the railway company. A possible reason might be the heavier die in this project. The heavier die might dampen the impact.

Additionally Figure 45 compares the diabase values from Austrian Railways to results from TUGraz. The reason is the unusually high SZ_{TU} -result for rock type 07 compared to the other diabase results. Diabase rocks show similar results, except for diabase 07. A comparison with the ÖBB results is displayed in order to show whether the trend can also be seen here. But the SZ_{RB} -value (ÖBB) for 07 is not unusually higher than the others; 08 Diabase shows the same result.

**Figure 45: comparison Diabase results SZ_{RB} ÖBB 2013 and results SZ_{TU} 2013.**

6. Discussion and Conclusion

The aim of this thesis has been to determine the effect of grain shape, angularity, and petrographic composition of railway ballast on the impact test. For this purpose angularity (as “Volume of Angles”), and flatness, and elongation ratio are determined with the help of the device Petroscope 4D[®]. Values from the impact test accomplish statistical analysis of the SZ_{TU} -value and strain value. Indirect analyses of device Petroscope 4D[®] data lead to the degree of fragmentation Z and are compared to the results of the impact test.

SZ_{TU} -value

350 impact tests are performed. The results vary for all rock types. SZ_{TU} -values differ within one rock type and within one supplier. There is no general trend detectable for one of the probed rock types concerning fragmentation performance. For example, one cannot consider diabase a better suitable rock type than granite. However, the samples of granite porphyr have the lowest SZ_{TU} -values and therefore the best fragmentation performance in this test series. Dolomite shows the worst fragmentation performance with the highest SZ_{TU} -values.

For a confidence interval of 95% to be achieved, with a limiting absolute value of 0.5% from the mean SZ_{TU} -value, between 2 and 39 test repeats are necessary (see Table 23). Variations occur in samples with and without subclasses. Subclasses show distinctly different SZ_{TU} -values for rock types 04, 07, 12, and 14. Clear distinctions in petrographic composition can be seen for rock type 07 and 14, which can explain the diversity of SZ_{TU} -results in subclasses.

The results for the various rock types and the results for two subclasses clarify the effect of petrographic composition on the impact test. Weak material like Dolomite shows high tendency to fragment. A lower trend to fragmentation can be seen for granitoid rock types and diabase. However, before the test, an assumption was made that fragmentation behavior is influenced by grain sizes (coarse grained material like granite → higher tendency to break than fine

grained material like diabase). This assumption was not confirmed, as granite and diabase have similar results.

Strain

During the test, strain is created by rearrangement and rearrangement processes linked with fragmentation. Strain values only differ slightly for the different rock types. Therefore, one can assume that the petrology plays only a minor role in the compaction of sample material in the mortar. Samples are inserted by hand inside the mortar. In Figure 26 and Figure 27, it can be concluded that the human impact has no effect on the test results.

Degree of fragmentation Z

The value Z expresses the resistance to fragmentation of particles. There is a strong correlation between the impact test result SZ_{TU} -value and the degree of fragmentation Z. This correlation is expressed by the equation $Z = 0.98SZ_{TU} + 3.40$. Value Z was determined by the grain size distribution. This leads to the assumption that the grain size undergoes large changes during the impact test. Many fines are produced. Samples break down to very fine (<8mm) and large (8mm-40mm) particles. Moreover, the correlation indicates that fragmentation takes place, but does not only create particles that are smaller than 8mm. In the mortar, rock aggregates break down to particles that are bigger than 8mm. One can assume that the SZ_{TU} -value reflects the degree of fragmentation very well.

The degree of fragmentation Z varies between the different rock types and also within one rock type. However, there is no clear trend detectable between the various subclasses within one rock type.

Particle Shape

The distribution of mean flatness ratio of different rock types varies between 0.6 and 0.85, while the mean elongation ratio varies between 0.65 and 0.8 for data taken before the impact test. The mean flatness ratio varies between 0.66 and 0.78 (prior to test) and the mean elongation ratio varies between 0.72 and 0.78. Smaller FR values lead to the assumption that there are more flat than elongated particles. Selected rock types have been analyzed in terms of ER and FR after the impact test. The change in mean flatness ratio varies between -1 and 8%. Positive change in mean FR means a decrease of flat particles and a negative change indicates an increase of flat particles. The change in mean elongation ratio only varies between 1 and 2%. Therefore, more flat particles are produced during the test than elongated particles.

Trends for different particle shape in subclasses are not detected except for rock type 04. Rock type 04 shows distinct different results for SZ_{TU} -values and particle shape, but the mineralogy does not differ between the subclasses. A possible reason for these different SZ_{TU} -values could be that subclasses have intuitively been built by particle shape. Therefore, one could also form subclasses based on particle shape and not only on the basis of mineralogy. As there are distinct changes in flatness and elongation ratio before and after the test, one can make the assumption that particle shape affects the mechanical behavior in the impact test.

Angularity

75% to 85% Volume-% of the particles tested are “angular” and “very angular” particles. This changes by about 5% Volume-% after the test in favor of more “subangular” particles. The change is very small and for selected subclasses only slight differences in angularity characteristics could be detected. As can be seen in Table 25 and Figure 41, there are positive and negative changes when comparing the mean angularity before and after the test. Positive changes indicate an increase in angularity and negative values indicate a decrease. Therefore, one can assume that although small changes in angularity are apparent, they do not have a large effect in the results, because fragmentation does not

influence the angularity of railway ballast. Fracture surfaces which are formed during the impact test, have similar surfaces as those generated in the crushers.

Furthermore angularity does not show a clear trend to be dependent on petrographic composition. Mean angularity values vary within one rock type, but there is not a clear trend detectable for different rock types.

Comparison ÖBB/TUGraz

A comparison of SZ_{RB} -values and SZ_{TU} -values shows that the latter have smaller values than the ones obtained in the test series by ÖBB in 2013 (see Figure 43 and Figure 44). These smaller values can be explained by the impact test device changes made to the European Standard. This theory is strengthened by the weak correlation of both SZ_{RB} - and SZ_{TU} -values. Subclasses are not considered here, as the distinction in subclasses only took place in the test series of TUGraz. As mentioned in section 3.1, the standard EN 1097-2 proposed a SZ_{RB} -value maximum of 22%. All rock types lie under this proposed value in both test series, except for the dolomite in the ÖBB test series.

Another unique feature of the TUGraz test series is that rock types 08 and 14 are the same rock type from the same quarry, but broken down in different crushing machines (see Figure 45). They have the same petrology, but different shapes and angularity, and different SZ_{TU} -values. One can assume that rocks with the same petrology lead to different mechanical properties when particle shape and angularity differ. Suppliers could produce railway ballast with higher quality by using a suitable crushing method.

Impact strength behavior of railway ballast is particularly dependent on particle shape, and petrology, and processing of the material. Due to blasting techniques and local crushers, geological factors that normally determine particle shapes (e.g. erosion, weathering, mineral size), are overridden. Angularity has a minor effect on the ballast during the impact test. The impact of different petrographic compositions and particle shape on the fragmentation are proved to be stronger than the angularity impact.

As initially mentioned, possible reasons shall be found that lead to the variations in the results of the impact test. Possible explanations are differences in petrology (inhomogeneity of material), diversity in grain shape, and less importantly is the angularity of the rock type.

References

- Bach, H., & Hofer, V. (2013), *Analyse des Gleisschotters* (Projektbericht), Graz, Technische Universität Graz.
- Bach, H. (2012), *Beanspruchungscharakteristik von Schotter im Gleis*. Institut für Eisenbahnwesen und Verkehrswirtschaft an der TU Graz (Ed.), Forschungstag 2012 (Schriftenreihe 1), pp. 76-93, Graz.
- Bach, H. (2013), *Evaluation of attrition tests for railway ballast*. Institut für Eisenbahnwesen und Verkehrswirtschaft an der TU Graz, Dissertation, Graz.
- Blott, S. J., & Pye, K. (2008), *Particle shape: A review and new methods of characterization and classification*, *Sedimentology*, vol. 55, pp. 31-63.
- Breyman, H., Nindl, G., & Scharler, D. (2012), *Mechanische Kriterien für den Gleisschotter - Punktlastversuch – Zeitreihen*, Projekt, Höhere Technische Bundeslehranstalt Saalfelden - Abteilung Bautechnik - Tiefbau, pp. 1-14.
- Daniel, J. S., & Lowe, J. (2011), *Petroscope evaluation*, Report, University of New Hampshire - Department of Civil Engineering, pp. 1-65.
- EUREKA. (2001), *Petroscope – an optical analyser for construction aggregates and rocks*, No. Tech. Rep. 2569, Brussels.
- EUREKA. (2005), *Petroscope II*, No. Tech. Rep. 3665, Brussels.
- Fendrich, L. (2007), *Handbuch Eisenbahninfrastruktur*, DE, Springer Berlin Heidelberg, pp.254-255.
- Hofer, V., Bach, H., Latal, C., & Neubauer, A. (2013), *Impact of geometric and petrographic characteristics on the variability of LA test values for railway ballast*, *Mathematical Geosciences*, vol. 45(6), pp. 727-752.
- Klotzinger, E. (2008), *Der Oberbauschotter Teil 1: Anforderungen und Beanspruchung*, *Eisenbahntechnische Rundschau*, vol. 57(1/2), pp. 34-41.
- Kuttelwascher, C. (2011), *Oberbauschotter in Österreich.*, Proc. 10. Unterbau-Expertentreffen DACH-Staaten, Nürnberg.
- Lee, J. R. J., Smith, M. L., & Smith, L. N. (2007), *A new approach to the three-dimensional quantification of angularity using image analysis of the size and form of coarse aggregates*, *Engineering Geology*, vol. 91, pp. 254-264.

- Liu, Q., Dr. (2010), *Statistische Schätzverfahren und Tests*, Vorlesungsskript „Angewandte Statistik“, Institut für Angewandte Geowissenschaften, TU-Graz.
- Moorhouse, W. W. (1959), *The study of rocks in thin section*, New York [u.a.], Harper, pp. 1-514.
- Nesse, W. (2012), In Oxford University Press I. (Ed.), *Introduction to mineralogy* (2nd Edition ed.), New York: Oxford University Press.
- Österreichische Bundesbahnen (ÖBB) (2007), BH 700 *Technische Lieferbedingungen für den Oberbauschotter*, Wien.
- Österreichisches Normungsinstitut (2004a), EN 13450 *Gesteinskörnungen für Gleisschotter*, Wien.
- Österreichisches Normungsinstitut (2004b), EN 1097-1 *Prüfverfahren für mechanische und physikalische Eigenschaften von Gesteinskörnungen - Teil 1: Bestimmung des Widerstandes gegen Verschleiß (Mikro-Deval)*, Wien.
- Österreichisches Normungsinstitut (2006), EN 1097-2 *Prüfverfahren für mechanische und physikalische Eigenschaften von Gesteinskörnungen - Teil 2: Bestimmung des Widerstandes gegen Zertrümmerung*, Wien.
- Pape, H. (1972), *Leitfaden zur Gesteinsbestimmung: Mit Tabellen zur Bestimmung der wichtigsten Gesteine nach einem Schlüssel mit mehrfachen Verzweigungen ; 9 Tabellen*, Stuttgart: Enke, pp. 1-152.
- Powers, M. C. (1953), *A new roundness scale for sedimentary particles*, Journal of Sedimentary Petrology, vol. 23(2), pp. 117-119.
- Wieden, P. (1969), *Erfassung der Gesteinseigenschaften durch Schlag- und Zertrümmerungswert und Los-Angeles-Test*, Berg- und Hüttenmännische Monatshefte, vol. 114(10), pp. 310-315.
- Zingg, T. (1935), *Beitrag zur Schotteranalyse - Die Schotteranalyse und ihre Anwendung auf die Glattalschotter*, Abteilung für Naturwissenschaften an der ETH Zürich, Schweizerische Mineralogische Und Petrographische Mitteilungen, vol. XV (Sonderband), Zürich.